Featuring work from the research teams of Dr Radislav A. Potyrailo, GE Global Research Center, Niskayuna, NY, USA.

Toward high value sensing: monolayer-protected metal nanoparticles in multivariable gas and vapor sensors

This review examines advances in multivariable sensors based on monolayer-protected nanoparticles and several principles of signal transduction that result in non-resonant and resonant electrical sensors as well as material- and structure-based photonic sensors.

As featured in:

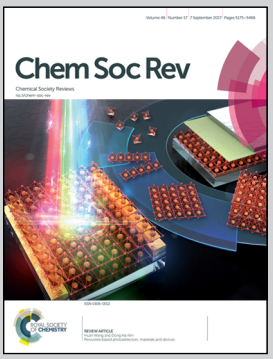

See Radislav A. Potyrailo, *Chem. Soc. Rev.*, 2017, **46**, 5311.

ROYAL SOCIETY OF CHEMISTRY

rsc.li/chem-soc-rev

Registered charity number: 207890

Chem Soc Rev

REVIEW ARTICLE

View Article Online
View Journal | View Issue

Cite this: *Chem. Soc. Rev.*, 2017, **46**, 5311

Toward high value sensing: monolayer-protected metal nanoparticles in multivariable gas and vapor sensors

Radislav A. Potyrailo

For detection of gases and vapors in complex backgrounds, "classic" analytical instruments are an unavoidable alternative to existing sensors. Recently a new generation of sensors, known as multivariable sensors, emerged with a fundamentally different perspective for sensing to eliminate limitations of existing sensors. In multivariable sensors, a sensing material is designed to have diverse responses to different gases and vapors and is coupled to a multivariable transducer that provides independent outputs to recognize these diverse responses. Data analytics tools provide rejection of interferences and multi-analyte quantitation. This review critically analyses advances of multivariable sensors based on ligand-functionalized metal nanoparticles also known as monolayer-protected nanoparticles (MPNs). These MPN sensing materials distinctively stand out from other sensing materials for multivariable sensors due to their diversity of gas- and vapor-response mechanisms as provided by organic and biological ligands, applicability of these sensing materials for broad classes of gas-phase compounds such as condensable vapors and non-condensable gases, and for several principles of signal transduction in multivariable sensors that result in non-resonant and resonant electrical sensors as well as material- and structure-based photonic sensors. Such features should allow MPN multivariable sensors to be an attractive high value addition to existing analytical instrumentation.

Received 5th January 2017

DOI: 10.1039/c7cs00007c

rsc.li/chem-soc-rev

1. Introduction

Detection of gases and vapors in complex backgrounds is needed for industrial safety, environmental surveillance, medical diagnostics, homeland protection, and many other applications.[1–5] When detection selectivity is critically required, "classic" analytical instruments based on gas chromatography (GC), mass spectrometry (MS), ion mobility spectrometry (IMS), and tunable diode laser absorption spectroscopy (TDLAS) are preferred despite their limitations of relatively high power consumption, cost, and size.[6–10] These instruments are often inconvenient and costly, even with the reduced carrier gas, vacuum, or power demands,[4] but are an unavoidable alternative to existing sensor systems.

The evolution in developments of diverse types of gas and vapor sensors is outlined in Fig. 1 as three technology curves. Initially, natural organisms have been used for detection of gases and vapors for industrial safety, homeland protection and other demanding applications (Fig. 1a and b).[11] While natural organisms such as canines continue to be applied in diverse scenarios of detection of drugs, explosives, and cancer, their applicability is limited by their costly training (~$50,000 per dog) and relatively low accuracy (90% in controlled conditions, <50% in real-life situations).[12,13]

Gas and vapor sensors have been under development for over 100 years, beginning with sensors based on catalytic metals, metal oxides, polymers, and formulated materials.[14–22] Sensors based on metal oxides are the most popular type of commercially available gas and vapor sensors[23–27] (Fig. 1c and d). Recent important advances in new gas sensors based on diverse sensing materials and single-output detection include outstanding sensitivity in vacuum and clean carrier gas[28–32] and rapid response times.[33–39] We see tremendous merits of single-output sensors based on resistivity, capacitance, light intensity, and other detection principles in providing excellent solutions to measurement needs in simple scenarios where selectivity of the response is not required. However, as the complexity of analyzed samples increases because of known and unknown chemical interferences and other environmental effects, single-output sensors rapidly lose their performance accuracy. Unfortunately, existing commercial- and research-grade sensors are quite non-selective because they struggle with antagonistic requirements for sensor reversibility *vs.* selectivity[1] that do not allow quantitation of gases and vapors in mixtures and in the presence of interferences.[5,40–44]

Combining sensors into arrays[45] is a common compromise to mitigate poor selectivity of sensors as shown in excellent

GE Global Research, Niskayuna, New York 12309, USA. E-mail: potyrailo@ge.com

studies with arrays of with up to thousands of elements.[37,45–48] Recent reviews cover different aspects of sensor arrays.[49–56] Examples of sensor arrays are illustrated in Fig. 1e and f. Over the years, the field of sensor arrays has matured to understanding of their limitations outside controlled laboratory conditions that include inability to operate in the presence of high levels of known and unknown interferences and an uncorrelated drift of each sensor in an array.[3,40–42,46–48,50,51,54,57–60] Thus, at present, ''classic'' analytical instruments successfully compete for high value applications where selective detection of gas-phase compounds is critical.

Recently, a new generation of gas and vapor sensors, known as multivariable sensors, has emerged with a fundamentally different perspective for sensing (Fig. 1g and h) to eliminate numerous limitations of existing commodity single-output sensors and their arrays.[61–76] Commodity sensors are technologically mature products that serve established markets, are widely available, inexpensive, and interchangeable. Unlike such commodity sensors, multivariable sensors quantify multiple individual vapors,[63,64,77] quantify multiple vapors in their mixtures,[61,73,78] accurately detect vapors in the presence of numerous interferences,[79] and reject interferences at a several million-fold excess level.[80] Such performance characteristics make multivariable sensors an attractive high value addition to existing analytical instruments.

These attractive performance characteristics of individual multivariable sensors have been achieved by applying new sensor-design criteria for selective gas and vapor sensing as illustrated in Fig. 2a. These design criteria involve (1) a sensing material with diverse responses to different gases and vapors, (2) a multivariable transducer with carefully chosen excitation conditions to provide independent outputs and to recognize these different responses to gas-phase compounds, and (3) data analytics to provide multi-analyte quantitation, rejection of interferences, and drift minimization.[73,81–83] These new multivariable sensor-design criteria bring a fundamentally new sensing philosophy that allows response to interferences with this new multivariable sensor but in different directions than the analyte response (Fig. 2b). This new sensing philosophy is the major departure from the existing sensing approach where a conventional sensor cannot differentiate between the analyte and interferences (Fig. 2**c**).

Numerous sensing materials have been demonstrated with recently developed multivariable sensors. Examples of sensing materials include dielectric and conducting polymers,[66–68,80,84–91] metal oxides,[92–96] catalytic metals,[97–99] macrocycles,[63,84,100] carbon allotropes,[101–103] ionic liquids,[104] composite materials,[105,106] semiconducting nanowires,[78] and functionalized metal nanoparticles.[42,72,74,80,88,107–112]

To recognize diverse responses of these sensing materials to different gases and vapors, three transducer types have been explored: (1) electrical transducers such as impedance devices[61,63,64,84,91,93,94,107] and field effect transistors,[62,78,98–100,113] (2) photonic transducers such as material-based[74,109–111] and nanostructure-based[70,71,73,105,114,115] resonators, and (3) electromechanical transducers such as thickness shear mode resonators.[104,106,108,116,117]

To process data from multivariable sensors, diverse data analytics and machine learning tools have been utilized such as Principal component analysis (PCA),[64,70,118] Discriminant Analysis (DA),[99,118] Artificial Neural Network (ANN),[119] Hierarchical cluster analysis (HCA),[73] Support Vector Machines (SVM),[79] Independent Component Analysis (ICA),[118] Partial least squares (PLS) regression,[73,109] and Principal Component Regression (PCR).[79]

Metal nanoparticles functionalized or capped with different organic or biological ligands – termed here as monolayer-protected nanoparticles (MPNs) – distinctively stand out from the rest of the sensing materials for multivariable sensors because of their three attractive attributes: (1) ability to produce diverse chemical functionality of nanoparticles, (2) applicability of these sensing materials for diverse classes of gas-phase compounds, and (3) broad principles of signal transduction in multivariable sensors.

There are several remaining needs in advancement of these sensing materials toward bringing them into practical applications. The very challenging needs include improvements of stability of these materials, expanding the temperature range of their operating conditions, and expanding further the range of detected gas-phase compounds. At present, inadequate stability is the biggest limitation of the majority of MPN materials, precluding them from advancing to commercial sensor products.

This review provides a comprehensive analysis of two key topics such as functionalized nanoparticles for sensing of gas-phase compounds and multivariable sensing using individual

Radislav A. Potyrailo

Dr Radislav Potyrailo is a Principal Scientist at GE Global Research in Niskayuna, New York, leading the growth of industrial, wireless, wearable, and harsh environment sensing technologies for GE applications. He holds an Optoelectronics degree from Kiev Polytechnic Institute and PhD in Analytical Chemistry from Indiana University. Radislav has been serving as the GE Principal Investigator on U.S. Government programs funded by AFRL, DARPA, DHS, NETL, NIH, NIOSH, and TSWG. Radislav delivered 80+ invited lectures and ten keynote/plenary lectures at National and International Meetings, has 100+ granted U.S. Patents and 150+ publications, and coauthored/coedited eight books. He serves as an editor of the Springer book series Integrated Analytical Systems. His recent awards include the 2010 Prism Award by SPIE and the 2012 Blodgett Award by GE Research. In 2011 Radislav was elected SPIE Fellow for achievements in fundamental breakthroughs in optical sensing and analytical systems. In 2013 Radislav was elevated to the grade of Senior Member of the IEEE.

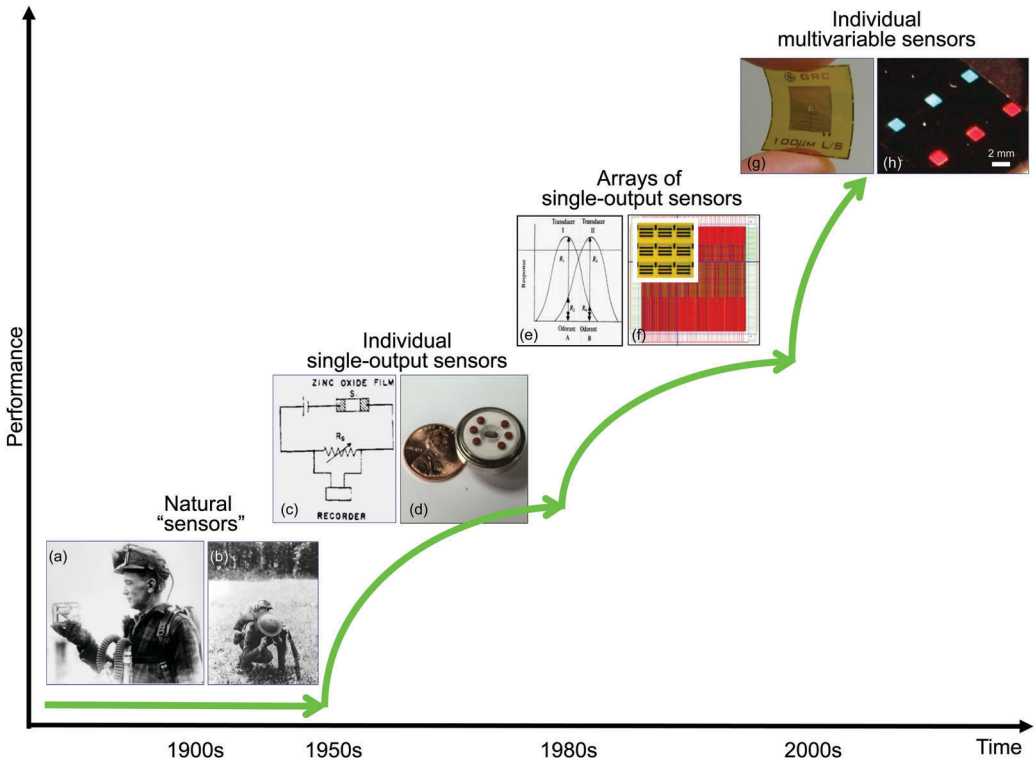

Fig. 1 Evolution in developments of diverse types of gas and vapor sensors as three technology curves. Natural organisms for detection of gases and vapors: (a) canary detecting carbon monoxide in underground mines[11] and (b) soldier detecting residual of mustard gas on the battlefield. Single-output sensors: (c) schematic of one of the first sensors[18] and (d) example of a modern commercially successful sensor. Sensor arrays as a compromise to mitigate poor selectivity of conventional sensors: (e) schematic of operation of the first sensor array[45] and (f) example of a modern sensor array with 65 536 sensors (the size of the die 2.1 cm × 2.1 cm); inset in (f) shows a segment with nine sensor elements having dimensions of 220 μm × 220 μm with 20 μm gap between the electrodes.[48] Multivariable sensors as a new generation of gas and vapor sensors: (g) radio-frequency sensor[72] and (h) photonic sensor.[73] (a) Reprinted with permission from ref. 11. Copyright 2005, RKI Instruments. (c) Reprinted with permission from ref. 18. Copyright 1962, The American Chemical Society. (e) Reprinted with permission from ref. 45. Copyright 1982, Nature Publishing Group. (f) Reprinted with permission from ref. 48. Copyright 2017, Elsevier. (g) Reprinted with permission from ref. 72. Copyright 2013, The Royal Society of Chemistry. (h) Reprinted with permission from ref. 73. Copyright 2015, Nature Publishing Group.

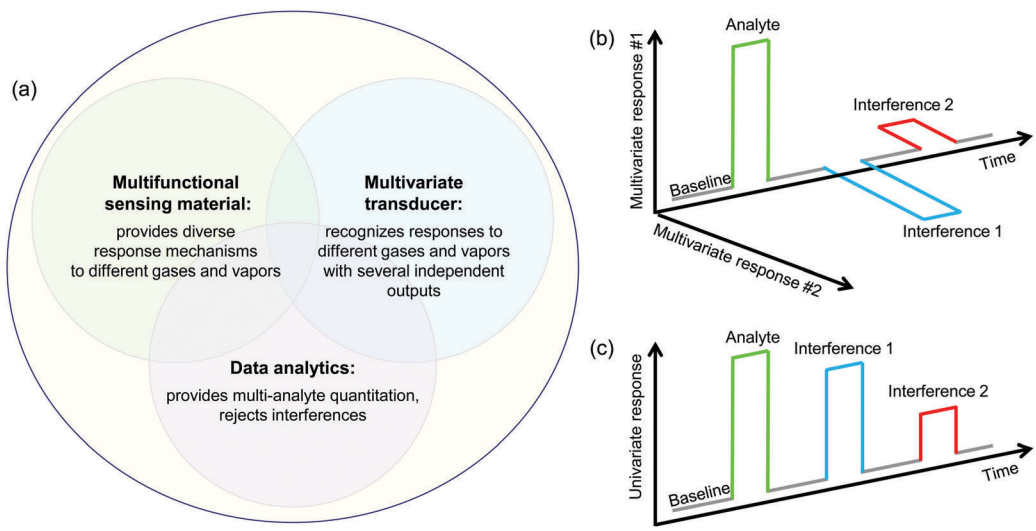

Fig. 2 Multivariable sensors as a new generation of gas and vapor sensors. (a) Design criteria for selective sensing of gas-phase compounds using individual multivariable sensors. (b) New sensing philosophy with multivariable sensors that allows response to interferences but in different directions than the analyte response. (c) Existing sensing approach where a conventional sensor does not differentiate between the analyte and interferences.

new generation sensors. Excellent recent reviews on nanoparticles/nanomaterials for gas and vapor sensing focus on single-output sensors and conventional sensor arrays[49,120–126] and do not analyze opportunities for multivariable sensors. Earlier published reviews on multivariable (also known as high-order or intelligent) sensors[40,42,44,127] do not analyze the diverse response mechanisms and opportunities for MPN materials in multivariable transducers based on different principles and possible solutions for the improvements of stability of these materials.

Thus, to accelerate the multi-disciplinary research in multivariable sensors, this review has six broad goals: (1) to provide critical analysis of design parameters of MPNs for multivariable sensors; (2) to demonstrate the opportunities of matching of MPNs with different transducers to achieve discrimination of different gases and vapors; (3) to highlight recent results on improvement of stability of MPNs for future operation in practical conditions; (4) to discuss insights on development of new generations of MPN-based sensors; (5) to adapt attractive attributes of MPN sensing materials toward development of new types of sensing materials for multivariable sensors; and (6) to unite the fundamental and applied aspects of the design of these MPN-based sensors to solve gas-measurement challenges of the 21st century society.

2. State-of-the-art in design of MPN sensing materials

Metal nanoparticles functionalized with a ligand monolayer is a natural progression of materials science of self-assembled monolayers on gold and other surfaces.[128,129] Ligand-capped metal nanoparticles have been introduced for gas sensing almost twenty years ago[130] demonstrating improvements in vapor-response sensitivity over traditional dielectric polymeric materials by at least one order of magnitude.[131] These functionalized metal nanoparticles were initially termed colloidal metal-insulator metal-ensemble (MIME) clusters,[130] followed by other names such as monolayer-protected clusters (MPCs),[131] monolayer-protected nanoparticles (MPNs),[132] monolayer-capped metal nanoparticles (MCNPs),[133] and thin film-capped metallic nanoparticles (TFCMNPs).[134] The terminology adapted in this review is monolayer-protected nanoparticles (MPNs).

These sensing materials have been used in a variety of single-output sensors including resistors,[47,131,135–140] capacitors,[107,141–143] quartz crystal microbalances,[132,144–146] colorimetric,[147,148] and Schottky-diode sensors.[149] Such individual single-output sensors are non-selective, requiring the use of a traditional sensor array format to achieve needed discrimination between gas-phase compounds.[47,138–140,146,147] The vapor-response mechanisms involve changes in the dielectric constant and/or dimensions of the ligand shell leading to the diverse effects in these sensing films as probed with different types of transducers. Several recent reviews describe single-output measurements using these materials.[150–152]

Typically, MPNs have a spherical shape because of its most straightforward synthetic choice.[130] Cubic MPNs have been demonstrated for resistive sensing with vapor-dependent 2–13-fold improvement in sensitivity over spherical nanoparticles.[133,153] Examples of nanoparticles of spherical and cubic shapes in MPN sensing materials are presented in Fig. 3a and b.[133,154] Numerous other shapes of nanoparticles such as rod-, rectangle-, hexagon-, triangle-, and starlike have been also grown using solution-based chemical routes.[155] However, these shapes have not found yet their applications in MPNs for sensing.

Metals that have been explored in the design of MPN sensing materials include Au,[130] Ag,[147,148] Pt,[133,156,157] Pd,[158–160] Ni,[161] and several types of alloys such as AuAg,[162,163] PdAg,[159] and PdAu.[159] The choice of a particular metal is driven by the ability to functionalize nanoparticles with the desired materials chemistry and by the transduction principle of the resulting sensor. For example, for certain analytes, chemiresistors with Pt nanoparticles have demonstrated 2–8-fold higher sensitivity as compared to Au nanoparticles.[156] Nanoparticles of different metals in MPN sensing materials are illustrated in Fig. 3a (Au[154]), Fig. 3b and c (Pt[133,156]), and Fig. 3d (Pd[160]).

Nanoparticle ligands can be categorized as soft and rigid ligands. Soft ligands change their length as a function of the type and amount of sorbed vapor, leading to the change in spacing between the nanoparticles. Rigid ligands do not appreciably change their length and enhance the effects of analyte-dependent changes of the dielectric constant of the film.[164] The majority of reported nanoparticle ligands for gas and vapor sensors are organic ligands for room-temperature operation. The long-range order of assembled particles is controlled by the thickness of the ligand shell; the improved order is proportional to the thickness of the ligand shell as illustrated in Fig. 3e and f.[165] In addition, biological ligands such as peptides[72] and DNA[166] were also used for expanding the range of detected gas-phase compounds and selectivity of sensors. Examples of particles with such biological ligands are presented in Fig. 3g and h.[72,166]

In situ nano-characterization of the MPN sensing films is critical in understanding of details of their vapor-response and degradation mechanisms. An example of a nano-characterization technique that has been applied *in situ* is wet scanning transmission electron microscopy (Fig. 3i and j[167]) where Au nanoparticles with a hydrophilic (poly(ethylene glycol)-thiol-stabilized) ligand were imaged under dry and hydrated conditions.

A summary of diverse organic and biological ligands utilized with MPNs, associated metal nanoparticles, and corresponding detected gases and vapors using single-output sensors and their arrays is presented in Table 1. This compilation illustrates several important points: (1) a wide variety of explored ligands, (2) the range of detected gas-phase compounds from organic condensable vapors to non-condensable gases, and (3) examples of uses of MPN-based sensors for model analytes and samples of practical interest.

Compared to surface-effect sensing materials (*e.g.* metal oxides, carbon nanotubes, graphene, semiconducting nanowires, porous silicon, *etc.*)[120,121,177,178] organic and biological ligands provide gas and vapor sorption into the bulk of the MPN sensing film and can be tailored to minimize effects from high humidity at

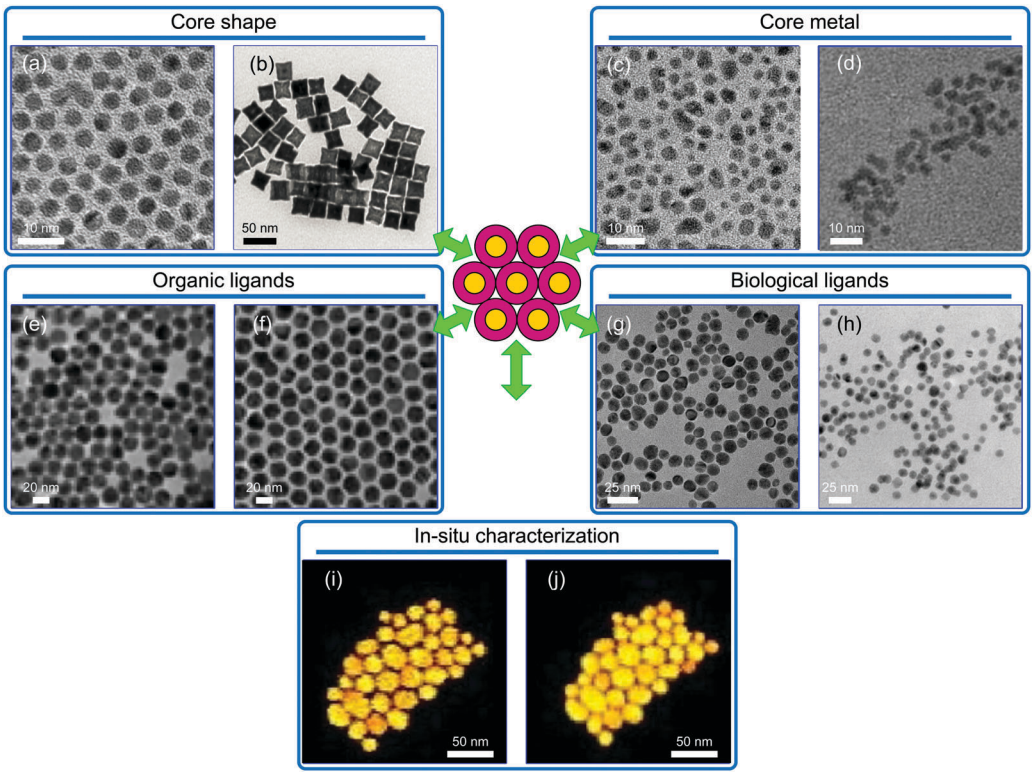

Fig. 3 Building blocks of MPN sensing materials. Examples of shapes of metal core: (a) spherical[154] and (b) cubic.[133] Examples of materials of metal core: (a) Au,[154] (b and c) Pt,[133,156] and (d) Pd.[160] Examples of ligand materials: (e) hexanethiolate,[165] (f) octadecylamine,[165] (g) peptide,[72] and (h) DNA.[166] Example of *in situ* nano-characterization: (i and j) visualization of Au nanoparticles of a drop-cast film of a hydrophilic ligand under hydrated and dry conditions.[167] (a) Reprinted with permission from ref. 154. Copyright 2004, The American Chemical Society. (b) Reprinted with permission from ref. 133. Copyright 2010, The American Chemical Society. (c) Reprinted with permission from ref. 156. Copyright 2004, Elsevier. (d) Reprinted with permission from ref. 160. Copyright 2011, The American Chemical Society. (e and f) Reprinted with permission from ref. 165. Copyright 2016, The American Chemical Society. (g) Reprinted with permission from ref. 72. Copyright 2013, The Royal Society of Chemistry. (h) Reprinted with permission from ref. 166. Copyright 2013, The American Chemical Society. (i and j) Reprinted with permission from ref. 167. Copyright 2016, The American Chemical Society.

realistic ambient conditions. In addition to permanent ligand functionalization of nanoparticles, another method to alter the sensor selectivity involves varying their functionalization *via* vapor-phase thiol place-exchange reactions.[139]

For sensing, functionalized metal nanoparticles have been self-assembled into random or ordered 3-D films with the inter-particle spacing controlled by ligand shell thickness. Such sensing films of MPN nanoparticles have been assembled by numerous methods including spraying,[130,131] drop-casting,[134,169,170] spin-casting,[179] printing,[180] layer-by-layer deposition,[134] self-assembly *via* exchange-crosslinking-precipitation,[162] and drain-to-deposit[181] methods. Gaps between nanoparticles consist of two regions such as a region formed by the ligand and a "region of lower ligand density"[130] formed by the air voids between particles and facilitating rapid diffusion of vapors into and out of the film.

3. Design guidelines for multivariable sensors based on MPN sensing materials

The gas and vapor response mechanisms of MPNs in electrical sensors involve (1) tunneling between metal cores and (2) charge hopping along the atoms of the organic ligand. Electronic conduction in a MPN film is described as:[132,182]

$$\sigma_{el} = \sigma_0 \exp(-\beta\delta)\exp(-E_A/k_BT) \quad (1)$$

where σ_0 is a constant pre-exponential tunneling factor, β is the electron tunneling coefficient, δ is interparticle surface-to-surface separation, k_B is Boltzmann's constant, T is the absolute temperature, and E_A is the tunneling activation energy. Two exponential terms in eqn (1) describe two types of contributions to electronic conductivity of the film. The first exponential term describes electron tunneling between the particles through the dielectric ligand shell. The second exponential term describes the activation energy E_A, required to generate a positive and a negative charged metal core from two initially neutral cores, given by:[132]

$$E_A = (e^2/(8\pi\varepsilon_0\varepsilon_{ligand}r_{core})) \times (1 - (r_{core}/(r_{core} + \delta))) \quad (2)$$

where e is electron charge, ε_0 is the permittivity of vacuum, ε_{ligand} is the dielectric constant of the dielectric ligand medium responsible for gas and vapor sensing, and r_{core} is the radius of each metal core. As shown by eqn (2), the activation energy E_A is inversely proportional to ε_{ligand}, r_{core}, and δ.

Table 1 Examples of MPN-based sensors and arrays for gases and vapors

Class of sensed compounds	Ligand	Type of nanoparticles (NPs)	System details and figures of merit[a]	Ref.
Hydrocarbon, polar aprotic and alcohol vapors	Straight-chain alkanethiols (1-butanethiol, 1-pentanethiol, 1-hexanethiol, 1-heptanethiol, 1-octanethiol, 1-nonanethiol, 1-decanethiol, 1-undecanethiol); branched alkanethiols (2-methyl-1-propanethiol, 2-methyl-1-butanethiol, 3-methyl-1-butanethiol, 1-cylohexanethiol, 2-ethyl-1-hexanethiol); aromatic ligands (1-phenylthiol, 1-naphthalenethiol, 4-biphenylthiol, 2-anthracenethiol, 1,1′,4′,1″-terphenyl-4-thiol); composite ligands (2-phenylethanethiol alone and with naphthalene, biphenyl, anthracene, or terphenyl)	Au NPs, <10 nm diam.	Detection: resistance; design: array of 5–20 sensors; analytics: PCA, LDA, up to 5 PCs	168 and 169
BTEXN volatiles (benzene, toluene, ethylbenzene, *p*-xylene, and naphthalene)	Screened 132 ligands: 1-hexanethiol, 4-nitrophenyl disulphide, benzyl mercaptan, *p*-tolyl disulfide, 4-(trifluoromethoxy)benzyl mercaptan, 1,4-benzenedimethanethiol, 1-thio-D-glucose, 4-methylbenzenethiol, 4-bromobenzenethiol, 4-chlorobenzenethiol, 1-propanethiol, 4-mercaptobenzoic acid, 6,8-thioctic acid, 3-mercaptopropionic acid, thiophenol, 1-butanethiol, 1-pentanethiol, 3,3′-thiodipropionic acid, 1-octanethiol, 1-dodecanethiol, 1,4-butanedithiol, 1,6-hexanedithiol, 1,8-octanedithiol, 1,10-decanedithiol, 4-aminothiophenol, 6-(ferrocenyl)hexanethiol, 3-mercaptohexyl hexanoate, 2-aminothiophenol, *trans*-4,5-dihydroxy-1,2-dithiane, 1-decanethiol, triphenylsilanethiol, 4-mercapto-1-butanol, triisopropylsilanethiol, cyclohexylmercaptan, 6-mercapto-1-hexanol, 1-heptanethiol, 3-amino-5-mercapto-1,2,4-triazole, cyclopentylmercaptan, *p*-terphenyl-4,4″-dithiol, 6-mercaptohexanoic acid, 4-nitrothiophenol, 4-methyl-4-mercaptopentan-2-one, 3-aminothiophenol, 4-mercaptophenylboronic acid, 2-mercaptobenzoxazole, 4-*tert*-butylbenzenethiol, *tert*-dodecanethiol, 4-mercapto-4-methylpentan-2-ol, 4-ethyl-4*H*-1,2,4-triazole-3-thiol, 1-octadecanethiol, hexadecyl mercaptan, 1*H*,1*H*,2*H*,2*H*-perfluorodecanethiol, 3,3,4,4,5,5,6,6,7,7,8,8,8-tridecafluoro-1-octanethiol, 3-mercaptophenylboronic acid, triphenylmethanethiol, 4-fluorothiophenol, 2-mercaptopyridine-3-carboxylic acid, 2-phenylethanethiol, 4-mercaptopyridine, 2-mercaptoisobutyric acid, 3-mercaptobenzoic acid, 4-isopropylbenzenethiol, 4-*tert*-butylbenzyl mercaptan, dithioglycolic acid, thioacetic acid, 3-mercapto-1-hexanol, L-cysteine, bis(4-methoxyphenyl)disulfide, 1,2-ethanedithiol, 2-mercaptobenzimidazole, 3,4-difluorothiophenol, thiourea, 4-methoxybenzylmercaptan, 4-mercaptophenol, trithiocyanuric acid, 4-(trifluoromethyl)-2,3,5,6-tetrafluorothiophenol, thioglycolic acid, biphenyl-4,4′-dithiol, 4-methoxybenzenethiol, mercaptosuccinic acid, 11-mercaptoundecanoic acid, 2-ethylhexanethiol, 2,3,5,6-tetrafluorobenzenethiol, 1,16-hexadecanedithiol, 2-(2-methoxyethoxy)ethanethiol, 1,1′,4′,1″-terphenyl-4-thiol, 2-naphthalenethiol, D-cysteine, 6-mercaptopyridine-3-carboxylic acid, 1-thioglycerol, 2-furanmethanethiol, 4-(3-methoxypropyl)-4*H*-1,2,4-triazole-3-thiol, 3-chloro-1-propanethiol, 4-mercaptophenylacetic acid, 2-(trimethylsilyl)ethanethiol, 2-methyl-1-butanethiol, 4-(mercaptomethyl)benzoic acid, 4-acetamidothiophenol, 2,4-dichlorobenzenethiol, 2-amino-4-chlorobenzenethiol, *N*-acetylcysteamine, 4-bromobenzyl mercaptan, 4-chlorobenzenemethanethiol, 4-fluorobenzyl mercaptan, 3-ethoxythiophenol, 4,4′-bis(mercaptomethyl)biphenyl, 2,5-dichlorobenzenethiol, 3,4-dichlorobenzenethiol, 2-chlorothiophenol, 3-methyl-1-butanethiol, 4-mercaptobutyric acid, 4-bromo-2-fluorobenzylmercaptan, 4-trifluoromethylbenzylmercaptan, 4-chloro-2-fluorobenzylmercaptan, 1-phenylethylmercaptan, 5-[(*e*)-2-phenylvinyl]-4*H*-1,2,4-triazole-3-thiol, 3-(trifluoromethoxy)thiophenol, 3-bromobenzylmercaptan, 2,4,6-trimethylbenzylmercaptan, (4-nitrobenzyl)mercaptan, 1,2-benzenedimethanethiol, 4,4′-dimercaptostilbene, 1-adamantanethiol, 4-(mercaptomethyl)benzoic acid, 2-(5-sulfanyl-4*H*-1,2,4-triazol-3-yl)phenol, benzene-1,3-dithiol, 2-bromothiophenol, 2,4-difluorothiophenol, 2-(butylamino)-ethanethiol, 3-chlorobenzenethiol, 3-bromothiophenol, 2,3-dimercapto-1-propanol	Au NPs, 4–6 nm diam.	Detection: resistance; design: arrays formed with 132 different thiols; analytics: random forest analysis; RMS error: 8–17 $\mu g\ L^{-1}$	170

Table 1 (*continued*)

Class of sensed compounds	Ligand	Type of nanoparticles (NPs)	System details and figures of merit[a]	Ref.
Organic vapors	Poly(propyleneimine) dendrimers, polyphenylene dendrimers	Au NPs, 4 nm diam.	Detection: simultaneous resistance and quartz crystal microbalance	171 and 172
Organic vapors	DNA oligomers: AAA AAA AAA GAG GAG GAA AAG GAG T, TTT TTA CTC CTT TTC CTC CTC TTT T, AAA AAA AAA AAA AAA AAA AAA AAA A, TTT TTT TTT TTT TTT TTT TTT TTT T, CCC CCC CCC CCC CCC CCC CCC CCC C	Au NPs, 10 nm diam.	Detection: resistance; LOD: 32 ppm (toluene), 326 ppm (methanol) 242 ppm (ethanol)	166
Organic vapors	Oleylamine, 11-mercaptoundecanol, 11-mercaptoundecanoic acid, and benzylmercaptan	Cubic Pt NPs, 17 nm side	Detection: resistance; design: array of four sensors; analytics: PCA, 3 PCs; LOD: 160 ppm octane	133
NH_3, CO, toluene	1,9-Nonanedithiol and dodecylamine	Au NPs, 4 nm diam. Pt NPs, 3 nm diam.	Detection: resistance; LOD: $<$100 ppb NH_3	156
NO_2, toluene	4-Methylbenzenethiol, 1-hexanethiol and 1-dodecanethiol	Au NPs, 3.1–3.6 nm diam.	Detection: resistance; LOD: $<$0.5 ppm NO_2	173
CO_2	Poly(ethylene glycol)monomethyl ether, 1,8-octanedithiol, 1,9-nonanedithiol, 1,10-decanedithiol	Au38	Detection: resistance; measurement range: 0–6.5 MPa	174
H_2	Hexanethiolate ligand, followed by further ozone and thermal activation	Pd NPs, 3 nm diam.	Detection: resistance; LOD: 0.11%	158
H_2	Tetraoctylammonium bromide ligand on Pd, PdAg; octylamine and dodecylamine ligands on Pd, PdAg, PdAu	Pd, PdAg, PdAu NPs, 3–7 nm diam.	Detection: resistance; LOD: 0.08–0.11%	159
H_2	Octylamine, hexanethiolate, and mixed monolayers of octylamine and hexanethiolate	Pd NPs, 3 nm diam.	Detection: resistance; LOD: 0.3%	160
Metabolites from bacterial species *Escherichia coli*, *Bacillussubtilis*, *Staphylococcus epidermidis*, and *Enterobacter aerogenes*	1-Hexanethiol, 1-10-decanedithiol, 2-ethylhexanethiol, 1-16-hexadecanedithiol, 3-mercaptohexylhexanoate, 1-heptanethiol	Au NPs, 4–6 nm diam.	Detection: resistance; design: array of 23 sensors analytics: PCA, 2 PCs; LOD: 3.7×10^6 CFU per mL *E. coli*	175
Lung cancer breath	Decanethiol, 11-mercaptoundecanoic acid, 16-mercaptohexadecanoic acid, 3-mercaptopropanoic acid, 1,3-propanedithiol, 1,4-butanedithiol, 1,5-pentanedithiol, 1,6-hexanedithiol	Au NPs, 2 nm diam.	Detection: resistance; design: array of 5–6 sensors; analytics: PCA, 3 PCs; LOD: 20 ppm acetone	138
Ovarian carcinoma from breath	2-Nitro-4-trifluoro-methylbenzenethiol, 4-chlorobenzene-methanethiol, 3-ethoxythiophenol, 4-*tert*-butylbenzenethiol, 2-naphthalenethiol	Au NPs, size not reported	Detection: resistance; design: array of 10 sensors; analytics: discriminant factor analysis, 3 factors	176

[a] Abbreviations: LOD = limit of detection, RMS = root mean square.

Soft ligands of MPNs change their length proportionally to the type and amount of sorbed compound. Film swelling upon analyte exposures causes an increase of film resistance with increased δ, an increase of film mass, and a change in the film viscoelastic properties. These types of effects participate in the gas and vapor response mechanisms of MPNs in electromechanical sensors.

Depending on the dielectric constant of the analyte vapor ε_A, the dielectric constant of the dielectric ligand medium responsible for vapor sensing ε_{ligand} can also either increase or decrease

causing change in electronic conduction (eqn (1) and (2)). Rigid ligands restrain film swelling and boost the effects of analyte-dependent changes of ε_{ligand}.

An exposure to a gas or a vapor affects the effective dielectric constant ε_{eff} of the film/analyte system:[183]

$$\varepsilon_{eff} = \varepsilon_{ligand} + \varphi_A \{(\varepsilon_A - 1) - Q(\varepsilon_{ligand} - 1)\} \quad (3)$$

where Q is swelling factor, ε_A is the dielectric constant of analyte gas or vapor, and φ_A is volume fraction of analyte gas or vapor in the film:

$$\varphi_A = K(M/\rho)(P_A/(RT)) \quad (4)$$

where M and ρ are liquid analyte molar mass and density, respectively, P_A is partial pressure of analyte, R is gas constant, and K is the film/analyte partition coefficient. The partition coefficient K is the ratio of the concentration of the analyte gas or vapor in the sensing film C_s to the concentration of the analyte in the gas phase C_A:[184,185]

$$K = C_s/C_A \quad (5)$$

The charge transport properties of MPNs films are also related to their optical properties and gas and vapor response mechanisms of MPNs in photonic sensors. In particular, variations of film conductivity are accompanied by a variations of the peak position and the width of the plasmon absorption band.[186] For small metal particles, their wavelength-dependent extinction cross section is given by the dipole absorption:[187]

$$\sigma_{abs} = 9(\omega/c)V_o\varepsilon_{eff}^{3/2}\{\varepsilon_2/(\varepsilon_1 + 2\varepsilon_{eff})^2 + \varepsilon_2^2\} \quad (6)$$

where ω is the angular frequency, V_o is the particle volume, and $\varepsilon = \varepsilon_1 + i\varepsilon_2$ is the dielectric constant of the particle.

The surface plasmon peak position of coated nanoparticles assembled on a substrate and exposed to a gas-phase analyte can be described as:[148,188]

$$\lambda_{max}^2 = \lambda_p^2\{(\varepsilon^\infty + 2\varepsilon_{eff}) - 2g(\varepsilon_{eff} - \varepsilon_r)/3\} \quad (7)$$

where λ_{max} is the surface plasmon peak position, λ_p is the bulk metal plasmon wavelength, ε^∞ is the optical dielectric function of the metal, and g is a coefficient corresponding to the volume fraction between core and shell of a monolayer-protected nanoparticle with radius of its metal core r_{core} and radius of its dielectric ligand shell r_{shell} given by:[188]

$$g = \{(r_{core} + r_{shell})^3 - (r_{core})^3\}/(r_{core} + r_{shell})^3 \quad (8)$$

Eqn (1)–(8) describe the fundamentals of analyte-modulated conductivity, dielectric constant, partition coefficient, film thickness, and optical extinction effects in MPNs that form the basis for MPN-based multivariable electrical, electromechanical, and photonic sensors.

Design guidelines for multivariable electrical sensors based on MPN sensing materials to achieve discrimination and quantitation of different gas-phase compounds with a single sensing film include gas- or vapor-induced modulation of interparticle surface-to-surface separation δ and dielectric constant ε_{eff} of the sensing film. Additional contributions include contact resistance and capacitance of the film/electrode and substrate/film interfaces and morphology of the film. In non-resonant multivariable electrical sensors, these variations affect measured resistance R and capacitance C responses of the sensor at different probing frequencies (Fig. 4a). In resonant multivariable electrical sensors, these variations affect measured resistance R, capacitance C, inductance L, quantity factor Q, and other resonant response parameters of the sensor (Fig. 4b).

In multivariable photonic sensors, two broad design concepts are utilized with MPNs such as material- and structure-based designs. Material-based designs comprise of MPNs as sensing units, which are much smaller than the wavelength of interrogation light. The structure-based designs comprise of structural units that are comparable with the wavelength of interrogation light with the MPN material deposited on such structure.

Design guidelines for material-based multivariable photonic sensors include gas- or vapor-induced modulation of interparticle surface-to-surface separation δ and dielectric constant ε_{eff} of the sensing film. In photonic sensors, these variations affect extinction cross section σ_{abs} and plasmon peak position λ_{max} of the sensing film. Combined with the thickness and morphology of the film, these parameters affect the measured spectral reflectance or transmission (Fig. 4c). Design guidelines for structure-based multivariable photonic sensors combine parameters of the material-based photonic sensors with extinction, scattering, and gas- or vapor-induced dimensional changes of the structural units (Fig. 4d).

Examples of capabilities of MPN-based multivariable sensors are presented in Table 2. These examples illustrate several new important aspects as compared to single-output sensors and their arrays (Table 1): (1) multivariable sensors take advantage of ligands earlier screened in single-output sensors but also utilize new ligands with predicted or expected diversity of response mechanisms to different gas-phase compounds, (2) dispersion dimensionality of individual multivariable sensors is similar to that of arrays of single-output sensors, and (3) signal excitation conditions and new data analytics are important to achieve high dispersion dimensionality.

The next sections will detail the fundamental aspects of the performance of multivariable electrical sensors as non-resonant and resonant circuits and photonic sensors as material-based and structure-based sensors. The applied aspects of these multivariable sensors will be demonstrated in quantitation of multiple individual analytes, quantitation of multiple analytes in their mixtures, accurate detection of analytes in the presence of numerous interferences, and rejection of interferences at a several million-fold excess.

4. Non-resonant multivariable electrical sensors

In multivariable electrical sensors, changes in dielectric constant and conductance of the MPN sensing materials as produced by diverse gas-phase compounds, predictably affect several measured outputs of the multivariable sensor at different probing frequencies. Gas- or vapor-modulated changes in resistance R and

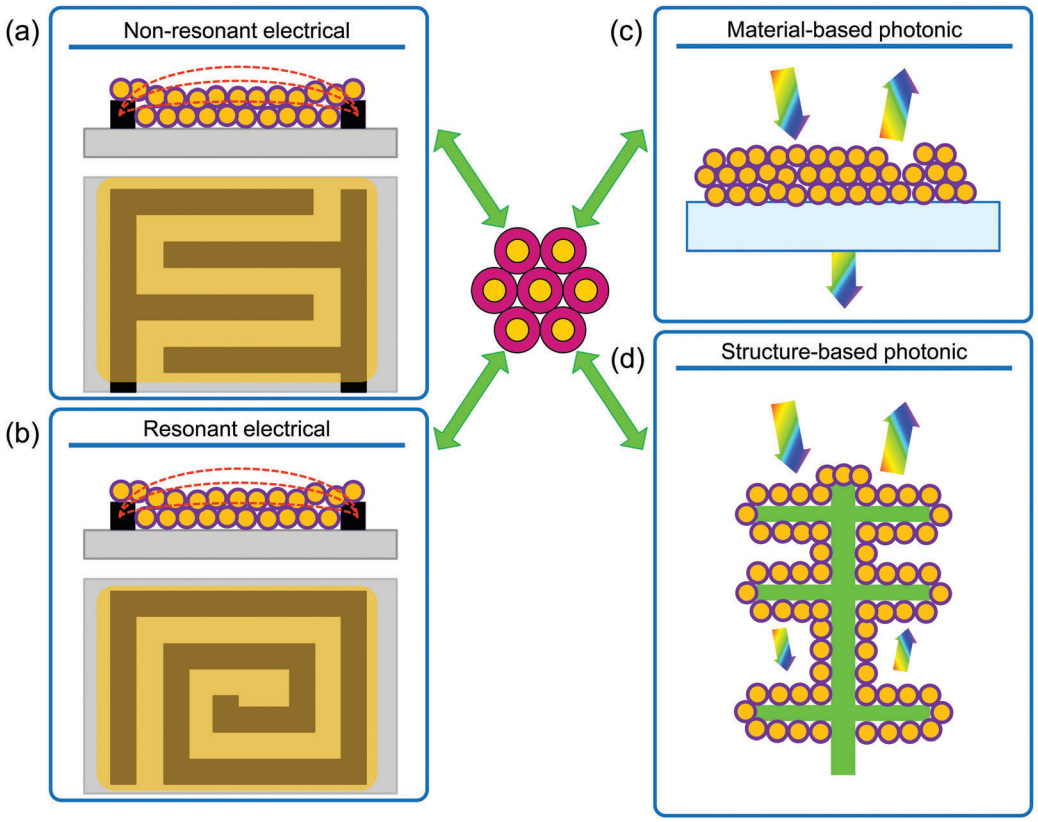

Fig. 4 Design guidelines for multivariable sensors based on MPN sensing materials for discrimination and quantitation of different gases and vapors with a single sensor: (a) non-resonant and (b) resonant electrical sensors, (c) material-based and (d) structure-based photonic sensors.

capacitance C of multivariable electrical sensors can be measured using impedance spectroscopy as illustrated in Fig. 5. Variations of real Z' and imaginary Z'' parts of impedance spectra of an RC circuit that contains MPN sensing material (Fig. 5a and b) can reveal independent changes of R and C and can provide multivariable sensor response. A simplified equivalent circuit of such a sensor with a single RC constant is depicted in the inset of Fig. 5a. Examples of electrodes employed with MPNs are presented in Fig. 5c–f.[39,47,180,192] Electrodes employed for resistance measurements with gaps ranging from 10 nm to several hundreds of micrometers[39,72,130,144,180,193–197] are also applicable for multivariable impedance measurements.

An example of impedance measurements of four model vapors (Fig. 6) illustrates capabilities and opportunities of multivariable impedance sensing with MPN materials.[190] Measurements were performed using a laboratory desktop system over the frequency range from 50 Hz to 1 MHz. A well-known "soft" ligand 1-octanethiol ($C_8H_{17}S$-Au, OCT) was used with its length of $\sim$0.8 nm and dielectric constant ε_{OCT} = 2–3.[198–200] Model vapors such as acetonitrile (ACN), tetrahydrofuran (THF), benzene (BEN), and ethyl acetate (EA) were selected to cover a diverse range of chemical properties. Dynamic Z' and Z'' responses of this single multivariable RC impedance sensor to tested vapors offered a whole suite of diversity as depicted at three exemplary frequencies of 100 Hz, 10 kHz, and 1 MHz (Fig. 6a–f). This diversity can be summarized as three classes such as different relative intensities, opposite directions, and different dynamics of responses. These different responses of the sensing film originate from the diverse effects of vapors on the MPNs sensing material at probed frequencies of the real Z' and imaginary Z'' impedance spectra (Fig. 6g and h). The Nyquist plots of these impedance spectra (Z' *vs.* Z'') shown in Fig. 6i and j reveal an existence of two RC time constants in the equivalent circuit of the sensor over the measured frequency range from 50 Hz to 1 MHz. The Nyquist plots also show that vapors have different effects on RC constants. These effects were resolved by performing PCA on the spectra. The built PCA model showed that the first two PCs provided strong contributions (Fig. 6k) and discriminated well between four vapors at their medium and high concentrations while PC3 had very nonlinear response to concentrations of vapors (Fig. 6l).

In another example with laboratory equipment, a comparison of resistance and capacitance responses of metal nanoparticles capped with a 2-mercapto-benzylalcoholthiol ligand was performed using impedance spectroscopy measurements in two important scenarios such as well-controlled and real-world applications of measurements of exhaled breath.[107] Sensor capacitance response to well-controlled analytes was more stable and had less baseline drift *vs.* resistance response (Fig. 7a). Sensor capacitance response to breath samples of patients also had lower baseline drift *vs.* resistance responses. As expected, the variable levels of humidity in these real-world samples produced

Table 2 Examples of capabilities of MPN-based multivariable sensors

Demonstrated performance[a]	Detection modality	Data analytics	Ligand and type of nanoparticles[b]	Ref.
Discrimination of EtOH, HE, AC, DCM, TOL, THF, and ACN vapors	Non-resonant impedance spectroscopy down to 100 mHz	Determination of ionic and electronic resistance from equivalent circuit model	Ionic ligand on 2.5 nm NPs	189
Discrimination of ACN, THF, BEN, and EA vapors	Non-resonant impedance spectroscopy	PCA, two PCs with strong contributions, PC3 with very nonlinear response to concentrations of vapors	1-Octanethiol on 2–4 nm NPs	190
Discrimination of HE and HEOH vapors and samples of exhaled breath	Non-resonant impedance spectroscopy	Determination of resistance and capacitance from equivalent circuit model	2-Mercapto-benzylalcoholthiol on 3–5 nm NPs	107
Detection of volatile metabolites of biological CHO cells in cell culture	Non-resonant impedance spectroscopy	Raw responses at two selected frequencies; PCA, two PCs	1-Octanethiol on 2–4 nm NPs	191
Discrimination of ACN, THF, BEN, and EA vapors	Resonant impedance spectroscopy	PCA, three PCs with strong contributions	1-Octanethiol on 2–4 nm NPs	190
Rejection of high levels of water vapor interference	Resonant impedance spectroscopy	PCA, two PCs; toluene detection: rejected humidity at ~3000-fold overloading, 1-nonanol detection: rejected humidity at ~2 000 000-fold overloading	1-Octanethiol on 2–4 nm NPs	80 and 88
Discrimination between vapors with similar dielectric constants	Resonant impedance spectroscopy	PCA, two PCs; discrimination between DCM (ε_r = 9.1) and MeS (ε_r = 9.0)	A3 peptide AYSSGAPPMPPF on 8–12 nm NPs	72
Discrimination between vapors with similar dielectric constants	Resonant impedance spectroscopy; excitation: at −10 and 0 dBm power levels	PCA, two PCs; discrimination between PA, SAH, and PEN (ε_r = 13.9–14.5)	1-Octanethiol on 2–4 nm NPs	80
Discrimination of complex aromas from seven common teas	Resonant impedance spectroscopy	PCA, four PCs	1-Mercapto-(triethylene glycol)methyl ether on 3.5–5.5 nm NPs	190
Quantitation of H_2O, MeS, SAH, and ACN vapors in binary, ternary, and quaternary mixtures	Resonant impedance spectroscopy	Classification using SVM followed by quantitation by PCR	1-Octanethiol on 2–4 nm NPs	79
Discrimination of TOL and HEP vapors	Two-wavelength reflected light measurements	Wavelength selection at the opposite sides of plasmonic band	1-Octanethiol on 4.3 ± 0.9 nm NPs	74
Discrimination of individual vapors H_2O, MeS, THF, DMF, EA, and BEN and mixtures of EA and BEN	White light reflected light measurements	PCA, two PCs	1-Mercapto-(triethylene glycol)methyl ether on 3.5–5.5 nm NPs	109
Discrimination of PCE, TOL, OCT, BAC, MEK, and IPA vapors	Three-wavelength reflected light measurements	Wavelength selection across plasmonic band, PCA, two PCs	6-Phenoxyhexane-1-thiol on 4-nm NPs, 1-octanethiol on 4-nm NP, dithianate on 40 nm NPs	76
Discrimination of vapors of the first nine linear alcohols of their homologous series and H_2O	White light reflected light measurements of functionalized *Morpho* nanostructures	PCA for dimensionality reduction followed by LDA for vapor classification and followed by non-linear PCR for quantitation	1-Octanethiol on 2–4 nm NPs	191

[a] Abbreviations of vapors: acetone (AC), acetonitrile (ACN), benzene (BEN), 2-butanone (MEK), butyl acetate (BAC), dichloromethane (DCM), dimethylformamide (DMF), ethanol (EtOH), ethyl acetate (EA), heptane (HEP), hexane (HE), hexanol (HEOH), methyl salicylate (MeS), *n*-octane (OCT), paraldehyde (PA), 1-pentanol (PEN), 2-propanol (IPA), salicylaldehyde (SAH), tetrachloroethylene (PCE), tetrahydrofuran (THF), toluene (TOL), and water (H_2O). [b] All reported here nanoparticles were spherical Au nanoparticles.

more significant baseline offsets of capacitance *vs.* resistance responses (Fig. 7b).

Measurements of impedance spectra down to 100 mHz allowed identification of new mechanisms for multivariable sensing that utilize ion and electron transport processes in ionic ligand-functionalized gold nanoparticles.[189] When an alkane ligand was synthesized with a positively charged group at its head and a mobile negative counter ion, the ionic R_{ionic} and electronic $R_{electron}$ resistance values of such MPNs were different and varied by several orders of magnitude upon exposure to diverse vapors (Fig. 8a). The values and relative magnitudes of R_{ionic} and $R_{electron}$ can be used for discrimination of vapors (Fig. 8b). This diversity of R_{ionic} and $R_{electron}$ responses was found to be dependent not only on the vapor-induced change in interparticle distance and the dielectric environment of the MPN film but also on the interplay between ion and electron transport, the equilibrium between the absorbed and free vapor molecules, and the vapor-induced ion mobility.

With the goal of developing field deployable, unobtrusive, low power sensor systems, application specific integrated circuits (ASICs) recently were implemented to replace desktop and fieldable sensor readers fabricated from discrete components.

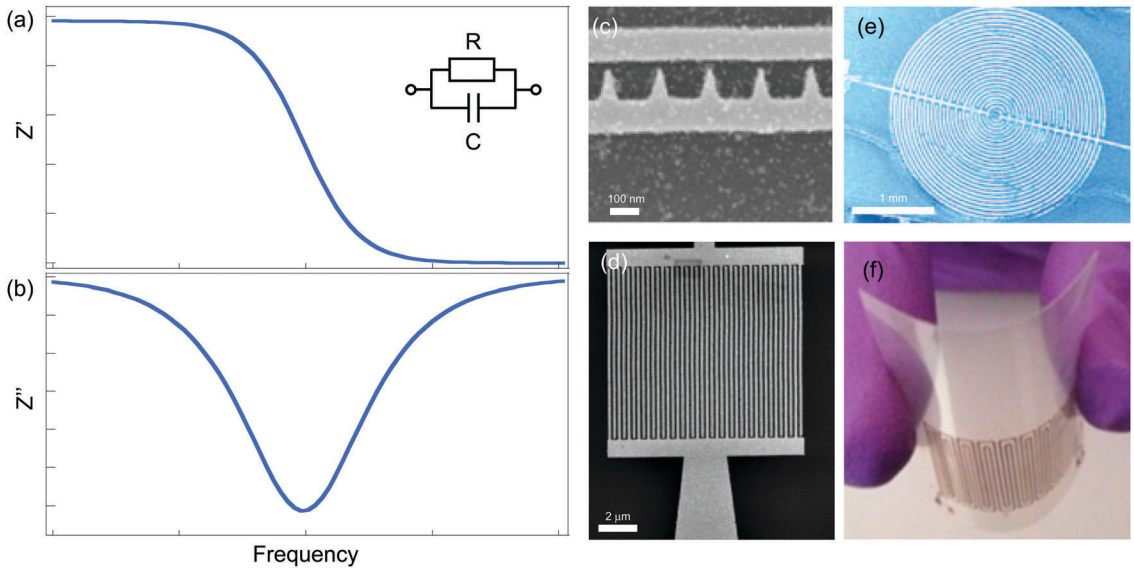

Fig. 5 Electrical measurements of MPN sensing materials using multivariable non-resonant impedance sensors. (a) Real Z' and (b) imaginary Z'' parts of impedance spectra, inset in (a) shows a simplified equivalent circuit with one RC constant with resistance R and capacitance C of the circuit. Examples of electrode structures employed with MPNs: (c) tooth electrodes with 50 nm gaps,[39] (d) interdigital electrodes with 100 nm gaps arranged in a square pattern,[192] (e) interdigital electrodes with 20 μm gaps arranged in a circular pattern,[47] (f) large-area electrodes with 90 μm gaps on a flexible substrate.[180] (c) Reprinted with permission from ref. 39. Copyright 2016, The American Chemical Society. (d) Reprinted with permission from ref. 192. Copyright 2009, IEEE. (e) Reprinted with permission from ref. 47. Copyright 2009, Nature Publishing Group. (f) Reprinted with permission from ref. 180. Copyright 2015, The American Chemical Society.

Such approach reduces the needed power, size, and cost of the sensor readers by several orders of magnitude as illustrated in Fig. 9.[201] These ASIC-based sensor readers allow implementations of multivariable sensors in their wearable and mobile formats.[202,203]

Recently, an ASIC-based impedance analyzer was implemented to measure effects of diverse vapors on a MPN film.[112] This impedance analyzer operated over the frequency range from 1 kHz to 100 kHz, had $<$100 mW power consumption, and had dimensions of only $\sim$1 cm $\times$ 1 cm $\times$ 0.2 cm. Three model vapors (water, toluene, and ethyl acetate) produced diverse Z' and Z'' responses of the multivariable sensor, for example as depicted in Fig. 10a–c at three representative frequencies such as 10 kHz, 35 kHz, and 100 kHz. These results demonstrated that ASIC-based measurements of outputs at different frequencies from this sensor provided desired diverse responses for differentiation of vapors. This response diversity was visualized using a scores plot of a developed PCA model as a function of time (Fig. 10d), experimentally validating sensing philosophy with multivariable sensors that brings response to diverse vapors into different response directions (Fig. 2b). The steady-state responses of the sensor were also processed using PCA (Fig. 10e), illustrating an improvement in the PC2 contributions.

Besides working with model vapors and their mixtures, discrimination of complex aromas has been also recently achieved using individual multivariable MPN-based sensors. In one application example, headspace atmosphere of a biopharmaceutical biological cell growth reaction was measured. Biopharmaceutical cell culture media have numerous nutrients to support growth of biological cells in biopharmaceutical cell culture production. During their growth, biological cells excrete a variety of metabolic products into the cell culture medium. Some of these metabolic products are small volatile molecules that partition into the headspace of a bioreactor. The level of these volatiles serves as indication of biological cell growth process. Because the headspace of bioreactor had relative humidity approaching 100%, the sensor should not be saturated with the high humidity but instead should be able to detect the presence of required volatile metabolites. Thus, gold nanoparticles with a hydrophobic 1-octanethiol ligand were utilized as a sensing material. Fig. 11 illustrates results of replicate measurements of the headspace of a biological cell culture medium and a medium with Chinese hamster ovary (CHO) cells. Measurements with this sensor were performed over the frequency range from 5 Hz to 15 MHz. Exemplary responses are illustrated in Fig. 11a–h. While sensor Z' and Z'' responses at some frequencies did not discriminate between high-humidity headspace without and with CHO cells (*e.g.* Fig. 11a, b, d and f), other frequencies were more appropriate for such discrimination (Fig. 11c and e). This developed sensor discriminated well between cell cultures without and with CHO cells using a developed PCA model based on whole measured impedance spectra (Fig. 11g–i) or using raw responses of the sensor at selected frequencies (Fig. 11e, f and j). Such capability of the individual multivariable sensor was competing with sensor arrays for the detection of metabolic volatile products from biological organisms.[175,204]

5. Resonant multivariable electrical sensors

Adding an inductor L to an electrical RC circuit provides an inductor–capacitor–resistor (LCR) resonator where vapor-modulated changes in resistance R and capacitance C of

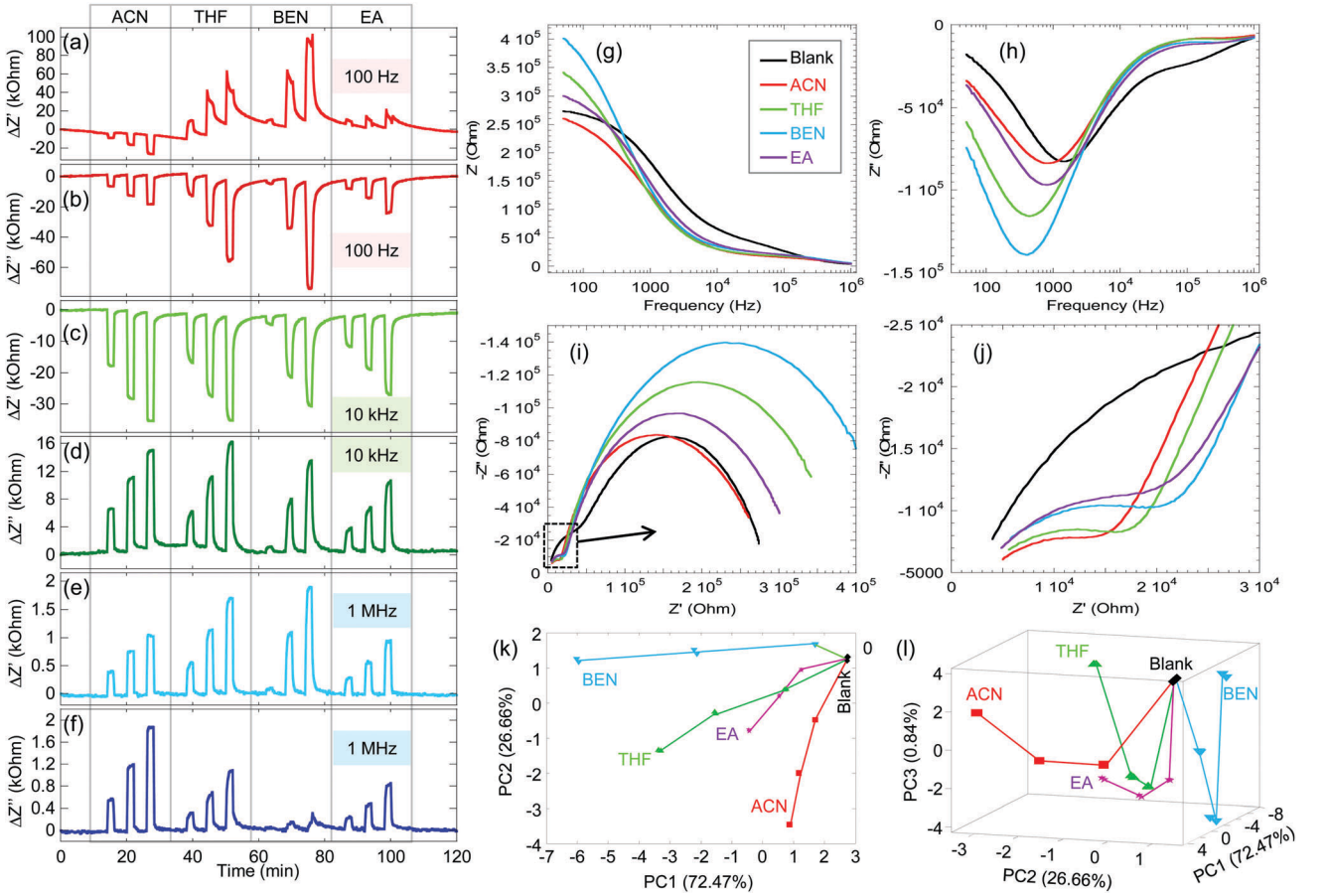

Fig. 6 Measurements of four model vapors using a multivariable non-resonant impedance sensor with 1-octanethiol-capped gold nanoparticles. Vapors: acetonitrile (ACN), tetrahydrofuran (THF), benzene (BEN), and ethyl acetate (EA). (a–f) Dynamic responses Z' and Z'' of the sensor upon exposures to four vapors at their three concentrations and illustrated at three representative frequencies of 100 Hz, 10 kHz, and 1 MHz, respectively. (g and h) Real Z' and imaginary Z'' impedance spectra, respectively upon exposure to a blank and to the highest tested concentrations of four vapors. (i and j) The Nyquist plots of Z' *vs.* Z'' reveal existence of two *RC* time constants and effects of different vapors on *RC* constants. The dotted-line region of the Nyquist plots in (i) is zoomed-in in (j). (k and l) Scores plots of PC1 *vs.* PC2 and PC1 *vs.* PC2 *vs.* PC3 of the developed PCA model, respectively.[190] Reprinted with permission from ref. 190. Copyright 2017, IEEE.

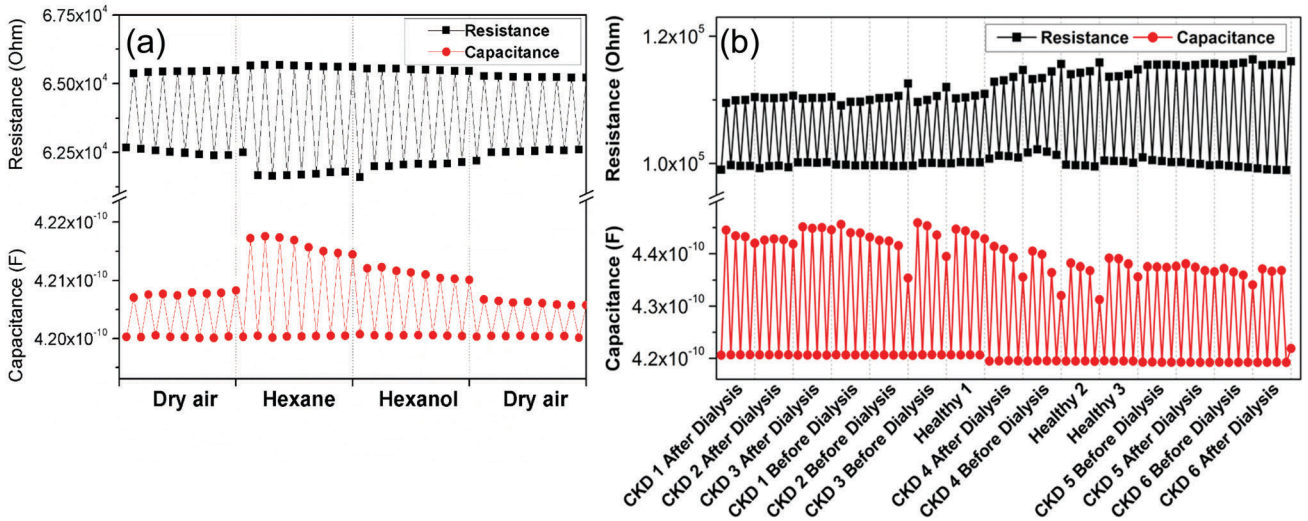

Fig. 7 Comparison of resistance and capacitance responses of 2-mercapto-benzylalcoholthiol-capped gold nanoparticles upon exposure to different volatiles. (a) Control experiment of exposures to dry air and to hexane and hexanol as two model volatiles. (b) Exposures to 15 breath samples obtained over a period of ~1 month.[107] Reprinted with permission from ref. 107. Copyright 2011, The American Chemical Society.

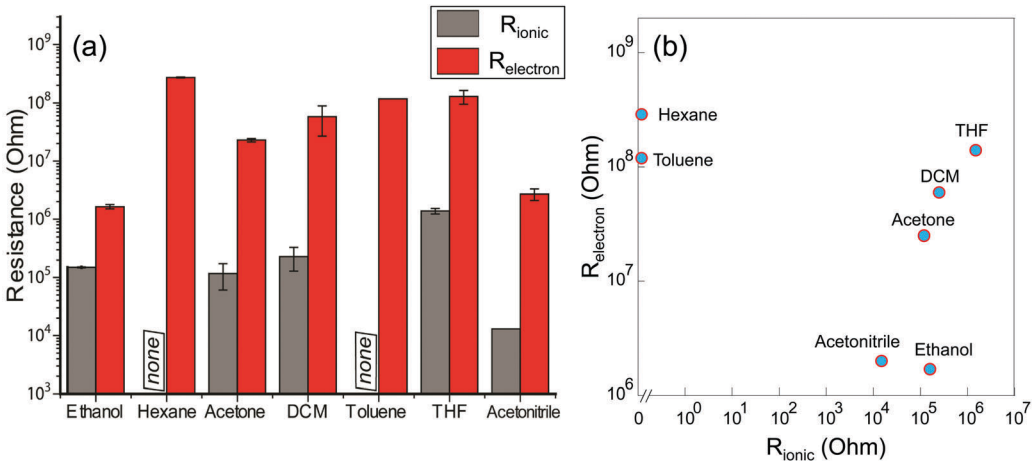

Fig. 8 Exploration of ion and electron transport processes of ionic ligand-functionalized gold nanoparticles using impedance spectroscopy down to 100 mHz as new mechanisms for multivariable sensing. (a) Ionic R_{ionic} and electronic $R_{electron}$ resistance of the sensing film upon exposure to diverse vapors, (b) Discrimination of vapors using diversity of R_{ionic} and $R_{electron}$ responses.[189] Reprinted with permission from ref. 189. Copyright 2015, Wiley-VCH.

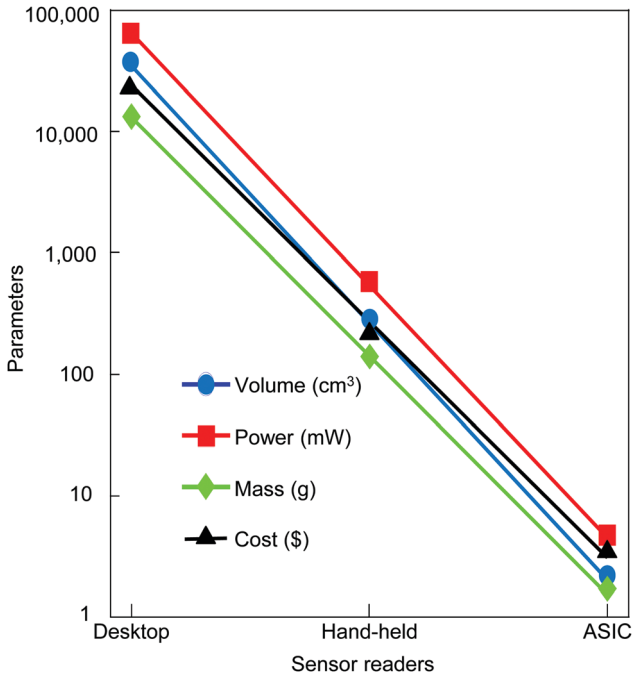

Fig. 9 Evolution of sensor readers for multivariable impedance sensors from desktop to hand-held and to ASIC-based readers in wearable and mobile formats.[201]

multivariable electrical sensors can be measured in a resonant circuit configuration as illustrated in Fig. 12. Variations of real Z' and imaginary Z'' parts of resonance impedance spectra of an LCR sensor that contains MPN sensing material (Fig. 12a and b) can reveal independent changes of R and C and provide multivariable sensor response. A simplified equivalent circuit of such a sensor with a single RC constant is depicted in the inset of Fig. 12a. Electrodes employed with MPNs in non-resonant sensor configurations (Fig. 5c–f) can be also applied in resonant sensors as RC transducers by connecting an appropriate inductor. An example of such electrode is presented in Fig. 12c.[72] Coiled electrodes simultaneously serve as inductors resulting in LCR transducers in the radio-frequency range with examples illustrated in Fig. 12d and e.[201,205] Split-ring resonators are LCR transducers in the microwave frequency range with an example shown in Fig. 12f.[206]

Application of resonant structures provides the ability to enhance sensitivity and selectivity of MPN sensors. Fig. 13 illustrates an example of measurements of same four vapors shown in Fig. 6 but using a single multivariable LCR impedance sensor. The sensing IDE coated with 1-octanethiol that has been applied for measurements in Fig. 6 has been coupled to a coil to form an LCR sensor and was wirelessly interrogated.[190] Dynamic Z' and Z'' responses of this single multivariable LCR sensor to tested vapors are presented as F_p, F_1, F_2, Z_p, Z_1, and Z_2 responses in Fig. 13a–f. The definitions of F_p, F_1, F_2, Z_p, Z_1, and Z_2 responses are provided in Fig. 12a and b. Similarly to the non-resonant responses illustrated in Fig. 6, the diversity of the LCR sensor can be summarized as three classes such as different relative intensities, opposite directions, and different dynamics of responses. These different responses of the 1-octanethiol sensing film when probed with an LCR transducer originate from the diverse effects of vapors on the LCR circuit components and are summarized in unique variations in the measured real Z' and imaginary Z'' resonance impedance spectra (Fig. 13g and h). The Nyquist plots of these resonant impedance spectra (not shown) revealed a single RC time constant in the equivalent circuit of the sensor over the measured frequency range from 27 MHz to 37 MHz. The built PCA model showed that the first two PCs provided strong vapor-dependent contributions (Fig. 13i) and discriminated well between four vapors at their all tested concentrations. The PC3 also provided contributions correlated with concentrations of vapors (Fig. 13j). Thus, the resonant sensor (Fig. 13) demonstrated an improved vapor resolution into three dimensions of the PCA scores plot as compared to the non-resonant sensor (Fig. 6).

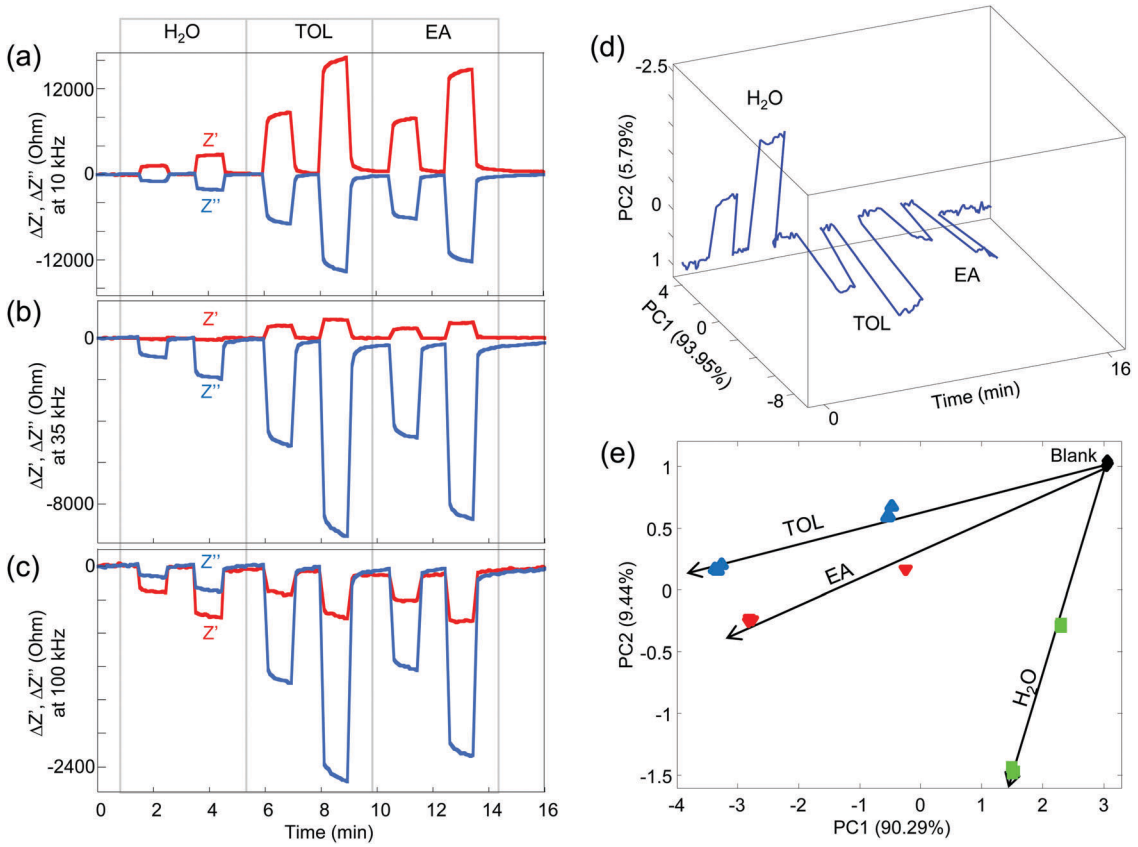

Fig. 10 Demonstration of ASIC-based multivariable sensing using 1-octanethiol-capped gold nanoparticles on a non-resonant impedance sensor and three model vapors (water (H_2O), toluene (TOL), and ethyl acetate (EA)) at their two concentrations. (a–c) Diverse Z' and Z'' sensor responses at 10 kHz, 35 kHz, and 100 kHz, respectively. (d) Visualization of response diversity using a scores plot of a PCA model of dynamic data. (e) Visualization of response diversity using a scores plot of a PCA model of steady-state data.[112]

The philosophy of multivariable sensing coupled with MPN sensing materials allowed straightforward rejection of interferences in mixtures of vapors. For example, mixtures of toluene and water vapors at their different ratios were measured using 1-octanethiol-capped metal nanoparticles on a resonant structure. The multivariate data analysis, as shown in a PCA scores plot *versus* experimental time (see Fig. 14a), illustrated different directions of the sensor response to toluene and water vapors.[102] Critical to the sensor performance, the sensing material applied onto the resonant structure had the same magnitude of response to the model analyte vapor in the presence of different humidity levels.[88] The sensor rejected humidity effect at a ~3000-fold overloading when calculated as the ratio of the highest tested water vapor concentration (40% RH = 12 000 ppm) to the resolution of detection of toluene concentration. Similar experiments and data analysis were performed with 1-nonanol and water vapors using 1-octanethiol-capped metal nanoparticles on a resonant structure but with the experimental ability to reach 75% RH in vapor mixtures (Fig. 14b). The sensor rejected humidity effect at a 2 000 000-fold overloading. Such rejection of interferences with a single sensor as schematically outlined in Fig. 2b and experimentally validated in Fig. 14 is one of the key performance characteristics of the developed individual multivariable sensors.

Discrimination between individual vapors of the similar dielectric constants has been also demonstrated using MPN sensing materials coupled with resonant LCR sensors. These advances have been achieved using two approaches – by using new capping ligands and by using new sensor-excitation conditions.

In the first approach, a biological capping ligand was used (Fig. 15).[72] The capping ligand was A3 peptide AYSSGAPPMPPF. As model analytes, toxic vapors and chemical warfare agent simulants, such as acetonitrile (ACN), dichloromethane (DCM), and methyl salicylate (MeS) were used with an added background of water vapor. Even through DCM has a dielectric constant $\varepsilon_r = 9.1$ which is close to that of MeS ($\varepsilon_r = 9.0$), direction of sensor response to DCM was opposite in comparison to response to MeS vapor (Fig. 15a and b). However, MeS was much bulkier in comparison to DCM and therefore was likely to affect the rigidity of the ligand differently as reflected in measured resonant spectral response. Results of multivariate analysis (Fig. 15c) illustrated the discrimination ability provided by this single A3-Au nanoparticle material. This new type of sensing materials can provide numerous opportunities for tailoring the vapor response selectivity based on the diversity of the amino acids composition of the peptides, and by the modulation of the nature of peptide–nanoparticle interaction through designed combinations of hydrophobic and hydrophilic amino acids.

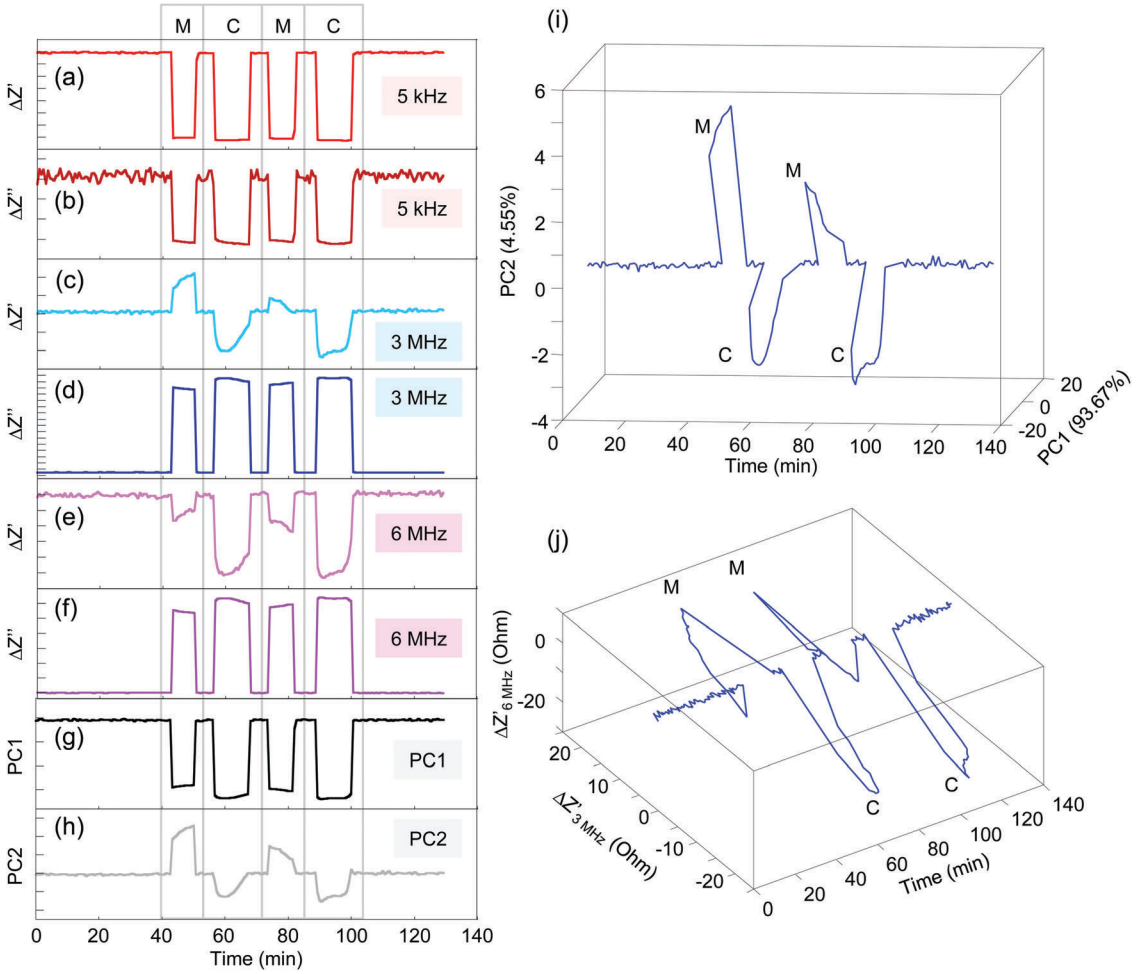

Fig. 11 Headspace measurements of a biological cell culture medium (M) and a medium with CHO cells (C) using a multivariable non-resonant impedance sensor with 1-octanethiol-capped gold nanoparticles. Responses of the real $\Delta Z'$ and imaginary $\Delta Z''$ impedance at representative frequencies as a function of experimental time: (a and b) 5 kHz, (c and d) 3 MHz, and (e and f) 6 MHz. Results of the developed PCA model: (g and h) PC1 and PC2, respectively as a function of experimental time and (i) PC1 *vs.* PC2 as a function of experimental time. For comparison, (j) illustrates $\Delta Z'$ at 3 MHz *vs.* $\Delta Z'$ at 6 MHz as a function of experimental time.

Acceptable response of the peptide-capped Au nanoparticles to target vapors only in the presence of humidity indicated that the peptides needed to be humidity-activated to exhibit the response to target vapors. Humidifying of tested gas streams is also common when using other biomolecular receptors.[166,207]

In the second approach, the sensor selectivity was controlled by excitation of an integrated circuit (IC) chip that was a part of the sensor at different power levels.[80] Such sensor was constructed using a passive radio frequency identification (RFID) tag normally operating at 13.56 MHz, connecting a sensing interdigital chip to the RFID antenna coil, and performing measurements with a wireless proximity readout. A sensing film made of 1-octanethiol-capped Au nanoparticles, was applied onto a sensing interdigital chip by drop casting. Different power levels applied to the sensor caused spectral distortions of the resonance spectra affecting differently the resonant and anti-resonant portions of the spectra. The power of operation of the RFID sensor was controlled from −10 dBm to 0 dBm. Discrimination between vapors of similar dielectric constants was demonstrated using three model vapors: 1-pentanol, paraldehyde, and salicylaldehyde with a range of dielectric constants of 14.5–13.9 (20–25 °C). Exemplary responses of the sensor at two power modulation levels are compared in Fig. 16a and b illustrating the change of the response pattern. The scores plots at two power levels (Fig. 16c and d) illustrate the desired improvement in sensor resolution of vapors at a carefully selected power level. This achievement adds a new independent variable toward higher sensor response dimensionality that can be used not only with MPN but also with other sensing materials.

Discrimination of complex aromas from numerous teas has been recently demonstrated using individual multivariable resonant MPN-based sensors (Fig. 17).[190] Bags of different types of teas were kept in jars to generate aromas in the jag headspace filled with ambient lab air (relative humidity ~40%). Gold nanoparticles were functionalized with a soft ligand such as 1-mercapto-(triethylene glycol) methyl ether ($C_7H_{15}O_3S$-Au, MTE). This ligand was chosen because of its amphiphilic properties to respond to both polar and nonpolar vapors. The length of the

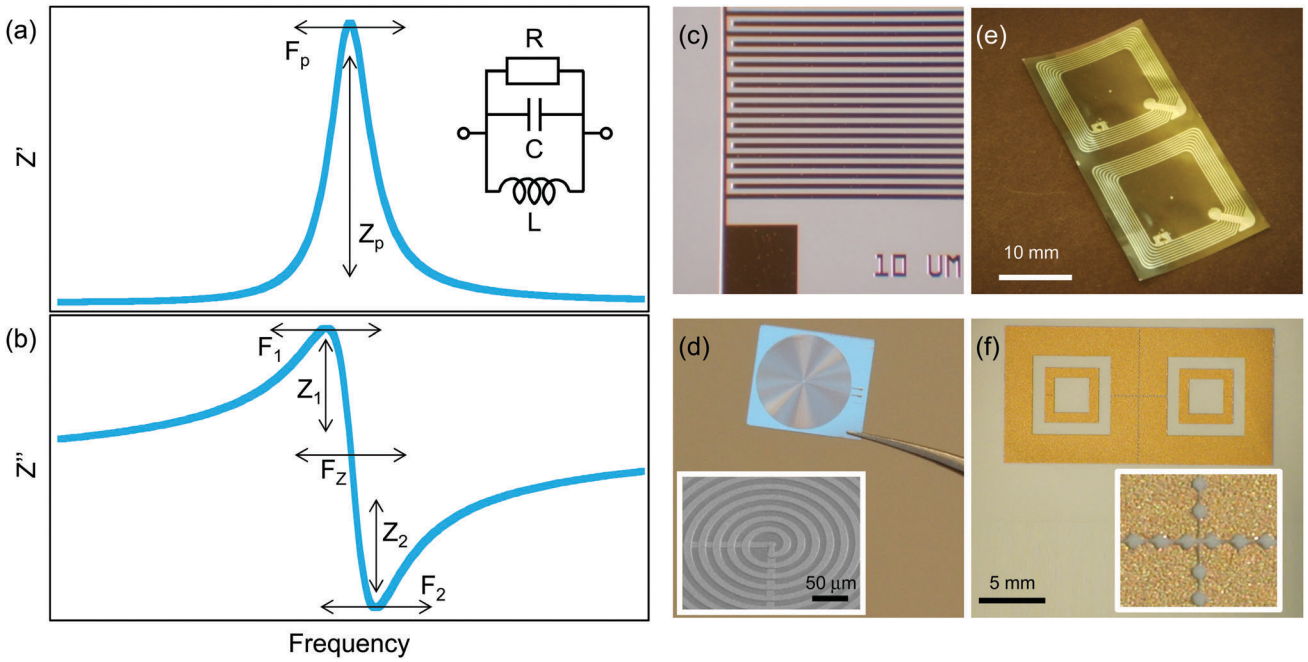

Fig. 12 Electrical measurements of MPN sensing materials using multivariable resonant impedance sensors. (a) Real Z' and (b) imaginary Z'' parts of impedance spectra, inset in (a) shows an equivalent *LCR* circuit with one *RC* constant with resistance *R*, capacitance *C*, and inductance *L* of the circuit. Multivariable measurements can be done of the Z' and Z'' spectra or their calculated parameters such as frequency F_p and magnitude Z_p of Z' spectrum, the resonant F_1 and antiresonant F_2 frequencies and zero-crossing frequency F_Z of Z'' spectrum, and impedance magnitudes Z_1 and Z_2 of Z'' spectrum. Other spectral parameters may be also calculated, *e.g.*, quality factor Q of resonance ($Q = F_p/\Delta f$, where Δf is the full width at half maximum). Examples of electrodes employed in *LCR* circuits with MPNs: (c) interdigital electrodes with 10 μm gaps arranged in a square pattern,[72] (d) coiled electrodes with 10 μm gaps,[201] (e) coiled electrodes with 270 μm gaps of a conventional RFID tag converted into a multivariable sensor,[205] and (f) patterned electrodes with 25/150 μm gaps (smallest/largest gaps) of a split-ring resonator.[206] (c) Reprinted with permission from ref. 72. Copyright 2013, The Royal Society of Chemistry. (e) Reprinted with permission from ref. 205. Copyright 2012, The American Chemical Society.

MTE ligand on the surface of nanoparticles in vacuum has been estimated to be ~1.5 nm.[208] Different parts of the ligand chain can be considered with their respective dielectric constants.[209] The triethylene glycol (TEG) chains have dielectric constant $\varepsilon_{TEG} = 23.69$, while the methyl ether (ME) groups have a much lower dielectric constant $\varepsilon_{ME} = 5.0$. Results presented in Fig. 17a–f illustrate diversity of F_p, F_1, F_2, F_Z, Z_p, and Q responses of the resonant sensor upon exposure to these complex volatile patterns. This diversity of individual responses of the multivariable sensor resulted in the PCA-based discrimination of volatiles patterns from these tested teas using four principal components as illustrated in Fig. 17g and h. Thus, in addition to discrimination of odors from the cell culture media with and without living biological cells using a non-resonant sensor (Fig. 11), an individual multivariable resonant sensor had high resolution of tea aromas competing with sensor arrays.[210–212]

In data analytics with multivariable sensors, multivariate statistical and machine learning methodologies are expanding their applicability not only for pattern recognition, but also for quantitative analysis of responses of multivariable sensors. It was recently demonstrated that binary, ternary, and even quaternary mixtures of model analytes were resolved and individual vapors in these mixtures were quantified with a single sensor. To achieve this attractive goal, SVM classification was performed to correctly determine types of vapors followed by PCR quantitation to determine concentrations of each vapor (Fig. 18).[79]

6. Material-based multivariable photonic sensors

Multivariable photonic sensors that utilize material-based designs comprise of units that are much smaller than the wavelength of interrogation light. These units are MPN sensing materials that exhibit plasmonic properties affected by gas-phase compounds. Fig. 19 illustrates examples of such materials that change their optical properties upon exposure to volatiles.[109,167] Visual observations capture color changes of macroscopic films of Au nanoparticles functionalized with mercapto-poly(ethylene glycol) (Fig. 19a and b) and MTE (Fig. 19c and d) ligands. Optical microscopy (Fig. 19e and f) illustrates that films can form color-changing microscopic islands of assembled nanoparticles. In multivariable material-based multivariable photonic sensors, not only the color change (wavelength shift) is of importance but also other optical parameters (extinction and band broadening) that lead to the multivariable sensor response (see Section 3).

In one study, two model vapors such as toluene and heptane were discriminated using a single sensing film of 1-octanethiol-capped Au nanoparticles.[74] Swelling of the sensing film dominated

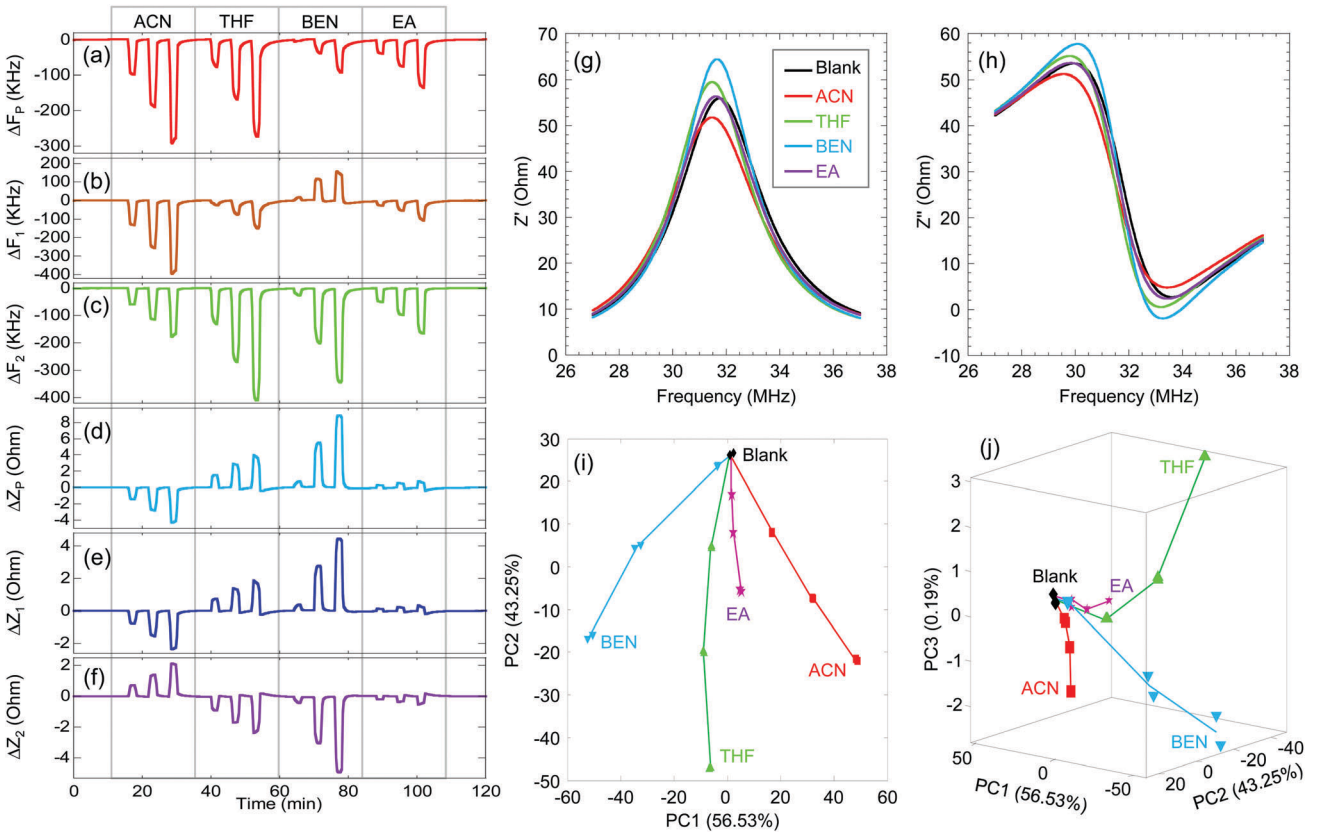

Fig. 13 Measurements of four model vapors (ACN, THF, BEN, and EA) using a multivariable resonant impedance sensor with 1-octanethiol-capped gold nanoparticles. (a–f) Dynamic responses F_p, F_1, F_2, Z_p, Z_1, and Z_2 of the sensor upon exposures to four vapors at their three concentrations. (g and h) Real Z' and imaginary Z'' resonance impedance spectra, respectively upon exposure to a blank and to the highest tested concentrations of four vapors. (i and j) Scores plots of PC1 *vs.* PC2 and PC1 *vs.* PC2 *vs.* PC3 of the developed PCA model, respectively.[190] Reprinted with permission from ref. 190. Copyright 2017, IEEE.

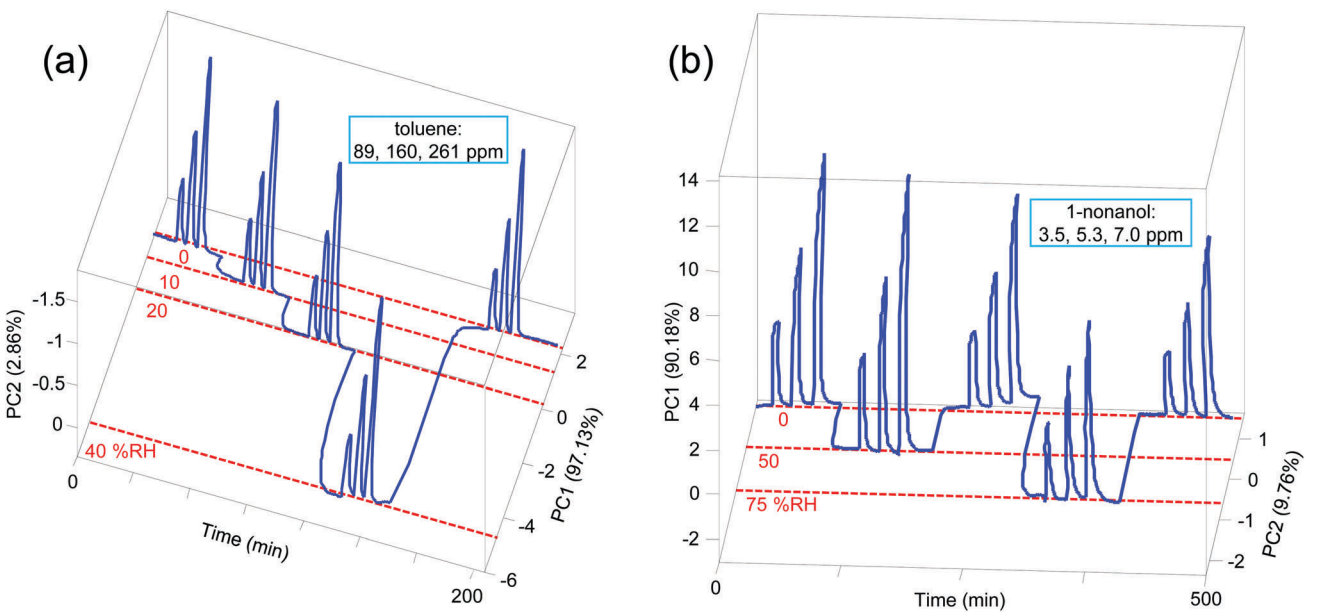

Fig. 14 Demonstration of humidity-independent operation using multivariable resonant impedance sensors. (a) Plot of PC1 *vs.* PC2 *vs.* time illustrating sensor selectivity in detection of toluene as a model vapor with a relatively high vapor pressure. (a) Plot of PC1 *vs.* PC2 *vs.* time illustrating sensor selectivity in detection of 1-nonanol as a model vapor with a relatively low vapor pressure. Sensing material was 1-octanethiol-capped gold nanoparticles.[80,88] (a) Reprinted with permission from ref. 88. Copyright 2012, Elsevier.

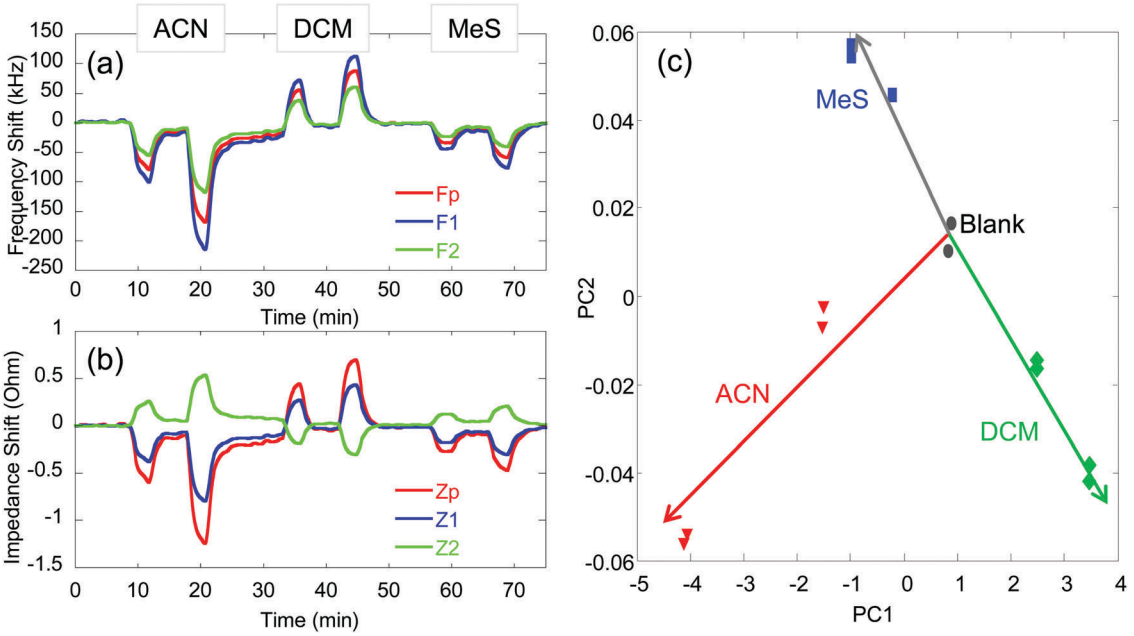

Fig. 15 Discrimination of individual vapors of similar dielectric constants using a multivariable resonant impedance sensor with A3 peptide-capped gold nanoparticles. (a) Sensor responses F_p, F_1, and F_2; (b) sensor responses Z_p, Z_1, and Z_2. (c) Scores plot of a PCA model of a sensor response with replicate (n = 2) data points for two concentrations of vapors such as acetonitrile (ACN), dichloromethane (DCM), and methyl salicylate (MeS).[72] Reprinted with permission from ref. 72. Copyright 2013, The Royal Society of Chemistry.

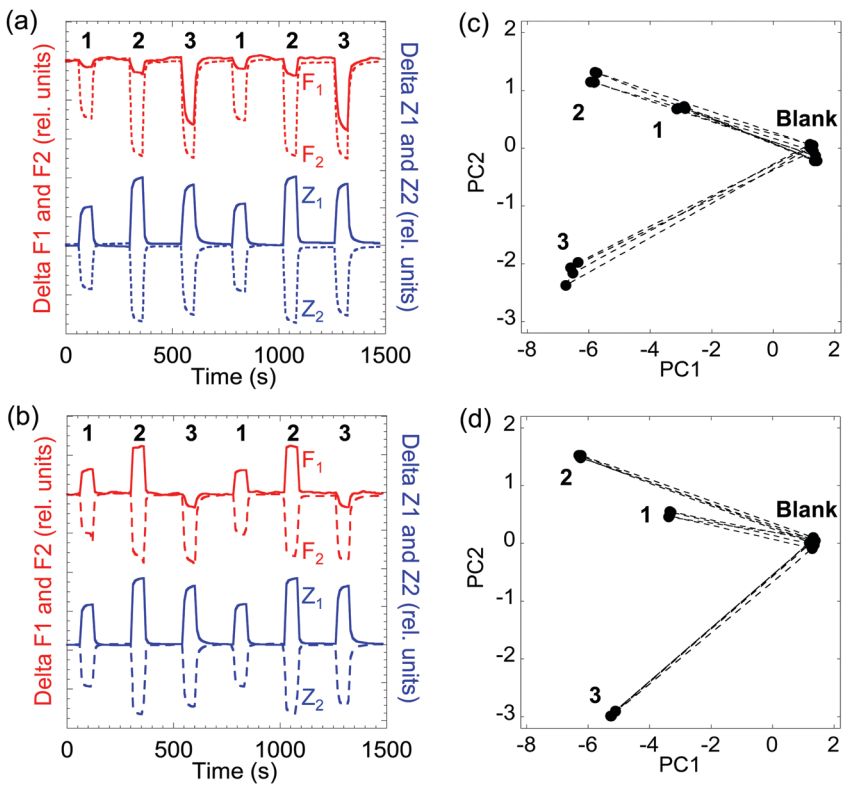

Fig. 16 Discrimination of individual vapors of similar dielectric constants using a multivariable resonant impedance sensor and its spectral distortions. Examples of F_1, F_2, Z_1, Z_2 responses at (a) −10 dBm and (b) 0 dBm and corresponding PCA scores plots (c and d). Model vapors: (1) 1-pentanol, (2) paraldehyde, and (3) salicylaldehyde. Sensing material was 1-octanethiol-capped gold nanoparticles.[80]

over the changes in the film refractive index. While the plasmonic peak of the sensing film was blue-shifted upon exposures to both vapors, the film absorbance increased upon exposure to toluene but decreased upon exposure to heptane (Fig. 20a).

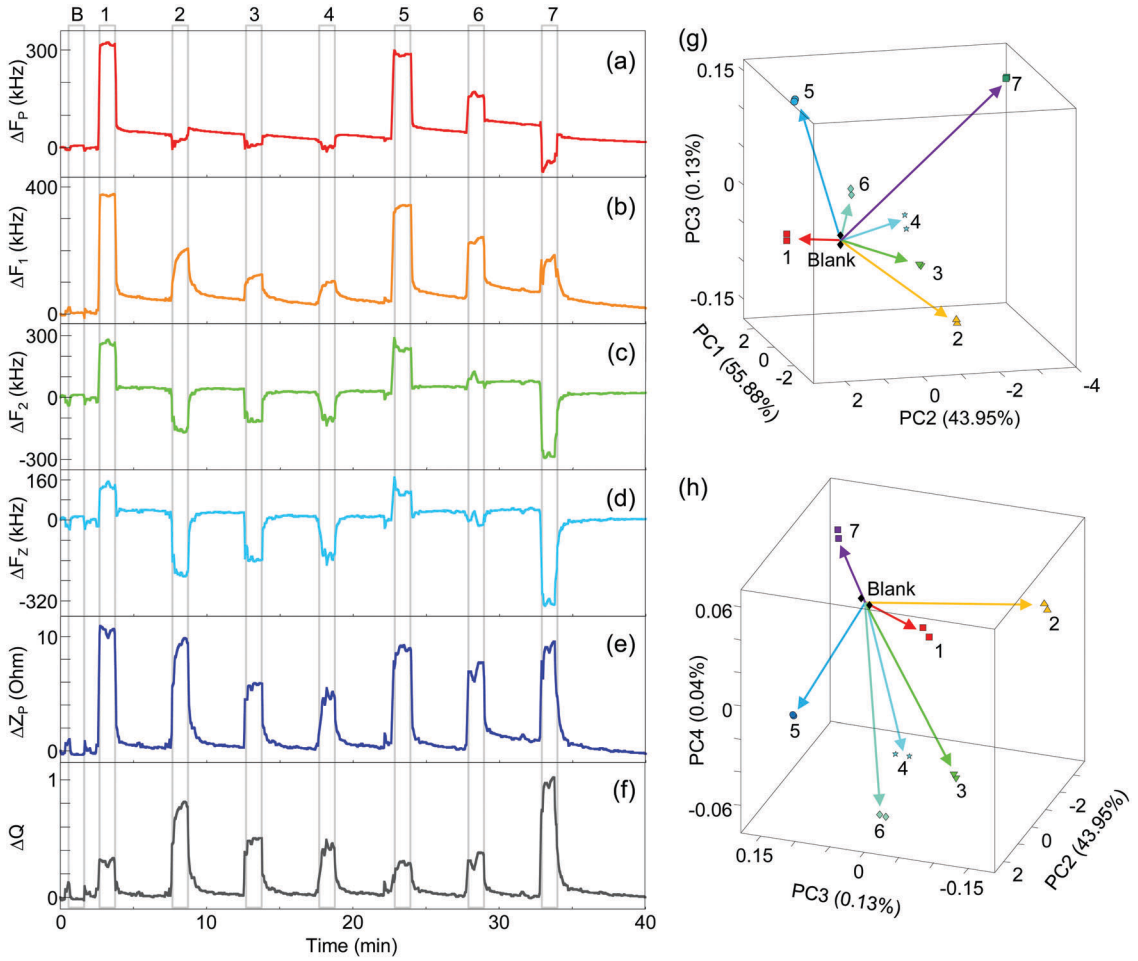

Fig. 17 Discrimination of complex aromas from teas using a multivariable resonant impedance sensor with MTE-capped gold nanoparticles. (a–f) Diversity of F_p, F_1, F_2, F_Z, Z_p, and Q responses of the sensor. Scores plots of the developed PCA model (g) PC1 *vs.* PC2 *vs.* PC3 and (h) PC2 *vs.* PC3 *vs.* PC4. Labels: (B) Blank ambient laboratory air, (1) Robert Roberts Blackcurrant Tea, (2) Dilmah Moroccan Mint Green Tea, (3) Bigelow Green Tea With Lemon, (4) Dilmah Pure Camomile Flowers Tea, (5) Bewley's Pure Rooibos Tea, (6) Numi Organic Jasmine Green Tea, and (7) Dilmah Earl Grey Tea.[190] Reprinted with permission from ref. 190. Copyright 2017, IEEE.

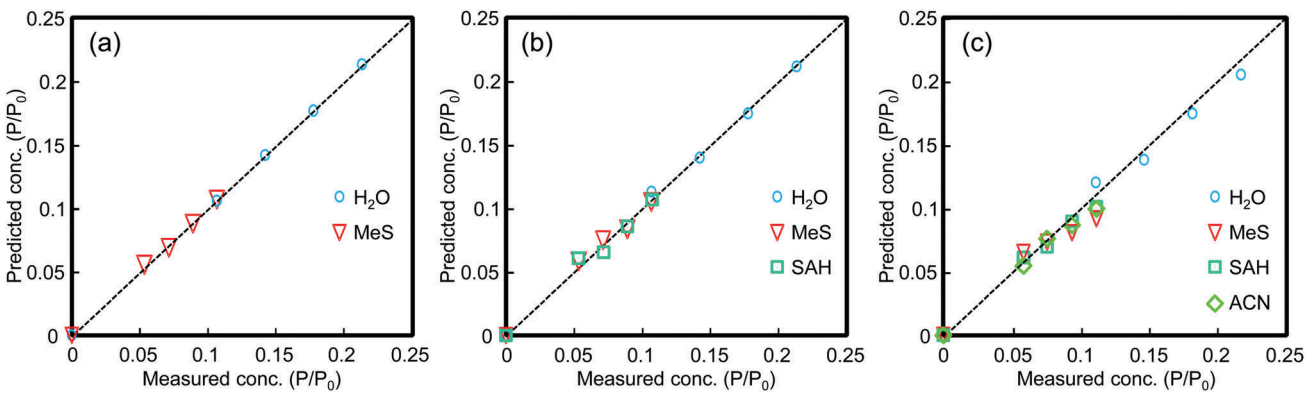

Fig. 18 Results of analysis of (a) binary, (b) ternary, and (c) quaternary mixtures using a multivariable resonant impedance sensor and SVM classification followed by PCR quantitation. Vapors: water (H_2O), methyl salicylate (MeS), salicylaldehyde (SAH), and acetonitrile (ACN). Sensing material was 1-octanethiol-capped gold nanoparticles.[79]

Quantitation of these vapors was further performed using dual-wavelength measurements of the intensity of the reflected light at the opposite sides of the absorption peak at 488 nm and 785 nm (Fig. 20b and c). The reflectance sensitivity ratios for toluene and n-heptane were of 0.68 and 0.80 at these two wavelengths, providing the ability for discrimination of these vapors (Fig. 20d).

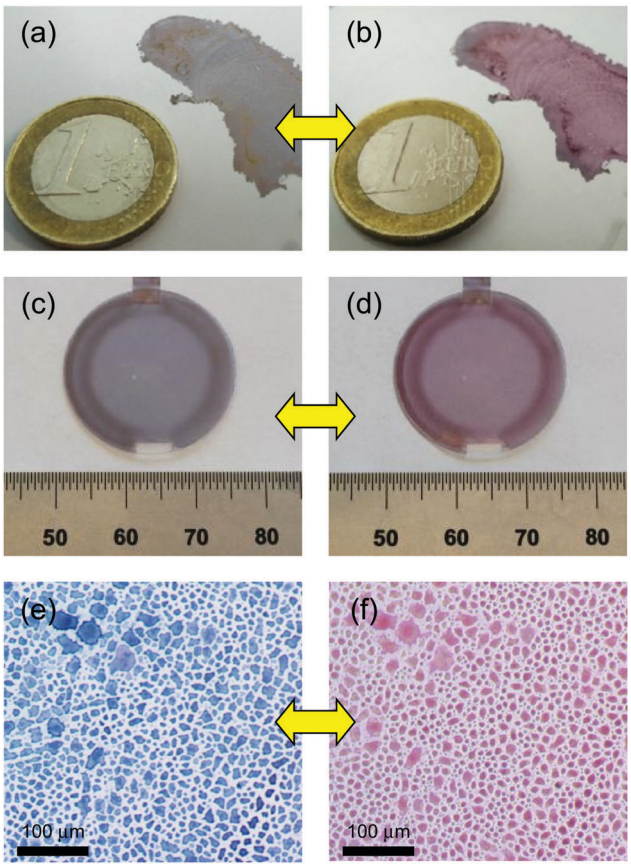

Fig. 19 Examples of MPN materials that change their visually-detected optical properties upon exposure to volatiles. Left and right panels – before and during vapor exposures, respectively. Color changes of macroscopic films of Au nanoparticles functionalized with mercapto-poly(ethylene glycol) (a and b)[167] and MTE (c and d) ligands.[109] (e and f) Color changes of microscopic islands of assembled nanoparticles.[167] (a, b, e and f) Reprinted with permission from ref. 167. Copyright 2016, The American Chemical Society. (c and d) Reprinted with permission from ref. 109. Copyright 2013, Wiley-VCH.

A MTE ligand was chosen in another study for discrimination of individual vapors and their mixtures because of its amphiphilic properties to respond to both polar and nonpolar vapors (Fig. 21).[109] The color of the sensing film with the MTE-based MPN film was changing from blue to the different shades of red upon exposure to different vapors. Six vapors with diverse range of their properties (water, methyl salicylate, tetrahydrofuran, dimethylformamide, ethyl acetate, and benzene) produced diverse plasmonic responses affecting the peak and the short- and long-wavelength shoulders of the plasmonic band (Fig. 21a–c). Irrespective to their refractive index, all vapors have led to the peak shift toward short wavelengths, indicating noticeable contributions of swelling effects of the organic soft shell upon interactions with vapors of different refractive index. The PCA scores plot illustrated that this sensing film discriminated most of the vapors (Fig. 21d). The vapors were ranked in the order of the solvent refractive index except for water vapor, likely because water was the only polar protic solvent among tested vapors. The film was further utilized to quantify ethyl acetate and benzene in their mixtures. The time-dependent responses of PC1 and PC2 from a built PCA model illustrate discrimination of individual vapors and their mixtures (Fig. 21e and f). The designed map of vapors concentrations (Fig. 21g) had good resemblance with the experimentally obtained map (Fig. 21h). This data shows the power of the application of MPN materials for the discrimination of vapors in their simple mixtures.

Several ligands and sizes of Au nanoparticles were compared for their ability to discriminate between multiple vapors with individual colorimetric films when probed at only three wavelengths such as 405, 532, and 600 nm across the plasmonic peak. Using experimentally measured changes in absorbance at these three wavelengths and adding a 5% of computed variation in responses, PCA models were constructed (Fig. 22).[76] The average recognition rate (RR) values were 51.5–99% among the six tested types of MPNs films. Tested vapors were tetrachloroethylene (PCE), toluene (TOL), *n*-octane (OCT), butyl acetate (BAC), 2-butanone (MEK), and 2-propanol (IPA). While a relatively poor discrimination of vapors was achieved using a 6-phenoxyhexane-1-thiol ligand (RR = 51.5%) (Fig. 22a), other types of MPN materials had outstanding discrimination. Excellent discrimination

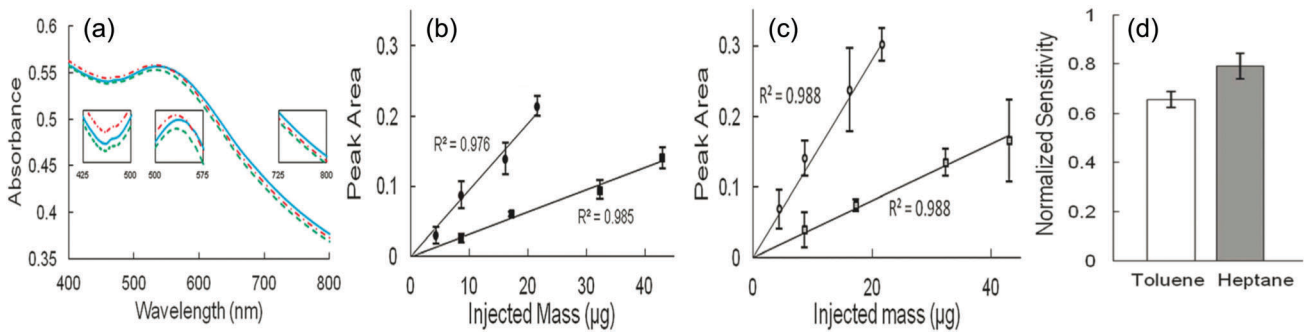

Fig. 20 Optical discrimination of individual vapors using a single sensing film of 1-octanethiol-capped Au nanoparticles and a two-wavelength detection. Model vapors: toluene and *n*-heptane. (a) Absorption spectra of the sensing film on a glass slide before exposure (solid blue line), and during exposures to *n*-heptane (dashed green line) and toluene (dashed-dotted red line). Insets show enlargements of selected spectral regions. Laser reflectance calibration curves at (b) 785 nm and (c) 488 nm for toluene (circles) and *n*-heptane (squares) of peak areas plotted *vs.* the injected mass of vapor. (d) Film sensitivity to each vapor at 785 nm upon normalization to the sensitivity at 488 nm.[74] Reprinted with permission from ref. 74. Copyright 2013, The Royal Society of Chemistry.

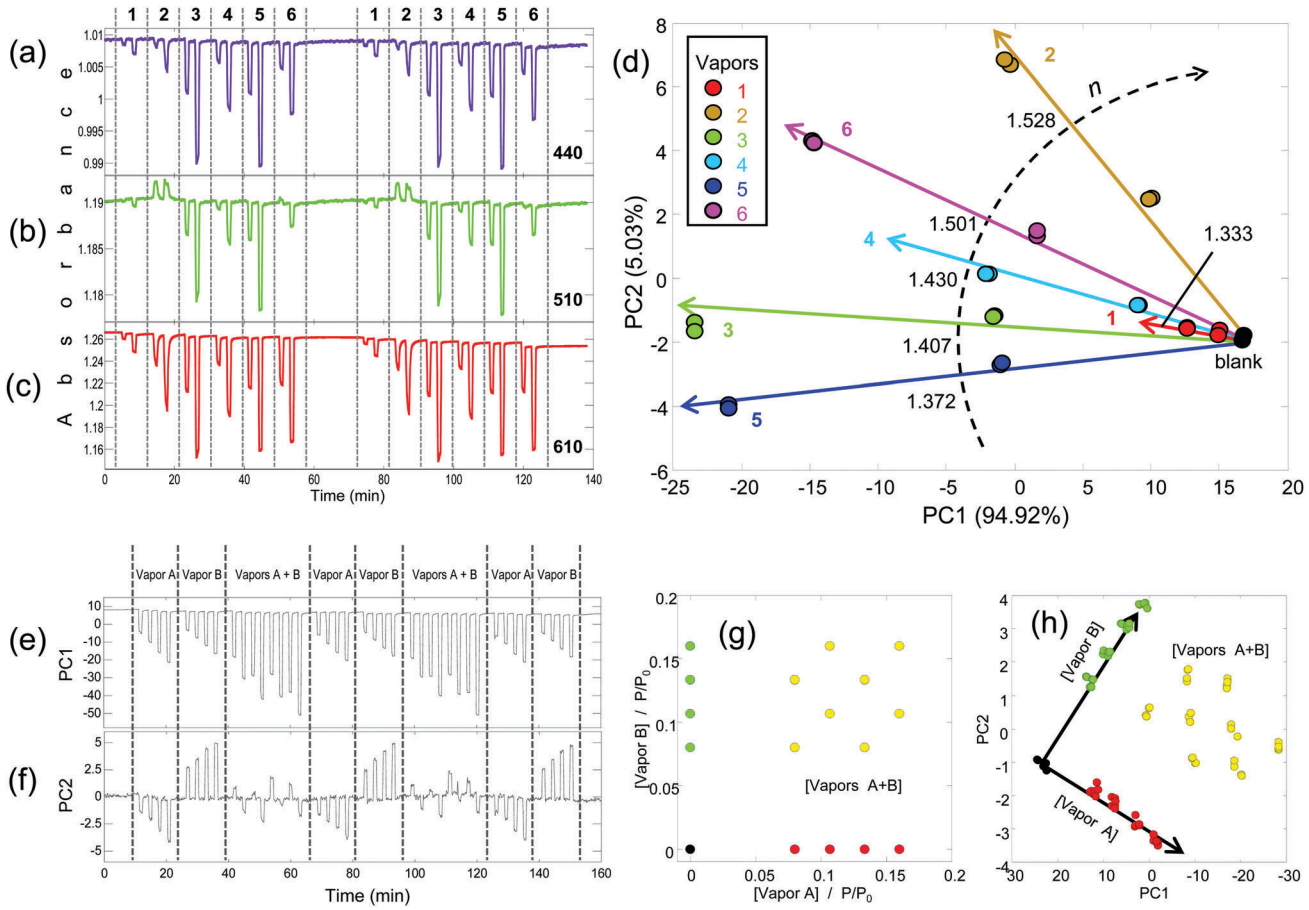

Fig. 21 Optical discrimination of individual vapors and their mixtures using a single sensing film of MTE-capped Au nanoparticles and a white-light detection. Model vapors: (1) water, (2) methyl salicylate, (3) tetrahydrofuran, (4) dimethylformamide, (5) ethyl acetate, and (6) benzene. (a–c) Dynamic response patterns of the sensing film to six vapors at representative wavelengths (440, 510, and 610 nm). (d) Scores plot of a developed PCA model. Each vapor concentration is represented by two replicate exposures. Dashed line is film response to different vapors in the order of the refractive index *n* of the corresponding solvent. (e and f) Responses PC1 and PC2, respectively from a built PCA model of detection of individual vapors A (ethyl acetate) and B (benzene) and their binary mixtures. (g and h) Comparison between a designed map and PCA results, respectively of detection of ethyl acetate and benzene.[109] Reprinted with permission from ref. 109. Copyright 2013, Wiley-VCH.

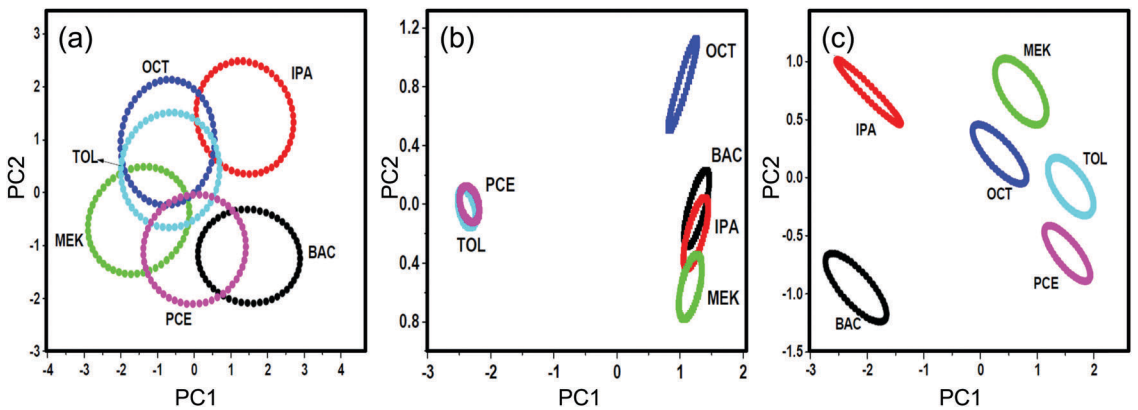

Fig. 22 PCA scores plots illustrating optical discrimination of vapors using individual MPN sensing films and a three-wavelength detection. Model vapors: tetrachloroethylene (PCE), toluene (TOL), *n*-octane (OCT), butyl acetate (BAC), 2-butanone (MEK), and 2-propanol (IPA). Ligands and sizes of Au nanoparticles (NPs): (a) 6-phenoxyhexane-1-thiol and 4 nm Au NP, (b) 1-octanethiol and 4 nm Au NP, and (c) dithianate and 40-nm Au NP. The 95% confidence ellipses were generated from experimental data with added 5% error.[76] Reprinted with permission from ref. 76. Copyright 2015, IEEE.

between six vapors was achieved with 1-octanethiol (RR = 98.4%) and dithianate (RR = 99.9%) ligands (see Fig. 22b and c, respectively). These results illustrated the strong ligand-dependent ability of MPN materials for the discrimination of vapors.

7. Structure-based multivariable photonic sensors

Structure-based photonic sensors comprise of units that are comparable with the wavelength of interrogation light.[213–220] Such sensors often operate based on single-output gas and vapor quantitation principles such as detection of wavelength shift of the resonance peak[221–225] or detection of signal intensity change at a single wavelength.[226] Monitoring of multiple analytes using these approaches requires traditional sensor arrays.[222,227,228] However, these physical structures facilitate multivariable performance of sensors when implemented as pristine structures[70,71,105,229] or when combined with the MPN material deposited on such structures.

Recently structure-based multivariable photonic sensors have been reported[70,71,73,105] that demonstrated the superior discrimination of diverse and closely related vapors as compared to other types of multivariable sensors.[191] These multivariable photonic sensors have been demonstrated using composite structurally colored colloidal crystal films self-assembled from polystyrene core nanospheres with a sol–gel shell,[105] natural biological nanostructures,[70,71] and fabricated bioinspired nanostructures.[73] The interest in natural biological nanostructures for vapor detection is driven by geometries that are attractive for sensing but difficult to reproduce using existing nanofabrication tools.[75,115,230–239]

A tree-like nanostructure of microscopic scales that produces iridescence of tropical *Morpho* butterflies was found to be attractive for sensing of volatiles[70] because of its open-air architecture that allows volatiles to interact with all its regions such as ridges, lamella, and microribs (Fig. 23a). Iridescent scales of *Morpho* butterflies yielded an unexpected diverse optical responses to different vapors.[70] This vapor-selectivity originated from a gradient of surface polarity of a conformal epicuticle layer of the ridge structure.[71] This polarity gradient runs from the polar tops to the less-polar bottoms of ridges. The mechanism of selective vapor response of the *Morpho* scales involves preferential sorption of vapors of different polarity onto the corresponding regions of the nanostructure (Fig. 23b).[71] Such vapor interactions are expressed in the corresponding regions

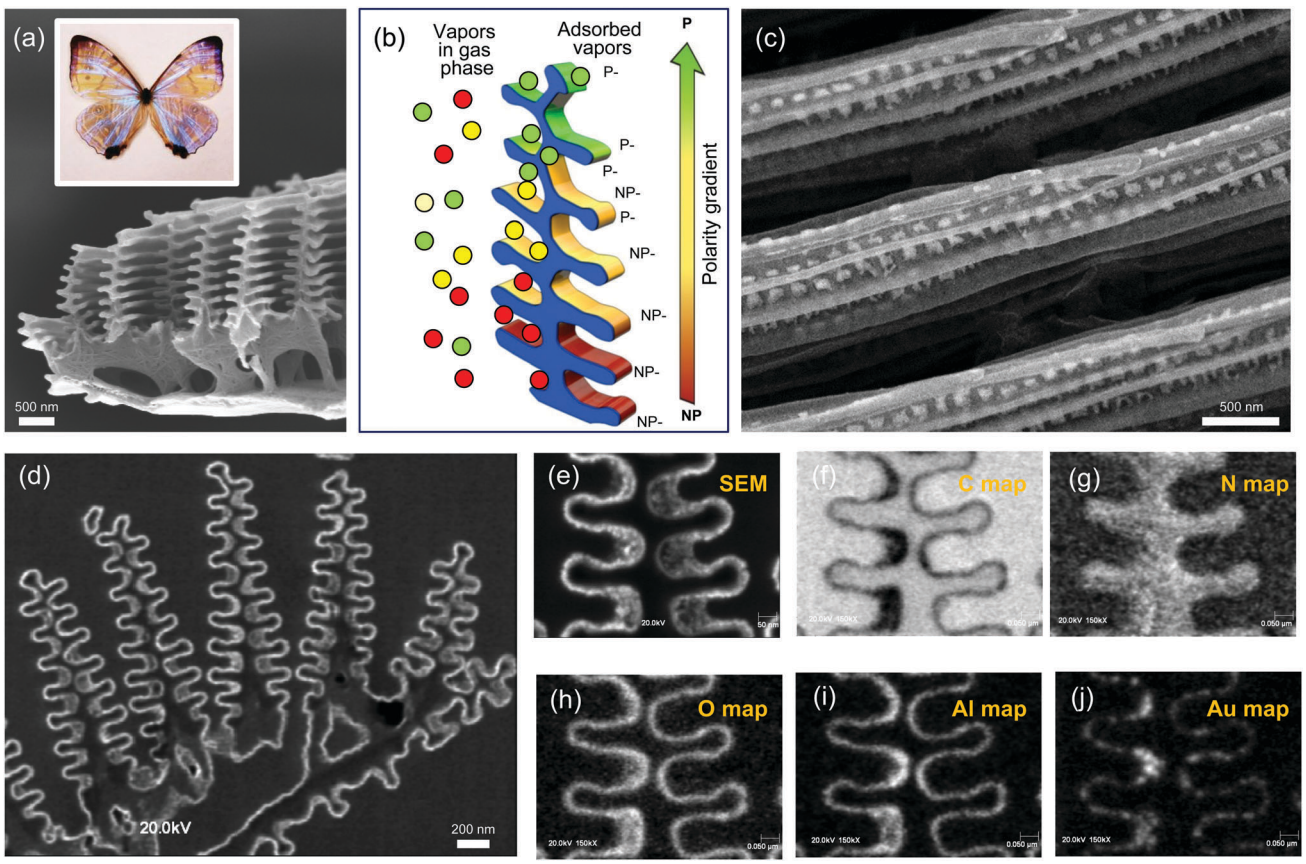

Fig. 23 Example of design of structure-based multivariable photonic sensors. (a) Open-air architecture of tree-like nanostructure of iridescent microscopic scales of tropical *Morpho* butterfly allows gas-phase compounds to interact with all its regions such as ridges, lamella, and microribs. Inset: Reflected light image of a *Morpho* butterfly.[71] (b) Origin of vapor-selectivity of structure-based multivariable photonic sensors. Interactions of vapors with different spatial regions of the nanostructure are expressed in the corresponding regions of the reflected light spectrum.[71] (c) *Morpho* nanostructure with 1-octanethiol-capped Au nanoparticles deposited from a toluene solution has formed clusters in the pockets between the microribs. (d–j) Visualization of deposited 1-octanethiol-capped Au nanoparticles by applying an Al_2O_3 ALD coating onto the *Morpho* nanostructure followed by deposition of MPNs: (d and e) SEM images with ALD conformal coating and deposited nanoparticles. (f–j) Auger elemental maps reveal distribution of respectively C, N, O, Al, and Au elements on the surface. (a and b) Reprinted with permission from ref. 71. Copyright 2013, The National Academy of Sciences USA.

of the reflected light spectrum, responsible for the unusual vapor response selectivity of the *Morpho* scales. To expand diversity of response to vapors, *Morpho* nanostructure was decorated with 1-octanethiol-capped Au nanoparticles forming clusters in the pockets between the microribs (Fig. 23c). To visualize better the deposited nanoparticles, an Al_2O_3 atomic layer deposition (ALD) coating was applied followed by deposition of MPNs. Fig. 23d and e illustrate SEM images with the ALD conformal coating and deposited nanoparticles. Auger elemental maps revealed distribution of elements on the surface (Fig. 23f–j).

Discrimination of vapors of the first nine linear alcohols of their homologous series and water was accomplished with Au nanoparticles capped with a 1-octanethiol ligand deposited onto a *Morpho* natural biological nanostructure. Detection of these closely related alcohol vapors is not straightforward even using gas chromatography and sensor arrays.[240] The MPN-functionalized *Morpho* natural biological nanostructure was exposed to ten vapors (water, methanol, ethanol, 1-propanol, 1-butanol, 1-pentanol, 1- hexanol, 1-heptanol, 1-octanol, and 1-nonanol, four concentrations of each vapor). Spectral data was processed using PCA followed by Linear Discriminant Analysis (LDA) for vapor classification and followed by non-linear Principal Component Regression (PCR) for quantitation. The PCA-LDA results demonstrated sensor discrimination of the vapors (Fig. 24a). Results of cross-validated PCR model are presented in Fig. 24b. From the experimentally measured four concentrations of each vapor, the cross-validated success rate was 100% as indicated by only diagonal contributions of actual *vs.* predicted vapors at their four concentrations.

Such ability to discriminate multiple vapors with a single sensor is surely attractive, however with a caveat of reproducibility of the structure-to-structure reflectance of natural samples.[71,73] The number of methodologies for fabrication of such bio-inspired structures is growing.[73,214,241–251] Controlled deposition of sensing moieties on these structures[252–254] should allow further tuning of multivariable response of these sensors.

8. Stability of MPN sensing materials

At present, inadequate stability of most of reported MPN materials is their biggest limitation. Stability evaluation of sensing materials and development of technical solutions to improve stability are important tasks toward bringing new sensors to their field applications.[255–257] Stability of MPN sensing films depends on stability of the metal particles, the ligand, and the particle–ligand linkage. General methods for stabilization of MPNs include utilization of end groups to modify the interactions between neighboring MPNs, incorporation of ionic functional groups in the adsorbate to provide electrostatic repulsion, diversification of the adsorbates to create chains of varying lengths and thereby enhance steric repulsion, development of chelating surfactants that reduce desorption, and addition of cross-links or polymerizable moieties into the adsorbate structure.[258]

Depending on the metal type, small metal particles oxidize at different rates in ambient air conditions. For example, it was shown that citrate-coated Ag nanoparticles (~8 nm diameter) deposited on a glass slide and stored in air were oxidized after one month of storage as determined from the disappearance of the plasmonic band of Ag nanoparticles.[148] Au and Pd nanoparticles demonstrate a significantly more stable performance over Ag nanoparticles in vapor sensing.[148]

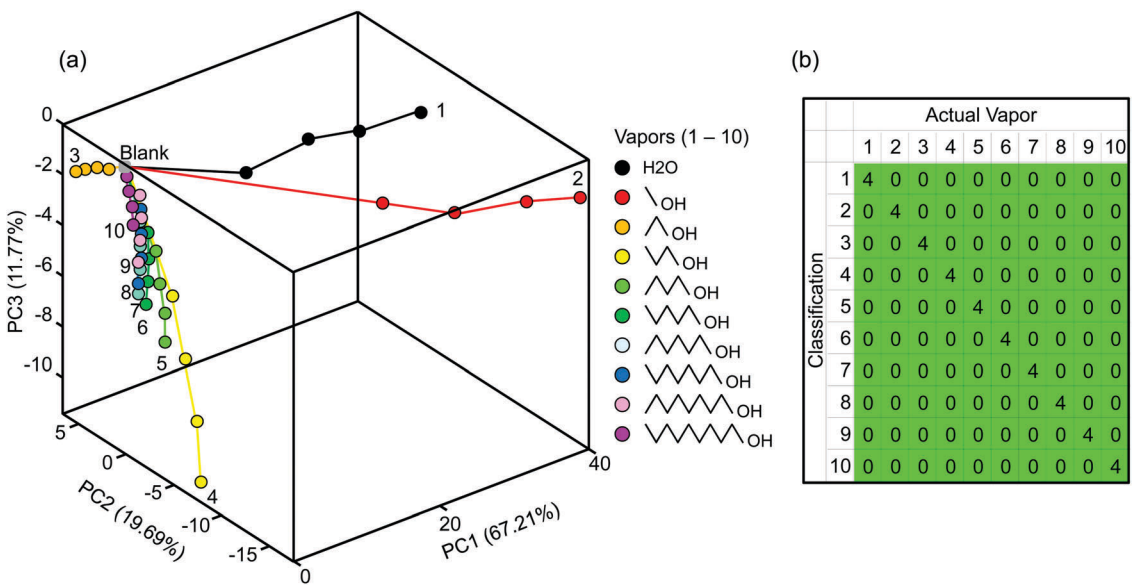

Classification \ Actual Vapor	1	2	3	4	5	6	7	8	9	10
1	4	0	0	0	0	0	0	0	0	0
2	0	4	0	0	0	0	0	0	0	0
3	0	0	4	0	0	0	0	0	0	0
4	0	0	0	4	0	0	0	0	0	0
5	0	0	0	0	4	0	0	0	0	0
6	0	0	0	0	0	4	0	0	0	0
7	0	0	0	0	0	0	4	0	0	0
8	0	0	0	0	0	0	0	4	0	0
9	0	0	0	0	0	0	0	0	4	0
10	0	0	0	0	0	0	0	0	0	4

Fig. 24 Optical discrimination of ten vapors using a structure-based multivariable photonic sensor with 1-octanethiol-capped Au nanoparticles applied onto *Morpho* nanostructure and a white-light detection. (a) The PCA–LDA results of discrimination of ten vapors. (b) Results of cross-validated non-linear PCR model. Cross-validation: leave-one-out. Vapors 1–10: water, methanol, ethanol, 1-propanol, 1-butanol, 1-pentanol, 1-hexanol, 1-heptanol, 1-octanol, and 1-nonanol.

Effects of nature of ligands on the stability of MPN sensing films in chemiresistors have been studied over 12–16 months of storage.[163] The studied ligands were hexanethiol (C6) and tetraoctylammonium bromide (TOABr) attached to Au nanoparticles. Stability of these sensing materials was characterized by exposure to model vapors (toluene and methanol) to determine changes in sensor sensitivity, by exposure to a blank gas to determine changes in intrinsic film conductivity, and by cyclic voltammetry to determine changes in ohmic and electron hopping behaviors. Response to model vapors decreased by ~60% and ~20% for C6- and TOABr-capped Au nanoparticles, respectively (Fig. 25a and b). The conductivity of C6 films decreased by a factor of two while the conductivity of TOABr films was almost unchanged. This decrease in conductivity and response for C6-Au MPNs was due to sulfur oxidation, which is well known to occur over time in air for thiols on Au. The cyclic voltammetry measurements revealed changes in electron hopping behavior for C6-Au films and changes in capacitive charging for TOABr films (Fig. 25c and d). This study demonstrated that chemiresistors made of TOABr-capped Au nanoparticles were at least 2× more stable than those comprised of C6-capped Au nanoparticles.

To understand better the origin of the instabilities of the MPN sensing films, effects of different conditions of 44-month storage of MPN films on the chemistry, morphology and vapor responses were evaluated.[259] The tested four types of storage conditions were (1) exposed to light in ambient air (“ambient/light”); (2) protected from light in ambient air (“ambient/dark”); (3) exposed to light in Argon (“inert/light”); and (4) protected from light in Argon (“inert/dark”). The studied ligands were 1,9-nonanedithiol and 1,16-hexadecanedithiol attached to Au nanoparticles. Vapor response resistance measurements to model vapors (toluene, 1-propanol, water, and hydrogen sulfide), X-ray photoelectron spectroscopy (XPS), and SEM were utilized for characterization of sensing films. Storage under ambient conditions resulted in oxidation of sulfur and carbon and appearance of nitrogen, a loss of sulfur and the increase of the particles size in the film. These effects were explained by the reaction of the thiol groups with ozone from the air, which destabilized the network. The XPS S 2p spectrum of the fresh 1,16-hexadecanedithiol film was dominated by thiols, bound and unbound to Au (Fig. 26a). During storage under ambient/light conditions the amount of both species decreased while oxidized sulfur species appeared and increased continuously with storage time (Fig. 26b). The responses of the 1,16-hexadecanedithiol films toward model vapors before and after storage are shown in Fig. 26c. Sensors under all storage conditions have changed their sensitivity and response patterns to model vapors. The films stored under argon showed a smaller change than those stored under ambient conditions, and their responses were very similar when comparing dark and light inert storage conditions.

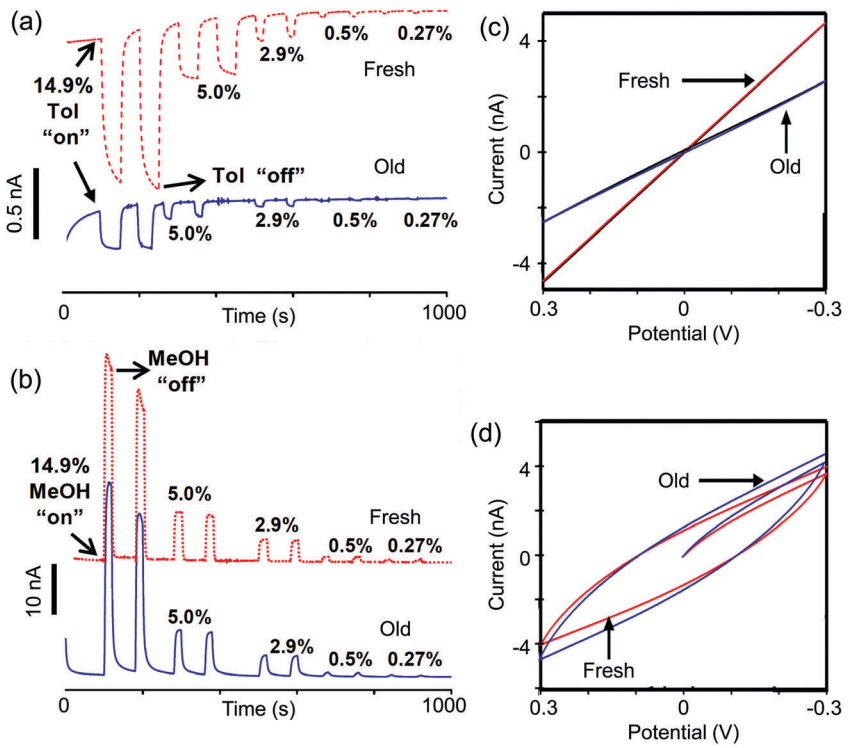

Fig. 25 Evaluation of effects of nature of ligands C6- and TOABr-attached to Au nanoparticles on the stability of MPN sensing films over 12–16 months of storage. (a) Response of C6-Au sensing material to toluene and (b) response of TOABr-Au sensing material to methanol before and after storage demonstrate changes in sensor sensitivity and changes in intrinsic film conductivity. (c) Changes in electron hopping behavior for C6-Au films and (d) changes in capacitive charging for TOABr films before and after storage.[163] Reprinted with permission from ref. 163. Copyright 2008, The American Chemical Society.

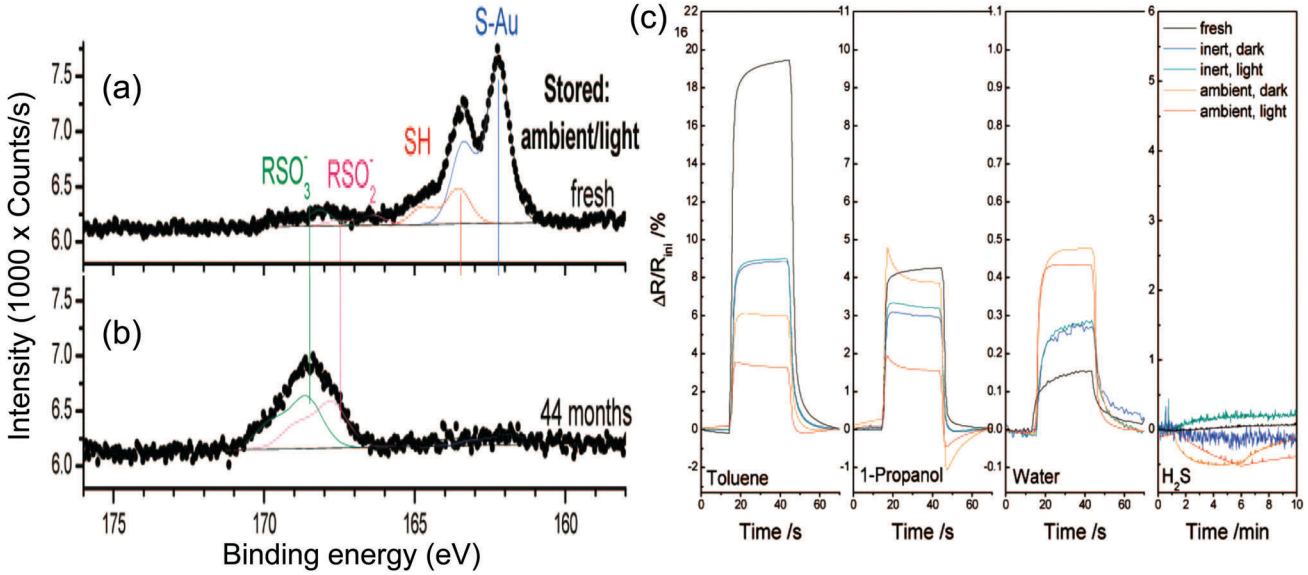

Fig. 26 Chemistry and vapor responses of MPN 1,16-hexadecanedithiol films upon 44-month storage. (a and b) S 2p XPS spectra of fresh and stored films, respectively. The spectrum of the fresh sample was dominated by thiols bound to Au at 162.1 eV and unbound thiols at 163.5. During storage, the amount of both species decreased while new oxidized sulfur species such as sulfinates at 167.4 eV and sulfonates at 168.5 eV appeared and increased continuously with storage time. (c) Responses of sensors before and after storage toward toluene, 1-propanol, water, and hydrogen sulfide.[259] Reprinted with permission from ref. 259. Copyright 2009, The American Chemical Society.

Stability of MPNs on chemiresistors has been studied for almost five years.[193] Six ligands have been tested by making replicate sensors (n = 2) for each ligand. Each replicate sensor had a very similar baseline current at the first day of the long term test; however, two types of variations were observed during the test. These variations were in baseline current over the duration of the test and between replicate sensors (Fig. 27).

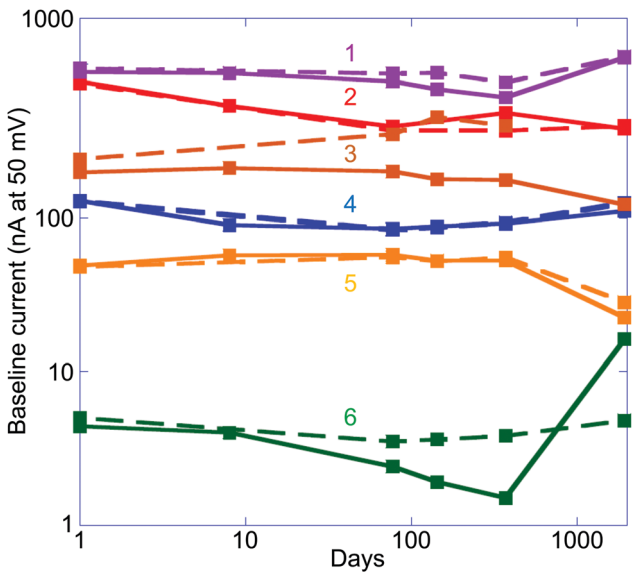

Fig. 27 Variations in the baseline current over time for MPN-based sensors with six different ligand shells and with two sensors tested of each type. Sensors: (1) 5 nm Au-HS$(CH_2)_7CH_3$, (2) 2 nm Au-HS$CH_2CH_2C_6H_5$, (3) 5 nm Au-HS$(CH_2)_9CH_3$, (4) 2 nm Au-HS$(CH_2)_5CH_3$, (5) 2 nm Au-HS$(CH_2)_5$COOH, and (6) 2 nm Au-HS$(CH_2)_7CH_3$.[193] Reprinted with permission from ref. 193. Copyright 2015, IEEE.

In addition to evaluations of stability of MPN sensing films using chemiresistors,[259–261] evaluations were also performed using multivariable optical readout.[109] It was found that the observed baseline drift was wavelength-dependent. While there was no significant drift over 400–500 nm, the drift increased from ~500 to 690 nm, stabilized at its maximum at ~690 nm, and decreased at longer wavelengths. There could be more than one degradation mechanism of the sensing film,[259–261] responsible for film instability.

The relatively poor long-term stability of thiol-capped Au nanoparticles has been improved by capping Au nanoparticles with trithiol ligands.[261] The nanoparticles with trithiol ligands had similar sensitivity towards different types of polar or non-polar volatile organic compounds (Fig. 28a) but were significantly more stable (Fig. 28b). Response of trithiol-Au to a 500 ppm toluene vapor had a ~10% sensitivity decrease *vs.* a ~50% sensitivity decrease of monothiol-Au. The known relatively poor stability of monothiol-Au nanoparticles was due to their ease of oxidization under ambient air conditions, forming sulfonyl-like oxidized products. In the case of trithiol-Au nanoparticles, the surface thiolate was less susceptible to oxidation due to binding to gold and the electron-rich nature of the gold core. Nevertheless, slow oxidation of the surface thiolate still occurred on a timescale of months to one year when exposed to air, light, and moisture under ambient conditions.

9. Conclusions and outlook: from MPN sensor ideas to products

Sensors research is a field with multi-disciplinary contributions where fundamental and applied sciences are united to produce

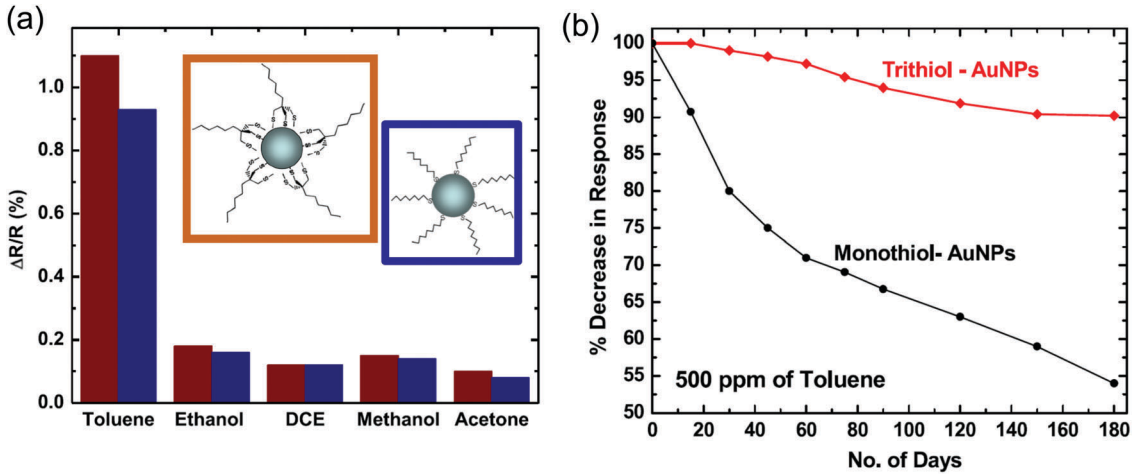

Fig. 28 Stability improvement of vapor sensors using trithiol-capped Au nanoparticles. (a) Responses of trithiol and monothiol-capped Au nanoparticle sensors to various volatile organic compounds. Inset: Structures of trithiol and monothiol-capped Au nanoparticles. (b) Response of trithiol-Au and monothiol-Au-based sensors to 500 ppm toluene over a six-month test period.[261] Reprinted with permission from ref. 261. Copyright 2010, Institute of Physics.

new sensing materials, couple them with physical transducers, and build sensor devices with previously unavailable capabilities. The growing number of disciplines involved in building innovative sensor systems is truly impressive. Materials science, organic, polymeric, inorganic, and biological chemistry, and nanotechnology are involved in the development of sensing materials. Engineering, analytical chemistry, and nanotechnology are involved in the design of physical transducers and building sensor devices. Other critically involved disciplines include informatics, statistics, machine learning, product management science, and product marketing. Ideally, these disciplines synergistically interact to produce solutions for new sensor systems to solve important measurement needs that cannot be solved by using existing technical approaches. This review was designed to give such a perspective for these new sensor systems.

As shown in this review, metal nanoparticles capped with different organic and biological ligands have been applied as attractive sensing materials in multivariable sensors. These MPN materials produce diverse chemical functionality for detection of different gas-phase compounds using several principles of multivariable signal transduction. As a result, these sensing materials provide vapor-induced changes in conductivity, dielectric constant, partition coefficient, film thickness, film mass, film viscoelastic properties, and optical extinction effects such as the peak position and the width of the plasmon absorption band. These changes in MPNs form the basis for MPN-based multivariable sensors.

From the initial demonstration of monolayer-protected nanoparticles as a sensing material for volatiles in the late 1990s,[130] the progress in development of MPN sensing materials expanded to studies of diverse types of organic and biological ligands, applications of transducers with different transduction principles, studies of sensor responses to model vapor mixtures and real-world samples, evaluation of materials degradation and improvements of material stability. Multivariable response of these MPN-based sensors typically has a 2D–3D dispersion and sometimes 4D dispersion,[72,80,88,112] close to 4D responses with multivariable sensors based on conjugated polymers[61] and silane-functionalized polymeric nanostructures.[73]

These developed MPN-based multivariable sensors were demonstrated in laboratory scenarios for quantitation of multiple individual model vapors, quantitation of multiple vapors in their mixtures, accurate detection of vapors in the presence of numerous interferences, rejection of interferences at a several million-fold excess, and discrimination of complex aromas. We believe that to bring these sensors outside pristine lab conditions, research activities should be focused on selectivity and stability improvements, expansion of temperature range of operating conditions, and further expansion of the range of detected gas-phase compounds. Sensitivity improvements may be also of interest to increase the signal-to-noise ratio in detection of ppm and ppb levels of analytes.

Selectivity improvements will continue to be driven by the general knowledge about functional groups of organic ligands to create networks of metal nanoparticles.[129] However, quantitative effects of different gas-phase compounds on selectivity of ligands in metal nanoparticle networks are difficult to rationally predict based on existing general knowledge, similar to the situation with other sensing materials.[44,262] Thus, high-throughput screening technologies should provide a desired ability to generate more rapidly new knowledge for the future design rules of ligands for needed gases and vapors.[170] Also, computational methodologies should be more proactively applied for the design of ligands for enhanced selectivity, especially given the growing speed and accuracy of computations[263–265] and the expanding impact of machine learning and artificial intelligence methods in materials science.[266–268] For further selectivity improvements, synergistic effects of the core and ligand shell of nanoparticles in producing electrical and optical effects should be explored. The inert nature of the metal core that is known to be responsible only for the electron hopping should be expanded for the

analyte-modulated electron hopping based on analyte-dependent changes in conductivity of the metal-like conducting core. Dynamic signatures of different gas-phase compounds and complex aromas can be further discriminated using bio-inspired approaches.[269,270]

Sensitivity improvements can be considered from the perspectives of material and transducer designs. Cubic nanoparticles in MPN-based sensors have been demonstrated to outperform spherical particles in sensitivity of electrical readout.[133,153] Other shapes of nanoparticles such as rod-, hexagon-, triangle-, and starlike shapes[155] and nanoporous nanoparticles with dendritic, branched, and nanocage structures[271] can be also evaluated for their vapor sensitivity. Further, by tailoring the number and position of MPNs in close-packed clusters, sensing materials can be made with plasmon modes of Fano-like narrow resonances[272] to enhance sensitivity of optical sensors.[273–275] From transducer design perspective, to enhance sensitivity of non-resonant and resonant impedance sensors, electrodes with nanometer gaps should be explored in combination with close-packed MPN clusters. To enhance sensitivity of impedance and photonic sensors, transducers can be designed with high-quality factor resonant structures. Impedance transducers can be designed as radio-frequency interferometers[276] or with a regenerative loop in the sensor reader to increase the quality factor of the system.[277] Photonic sensors can be designed with high-quality factor resonances in 3D bioinspired structures.[73,278]

Stability improvements will become critical for the broad acceptance of MPN sensing materials in practical applications. These improvements will originate from better understanding of the degradation mechanisms followed by the development of design rules for more stable MPN materials. More stable ligands and their linkers to nanoparticles of different metals should be developed using high-throughput experimental screening and computational methodologies, perhaps in parallel with screening for material selectivity.

Expansion of temperature range of operating conditions of MPNs beyond room temperature for sensing at elevated temperatures will be important for industrial applications. At present, nanoparticle-based sensing materials operating at elevated temperatures of 300–800 °C utilize plasmonic nanoparticles incorporated into an inorganic rigid metal oxide matrix rather than having a ''ligand'' layer around individual nanoparticles. Materials of nanoparticles in these high-temperature sensors are typically Au or Au alloys. Examples of metal oxides in such films include CuO, ZnO, TiO_2, NiO-SiO_2, SiO_2, BaO, CeO_2, and yttria-stabilized zirconia (YSZ, ZrO_2 and Y_2O_3).[110,111,279–285] The mechanisms of vapor response of such nanocomposite films involve the charge exchange with the nanoparticles or a change in the dielectric constant surrounding the nanoparticles, dependent on the type of a metal oxide and its morphology.[110] Materials developments with a ''ligand'' layer around individual nanoparticles for these high-temperature sensors should provide enhanced sensitivity and possibly selectivity control.

Expanding the range of detected gas-phase compounds to include gases of environmental and industrial importance should be beneficial because of the large demand for new sensors with higher reliability, lower power consumption, and lower cost as compared to existing technical solutions.[201] Examples of gas-phase compounds of such interest include environmental background (*e.g.* O_2, CO_2), atmospheric pollutants (*e.g.* O_3, NO_x, CH_4, waste odors), and public/homeland safety hazardous volatiles (*e.g.* toxic industrial chemicals, explosives).

We believe that adequate comparison of MPN materials should include understanding of the levels of remaining impurities and the density of ligand moieties on the surface of nanoparticles. Often, such information is not provided, thus results from different research teams may not be the same.

The general state of the art of gas and vapor sensing is remarkable. This field is thriving with commercially successful technologies such as catalytic combustion pellistors, metal oxide and polymer chemiresistors, electrochemical sensors, and catalytic field effect transistors.[44,286–289] The number of annually published research papers with ''vapor sensor'' and ''gas sensor'' concepts follows an exponential growth curve with over 5000 papers published in 2016 alone. From these remarkable developments, we see several key learnings that can be applied to the MPN-based and other types of multivariable sensors.

First, a ''low cost sensor'' argument is often used as the key sensor-technology differentiator. This argument is important when viewing sensor elements initially only as a stand-alone component, *e.g.* <$1 sensor elements manufactured using MEMS processes or <$0.001–$0.01 sensor elements that can be manufactured using new roll-to-roll and printing processes.[201,290] It is also recognized that a sensor element is typically a part of a sensor system. An appropriate standard packaging of such sensing elements adds cost – for example, up to a dollar when packaged on a flexible electronic circuit, up to several dollars when packaged in a standardized semiconductor package, or up to several tens of dollars when packaged for intrinsic safety compliance. With added electronics, gas sampling, housing, and other necessities, the whole system can be hundreds or thousands of dollars – for example, a little more than $100 for a hand-held food spoilage sensor system[291] or a little less than $8000 for a hand-held sensor system for complex chemical mixtures.[292]

We witness that some classes of gas and vapor sensors are becoming or have already become technologically mature, also known as ''commodity products''. The most prominent examples are polymeric capacitor sensors for ambient humidity and metal oxide resistor and pellistor sensors for diverse gases. These sensors serve established markets, are widely available, interchangeable, and inexpensive. Because these sensors are based on mature technologies, their advancements are mostly in cost reduction. However, we will also emphasize that when sensors bring high value to users that is unavailable from other technologies, these sensors do not need to be low cost for their acceptance by the markets – the ''low cost'' belief is for commodity products. For example, in numerous industrial applications humidity should be reliably detected down to ppb levels. It is accomplished using sensors that are in high demand even though they are 100–1000 times more expensive than commodity sensors for ambient humidity. As another example, monitoring

of fugitive methane gas emissions is critical for industrial safety, environmental compliance, and productivity. Thus, industrial companies utilize methane imaging systems that are $100 000 each. These and many other scenarios require high value sensors to perform monitoring tasks that cannot be accomplished using commodity sensors.

Second, an "acceptable low quality sensing" argument sometimes is used by developers with an assumption that for the next generation of sensors it will be acceptable to have data of relatively low quality (*e.g.* poor selectivity, drift, *etc.*), yet valuable to users. As a prominent example, environmental pollution sensors when made at a significantly reduced cost and, as a trade-off, relatively poor performance, are sometimes viewed as the next big breakthrough to allow ubiquitous air quality sensor networks. Commercial air quality sensors are being compared to reference methods[293] with sensor data reliability and accuracy as the key factors[294] and a relaxed objective of allowed 25–30% of response uncertainty.[295,296] Unfortunately, recent studies have reiterated the known fact that those "low cost" sensors do generate sensor responses much stronger to interferences than to analytes.[5,43] It was concluded that "most of these devices are unreliable and some are practically useless".[297] If these sensors to be used in critical applications – for example, by people with asthma to make personal decisions on medication, by public to trigger legal actions on exceeding local air-quality standards, by municipal officials to close roads based on live sensor data, and in many other realistic scenarios – the cost of false alarms would be overwhelming.[5] Manufacturers were encouraged to be more open about limitations of these low-cost sensors.[297]

Third, the field of sensors for gases and vapors should learn from other sensors to bring the high-quality data to low cost formats. For example, recent wearable sensors for physiological parameters have inspired numerous applications. It has been further recognized that many of the early wearable physiological sensors had insufficient accuracy. Such poor accuracy went initially un-noticed due to the excitement of potential applications. However, soon thereafter it has been realized that to be broadly accepted and sustainable, wearable physiological sensors should significantly improve their accuracy.[298–305] Thus, at present, the number of wearable sensors that have same accuracy as medical devices or hospital equipment is increasing.[306–309]

Fourth, to bring new sensor ideas from laboratory to practical applications, these sensors must demonstrate a new value to users by outperforming existing sensors and/or other technical solutions.[2,288,310–312] Such sensor development process typically takes several years from an idea to product launch.[313–315] We summarize the state of the development of MPN sensors in Fig. 29 highlighting research and product development phases that are linked by the "valley of death" – the gap between innovative sensor ideas and their commercial implementation. This progress can be described using technology readiness levels[316] as key milestones. Other metrics can be manufacturing,[317] data,[318,319] system,[320,321] or commercial[322,323] readiness levels. To successfully cross the "valley of death", the key technical risks relevant to specific applications of MPN sensors should be eliminated during the research phase. Risk reduction steps are a part of research activities on the research and development (R&D) roadmap of MPN sensors (Fig. 30). Specifics of these steps are related to sensor and system performance targets in intended applications. Assessment of expected markets provides important information on desired features of sensor products.

Productization and commercialization of sensors is more costly than research – investments are typically 1 : 10 : 100 : 1000 when advancing from proof-of-concept, to prototype, pilot scale production, and product launch.[324] However, in our opinion, the importance of early phases of sensor development is tremendous and will increase further in future in MPN and other sensors. These future ideas and feasibility demonstrations should focus on outperforming existing sensor concepts by at least 10–100 fold. These performance breakthroughs will result in "high value sensors" and will separate these new sensor ideas from the pack of commodity research results. Such performance advantages as to be tested first in pristine lab conditions and then to be further sustained in field tests will be the catalyst to secure interest of governmental and private organizations to invest in commercialization of new generations of sensors.

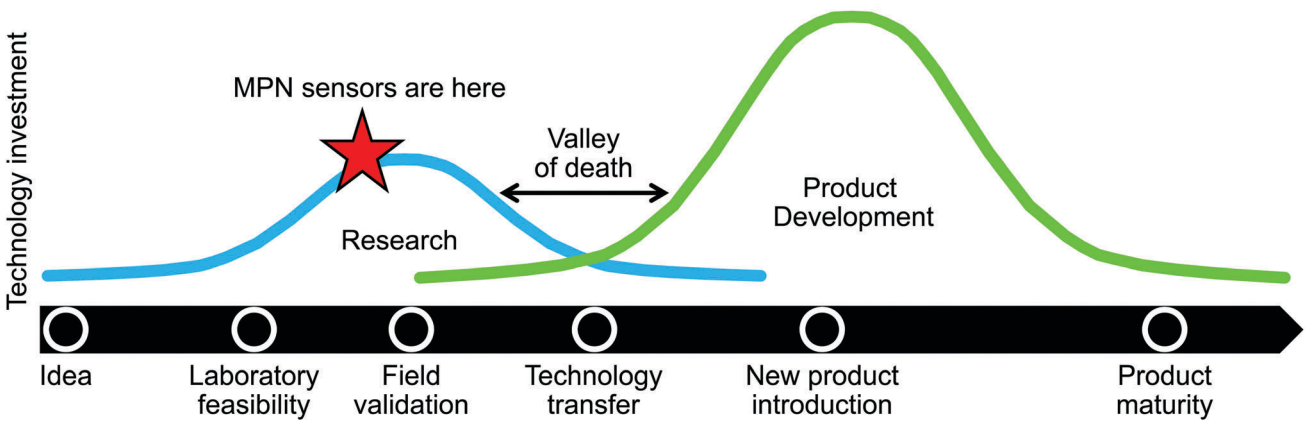

Fig. 29 Present state of the development of MPN sensors.

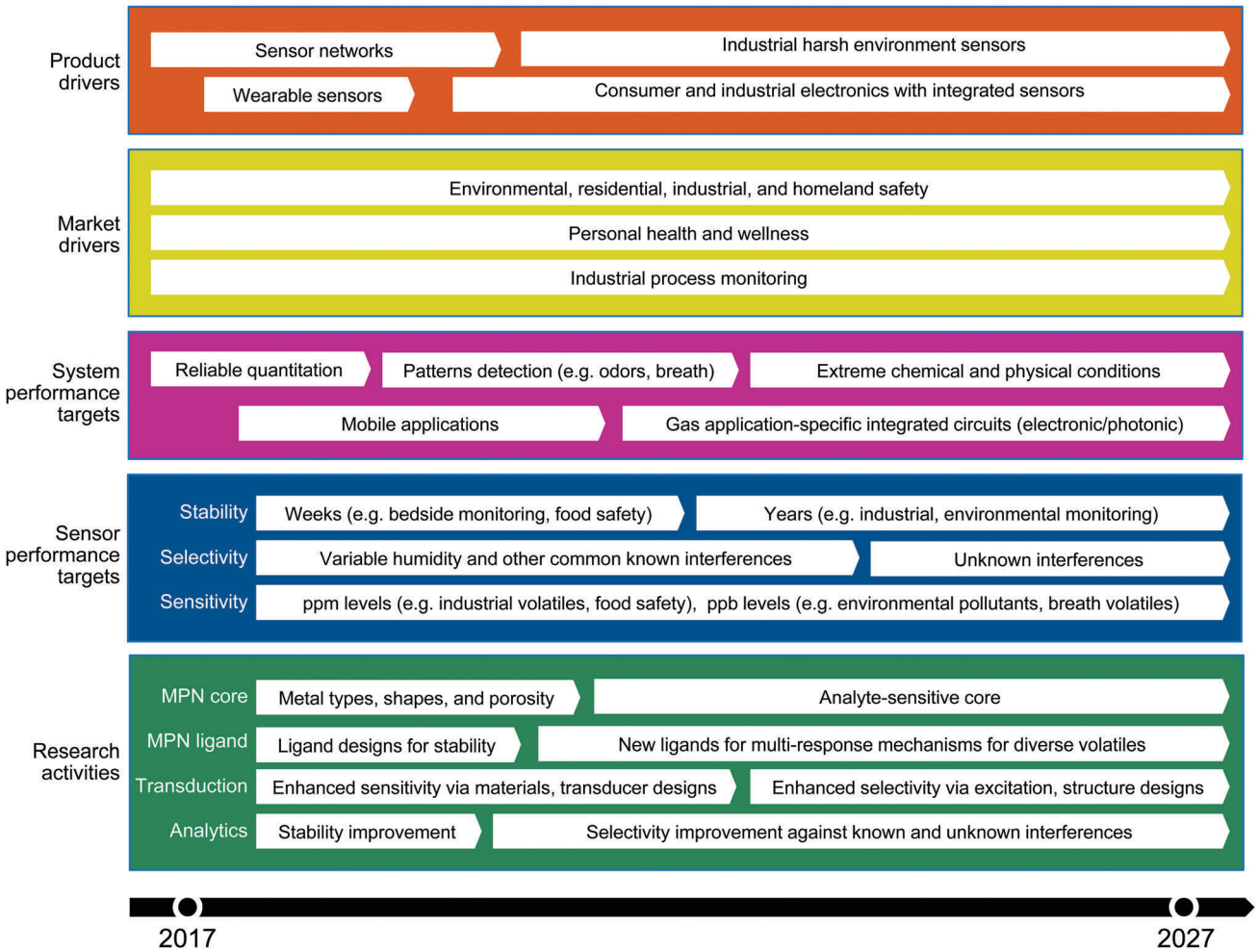

Fig. 30 R&D roadmap of MPN sensors that incorporates research activities, sensor and system performance targets as well as market and product drivers.

New generations of MPN-based and other high value sensors will continue to impact our society in many positive ways in being able to provide accurate real-time surveillance data about environmental and industrial pollutants, to provide real-time monitoring capabilities for improved process and asset control, and to measure and assess health and wellness of individuals. For these and other applications, new generations of sensors will compete with other micro-analytical technologies. The achieved performance characteristics of sensing and other technologies will guarantee their acceptance by users.

Acknowledgements

The author is thankful for discussions with many users of gas and vapor sensors across a wide variety of industries such as Food & Beverage, Oil & Gas, Military & Homeland Security, Transportation, and Healthcare & Biopharmaceutical who were requesting sensors with enhanced selectivity and stability, reduced power consumption, and low acquisition and operation cost *vs.* available sensors. This Review has been inspired by those discussions. Creative scientists and engineers of GE's collaborative teams who coauthored original referenced contributions are gratefully acknowledged. Special thanks go to L. Le Tarte, T. Deng, and S. Zhong for fabricating and analysis of structures in Fig. 23 and to M. Pietrzykowski for computing data in Fig. 18 and 24. GE's work on multivariable gas and vapor sensors has been supported in part from GE Advanced Technology research funds, U.S. Department of The Air Force, Air Force Research Laboratory (AFRL) Contract FA8650-08-C-6869, U.S. Department of Health and Human Services, National Institute of Environmental Health Sciences (NIEHS) Grant 1R01ES016569-01A1, U.S. Department of Defense, Defense Advanced Research Projects Agency (DARPA) Contract W911NF-10-C-0069, U.S. Department of Defense, Technical Support Working Group (TSWG) Project ED.TD.3574, U.S. Department of Energy, National Energy Technology Laboratory Cooperative Agreement FE0027918, U.S. Department of Health and Human Services, and National Institute for Occupational Safety and Health (NIOSH) Contract 211-2015-63806. The findings and conclusions in this review should not be construed to represent any determination or policy of the agencies. The content of the

review does not necessarily reflect the position or the policy of the US Government. Mention of any commercial product does not imply endorsement.

References

1 J. Janata, *Principles of Chemical Sensors*, Springer, New York, NY, 2nd edn, 2009.
2 T. R. Fadel, D. F. Farrell, L. E. Friedersdorf, M. H. Griep, M. D. Hoover, M. A. Meador and M. Meyyappan, *ACS Sens.*, 2016, **1**, 207–216.
3 A. P. F. Turner and N. Magan, *Nat. Rev. Microbiol.*, 2004, **2**, 160–166.
4 D. Janasek, J. Franzke and A. Manz, *Nature*, 2006, **442**, 374–380.
5 A. Lewis and P. Edwards, *Nature*, 2016, **535**, 29–31.
6 R. G. Cooks, Z. Ouyang, Z. Takats and J. M. Wiseman, *Science*, 2006, **311**, 1566–1570.
7 O. S. Wolfbeis, *Angew. Chem., Int. Ed.*, 2013, **52**, 9864–9865.
8 D. T. Allen, V. M. Torres, J. Thomas, D. W. Sullivan, M. Harrison, A. Hendler, S. C. Herndon, C. E. Kolb, M. P. Fraser, A. D. Hill, B. K. Lamb, J. Miskimins, R. F. Sawyer and J. H. Seinfeldi, *Proc. Natl. Acad. Sci. U. S. A.*, 2013, **110**, 17768–17773.
9 J. B. McManus, M. S. Zahniser, D. D. Nelson, J. H. Shorter, S. C. Herndon, D. Jervis, M. Agnese, R. McGovern, T. I. Yacovitch and J. R. Roscioli, *Appl. Phys. B: Lasers Opt.*, 2015, **119**, 203–218.
10 L. Zhang, G. Tian, J. Li and B. Yu, *Appl. Spectrosc.*, 2014, **68**, 1095–1107.
11 RKI Instruments, http://www.rkiinstruments.com/pdf/History.pdf.
12 Priceonomics, 2015, https://priceonomics.com/how-do-you-train-a-dog-to-sniff-bombs/.
13 R. Leung, *60 Minutes CBS News* 2004, http://www.cbsnews.com/news/does-the-nose-know/.
14 A. Williams and L. D. Williams, *Contrivance for automatically detecting the presence of certain gases and vapors*, *US Pat.*, 1143473, 1915.
15 S. Ruben, *Gas and vapor indicating device*, *US Pat.*, 1559461, 1925.
16 A. Bielanski, J. Deren and J. Haber, *Nature*, 1957, **179**, 668–669.
17 J. P. Dolan and W. M. Jordan, *Detection Device*, *US Pat.*, 3045198, 1962.
18 T. Seiyama, A. Kato, K. Fujiishi and M. Nagatani, *Anal. Chem.*, 1962, **34**, 1502–1503.
19 W. H. King, Jr., *Anal. Chem.*, 1964, **36**, 1735–1739.
20 I. Bergman, *Nature*, 1968, **218**, 396.
21 E. E. Hardy, D. J. David, N. S. Kapany and F. C. Unterleitner, *Nature*, 1975, **257**, 666–667.
22 I. Lundström, S. Shivaraman, C. Svensson and L. Lundkvist, *Appl. Phys. Lett.*, 1975, **26**, 55–57.
23 W. Göpel and K. D. Schierbaum, *Sens. Actuators, B*, 1995, **26-27**, 1–12.
24 A. Kolmakov and M. Moskovits, *Annu. Rev. Mater. Res.*, 2004, 151–180.
25 N. Barsan, D. Koziej and U. Weimar, *Sens. Actuators, B*, 2007, **121**, 18–35.
26 K. Govardhan and A. Nirmala Grace, *Sens. Lett.*, 2016, **14**, 741–750.
27 G. Korotcenkov and B. K. Cho, *Sens. Actuators, B*, 2017, **244**, 182–210.
28 R. M. Ma, S. Ota, Y. Li, S. Yang and X. Zhang, *Nat. Nanotechnol.*, 2014, **9**, 600–604.
29 R. Lv, G. Chen, Q. Li, A. McCreary, A. Botello-Méndez, S. V. Morozov, L. Liang, X. Declerck, N. Perea-López, D. A. Cullen, S. Feng, A. L. Elías, R. Cruz-Silva, K. Fujisawa, M. Endo, F. Kang, J. C. Charlier, V. Meunier, M. Pan, A. R. Harutyunyan, K. S. Novoselov and M. Terrones, *Proc. Natl. Acad. Sci. U. S. A.*, 2015, **112**, 14527–14532.
30 S. Y. Cho, S. J. Kim, Y. Lee, J. S. Kim, W. B. Jung, H. W. Yoo, J. Kim and H. T. Jung, *ACS Nano*, 2015, **9**, 9314–9321.
31 S. M. Mortazavi Zanjani, M. M. Sadeghi, M. Holt, S. F. Chowdhury, L. Tao and D. Akinwande, *Appl. Phys. Lett.*, 2016, **108**, 033106.
32 W. T. Koo, S. J. Choi, S. J. Kim, J. S. Jang, H. L. Tuller and I. D. Kim, *J. Am. Chem. Soc.*, 2016, **138**, 13431–13437.
33 F. Favier, E. C. Walter, M. P. Zach, T. Benter and R. M. Penner, *Science*, 2001, **293**, 2227–2231.
34 A. Salehi-Khojin, K. Y. Lin, C. R. Field and R. I. Masel, *Science*, 2010, **329**, 1327–1330.
35 G. S. Kulkarni, K. Reddy, Z. Zhong and X. Fan, *Nat. Commun.*, 2014, **5**, 4376.
36 W. Xuan, M. He, N. Meng, X. He, W. Wang, J. Chen, T. Shi, T. Hasan, Z. Xu, Y. Xu and J. K. Luo, *Sci. Rep.*, 2014, **4**, 7206.
37 A. Lichtenstein, E. Havivi, R. Shacham, E. Hahamy, R. Leibovich, A. Pevzner, V. Krivitsky, G. Davivi, I. Presman, R. Elnathan, Y. Engel, E. Flaxer and F. Patolsky, *Nat. Commun.*, 2014, **5**, 4195.
38 R. Zhang, T. Zhang, T. Zhou, Z. Lou, J. Deng and L. Wang, *RSC Adv.*, 2016, **6**, 66738–66744.
39 K. Fu, S. Chen, J. Zhao and B. G. Willis, *ACS Sens.*, 2016, **1**, 444–450.
40 A. Hierlemann and R. Gutierrez-Osuna, *Chem. Rev.*, 2008, **108**, 563–613.
41 F. Röck, N. Barsan and U. Weimar, *Chem. Rev.*, 2008, **108**, 705–725.
42 R. A. Potyrailo, C. Surman, N. N. Nagraj and A. Burns, *Chem. Rev.*, 2011, **111**, 7315–7354.
43 A. C. Lewis, J. D. Lee, P. M. Edwards, M. D. Shaw, M. J. Evans, S. J. Moller, K. R. Smith, J. W. Buckley, M. Ellis, S. R. Gillot and A. White, *Faraday Discuss.*, 2016, **189**, 85–103.
44 R. A. Potyrailo, *Chem. Rev.*, 2016, **116**, 11877–11923.
45 K. Persaud and G. Dodd, *Nature*, 1982, **299**, 352–355.
46 S. H. Lim, L. Feng, J. W. Kemling, C. J. Musto and K. S. Suslick, *Nat. Chem.*, 2009, 562–567.
47 G. Peng, U. Tisch, O. Adams, M. Hakim, N. Shehada, Y. Y. Broza, S. Billan, R. Abdah-Bortnyak, A. Kuten and H. Haick, *Nat. Nanotechnol.*, 2009, **4**, 669–673.

48 R. Beccherelli, E. Zampetti, S. Pantalei, M. Bernabei and K. C. Persaud, *Sens. Actuators, B*, 2010, **146**, 446–452.
49 J. R. Askim, M. Mahmoudi and K. S. Suslick, *Chem. Soc. Rev.*, 2013, **42**, 8649–8682.
50 P. Boeker, *Sens. Actuators, B*, 2014, **204**, 2–17.
51 S. W. Brooks, D. R. Moore, E. B. Marzouk, F. R. Glenn and R. M. Hallock, *Cancer Invest.*, 2015, **33**, 411–419.
52 K. J. Johnson and S. L. Rose-Pehrsson, *Annu. Rev. Anal. Chem.*, 2015, **8**, 287–310.
53 M. Peris and L. Escuder-Gilabert, *Trends Food Sci. Technol.*, 2016, **58**, 40–54.
54 J. Burlachenko, I. Kruglenko, B. Snopok and K. Persaud, *Trends Anal. Chem.*, 2016, **82**, 222–236.
55 M. J. Kangas, R. M. Burks, J. Atwater, R. M. Lukowicz, P. Williams and A. E. Holmes, *Crit. Rev. Anal. Chem.*, 2017, **47**, 138–153.
56 T. Wasilewski, J. Gębicki and W. Kamysz, *Biosens. Bioelectron.*, 2017, **87**, 480–494.
57 H. V. Shurmer, *Sens. Actuators, B*, 1990, **1**, 48–53.
58 W. Bourgeois, A.-C. Romain, J. Nicolas and R. M. Stuetz, *J. Environ. Monit.*, 2003, **5**, 852–860.
59 R. Gutierrez-Osuna and A. Hierlemann, *Annu. Rev. Anal. Chem.*, 2010, **3**, 255–276.
60 S. E. Stitzel, M. J. Aernecke and D. R. Walt, *Annu. Rev. Biomed. Eng.*, 2011, **13**, 1–25.
61 M. E. H. Amrani, R. M. Dowdeswell, P. A. Payne and K. C. Persaud, *Sens. Actuators, B*, 1997, **44**, 512–516.
62 L. Torsi, A. Dodabalapur, L. Sabbatini and P. G. Zambonin, *Sens. Actuators, B*, 2000, **67**, 312–316.
63 R. D. Yang, B. Fruhberger, J. Park and A. C. Kummel, *Appl. Phys. Lett.*, 2006, **88**, 074104.
64 R. A. Potyrailo and W. G. Morris, *Anal. Chem.*, 2007, **79**, 45–51.
65 R. A. Potyrailo and W. G. Morris, *Rev. Sci. Instrum.*, 2007, **78**, 072214.
66 R. A. Potyrailo, H. Mouquin and W. G. Morris, *Talanta*, 2008, **75**, 624–628.
67 R. A. Potyrailo, W. G. Morris, T. Sivavec, H. W. Tomlinson, S. Klensmeden and K. Lindh, *Wirel. Commun. Mob. Comput.*, 2009, **9**, 1318–1330.
68 R. A. Potyrailo, C. Surman, S. Go, Y. Lee, T. Sivavec and W. G. Morris, *J. Appl. Phys.*, 2009, **106**, 124902.
69 R. A. Potyrailo, C. Surman and W. G. Morris, *J. Comb. Chem.*, 2009, **11**, 598–603.
70 R. A. Potyrailo, H. Ghiradella, A. Vertiatchikh, K. Dovidenko, J. R. Cournoyer and E. Olson, *Nat. Photonics*, 2007, **1**, 123–128.
71 R. A. Potyrailo, T. Starkey, P. Vukusic, H. Ghiradella, M. Vasudev, T. Bunning, R. R. Naik, Z. Tang, M. Larsen, T. Deng, S. Zhong, M. Palacios, J. C. Grande, G. Zorn, G. Goddard and S. Zalubovsky, *Proc. Natl. Acad. Sci. U. S. A.*, 2013, **110**, 15567–15572.
72 N. Nagraj, J. M. Slocik, D. M. Phillips, N. Kelley-Loughnane, R. R. Naik and R. A. Potyrailo, *Analyst*, 2013, **138**, 4334–4339.
73 R. A. Potyrailo, R. K. Bonam, J. G. Hartley, T. A. Starkey, P. Vukusic, M. Vasudev, T. Bunning, R. R. Naik, Z. Tang, M. Palacios, M. Larsen, L. A. Le Tarte, J. C. Grande, T. Deng and S. Zhong, *Nat. Commun.*, 2015, **6**, 7959.
74 K. Scholten, K. Reddy, X. Fan and E. T. Zellers, *Anal. Methods*, 2013, **5**, 4268–4272.
75 L. P. Biró, K. Kertész, Z. Vértesy and Z. Bálint, *Proc. SPIE*, 2008, **7057**, 705706.
76 C. Zhang, L. K. Wright, K. Scholten, X. Fan and E. T. Zellers, *Proc. Transducers '15*, 2015, 1448–1451.
77 G. Piszter, K. Kertész, Z. Bálint and L. P. Biró, *Sensors*, 2016, **16**, 1446.
78 B. Wang, J. C. Cancilla, J. S. Torrecilla and H. Haick, *Nano Lett.*, 2014, **14**, 933–938.
79 R. A. Potyrailo, M. D. Pietrzykowski and Y. Lee, *Methods for analyte detection*, *US Pat.*, 9052263, 2015.
80 R. A. Potyrailo, C. M. Surman, A. A. P. Burns and N. Nagraj, *Highly selective chemical and biological sensors*, *US Pat.*, 9638653, 2017.
81 R. A. Potyrailo, C. Surman, W. G. Morris, S. Go, Y. Lee, J. A. Cella and K. S. Chichak, *IEEE Int. Conf. on RFID, IEEE RFID*, 2010, 22–28.
82 R. A. Potyrailo, A. Burns, C. Surman, D. J. Lee and E. McGinniss, *Analyst*, 2012, **137**, 2777–2781.
83 R. A. Potyrailo and R. R. Naik, *Annu. Rev. Mater. Res.*, 2013, **43**, 307–334.
84 F. Josse, R. Lukas, R. Zhou, S. Schneider and D. Everhart, *Sens. Actuators, B*, 1996, **35-36**, 363–369.
85 F. Musio and M. C. Ferrara, *Sens. Actuators, B*, 1997, **41**, 97–103.
86 M. E. H. Amrani, K. C. Persaud and P. A. Payne, *Meas. Sci. Technol.*, 1995, **6**, 1500–1507.
87 M. E. H. Amrani, P. A. Payne and K. C. Persaud, *Sens. Actuators, B*, 1996, **33**, 137–141.
88 R. A. Potyrailo, N. Nagraj, C. Surman, H. Boudries, H. Lai, J. M. Slocik, N. Kelley-Loughnane and R. R. Naik, *Trends Anal. Chem.*, 2012, **40**, 133–145.
89 R. A. Potyrailo, J. A. Cella, C. M. Surman, K. S. Chichak and S. Go, *Sensor system and methods for selective analyte detection using resonance sensor circuit*, *US Pat.*, 8364419, 2013.
90 R. A. Potyrailo, *Method and system for performance enhancement of resonant sensors*, *US Pat.*, 8736425, 2014.
91 W. T. Chen, K. M. E. Stewart, R. R. Mansour and A. Penlidis, *Sens. Actuators, A*, 2015, **230**, 63–73.
92 U. Weimar and W. Göpel, *Sens. Actuators, B*, 1995, **26**, 13–18.
93 Y. Liu and Y. Lei, *Sens. Actuators, B*, 2013, **188**, 1141–1147.
94 M. W. K. Nomani, D. Kersey, J. James, D. Diwan, T. Vogt, R. A. Webb and G. Koley, *Sens. Actuators, B*, 2011, **160**, 251–259.
95 R. A. Potyrailo, H. T. Lam, Z. Tang and N. Nagraj, *Sensors for gas dosimetry*, *US Pat.*, 9494541, 2016.
96 R. A. Potyrailo, Z. Tang, B. Bartling, N. Nagraj and V. Bromberg, *Materials and Sensors For Detecting Gaseous Agents*, *US Pat.*, Application 20160187280, 2016.
97 S. Nakagomi, A. Fukumura, Y. Kokubun, S. Savage, H. Wingbrant, M. Andersson, I. Lundström, M. Löfdahl and A. L. Spetz, *Sens. Actuators, B*, 2005, **108**, 501–507.

98 C. Bur, M. Bastuck, A. L. Spetz, M. Andersson and A. Schütze, *Sens. Actuators, B*, 2014, **193**, 931–940.
99 C. Bur, M. Bastuck, D. Puglisi, A. Schütze, A. Lloyd Spetz and M. Andersson, *Sens. Actuators, B*, 2015, **214**, 225–233.
100 J. E. Royer, E. D. Kappe, C. Zhang, D. T. Martin, W. C. Trogler and A. C. Kummel, *J. Phys. Chem. C*, 2012, **116**, 24566–24572.
101 E. S. Snow and F. K. Perkins, *Nano Lett.*, 2005, **5**, 2414–2417.
102 R. A. Potyrailo, H. Boudries, H. Lai, N. Nagraj, Z. Tang, C. Surman, W. G. Morris, J. Ashe and H. Lam, The 2011 Chemical and Biological Defense Science and Technology (CBD S&T) Conference, Las Vegas, Nov 14–18, 2011, M19-012.
103 S. Rumyantsev, G. Liu, M. S. Shur, R. A. Potyrailo and A. A. Balandin, *Nano Lett.*, 2012, **12**, 2294–2298.
104 N. C. Speller, N. Siraj, B. P. Regmi, H. Marzoughi, C. Neal and I. M. Warner, *Anal. Chem.*, 2015, **87**, 5156–5166.
105 R. A. Potyrailo, Z. Ding, M. D. Butts, S. E. Genovese and T. Deng, *IEEE Sens. J.*, 2008, **8**, 815–822.
106 B. P. Regmi, J. Monk, B. El-Zahab, S. Das, F. R. Hung, D. J. Hayes and I. M. Warner, *J. Mater. Chem. C*, 2012, **22**, 13732–13741.
107 G. Shuster, S. Baltianski, Y. Tsur and H. Haick, *J. Phys. Chem. Lett.*, 2011, **2**, 1912–1916.
108 R. A. Potyrailo, N. Nagraj, Y. Lee, C. Surman, J. M. Slocik, D. M. Gallagher, J. A. Hagen, R. R. Naik, N. Kelley-Loughnane and W. Lyon, The 2011 Chemical and Biological Defense Science and Technology (CBD S&T) Conference, Las Vegas, Nov 14–18, 2011, W11-009.
109 R. A. Potyrailo, M. Larsen and O. Riccobono, *Angew. Chem., Int. Ed.*, 2013, **52**, 10360–10364.
110 N. A. Joy, M. I. Nandasiri, P. H. Rogers, W. Jiang, T. Varga, S. V. N. T. Kuchibhatla, S. Thevuthasan and M. A. Carpenter, *Anal. Chem.*, 2012, **84**, 5025–5034.
111 N. Karker, G. Dharmalingam and M. A. Carpenter, *ACS Nano*, 2014, **8**, 10953–10962.
112 R. A. Potyrailo, D. W. Sexton and S. Y. Go, *Sensing system and method*, *US Pat.*, Application 20160187277, 2016.
113 R. Ionescu, Y. Zilberman and H. Haick, *Proc. IEEE Sens.*, 2011, 1070–1073.
114 G. Piszter, K. Kertész, Z. Vértesy, Z. Bálint and L. P. Biró, *Opt. Express*, 2014, **22**, 22649–22660.
115 G. Piszter, K. Kertész, Z. Vértesy, Z. Bálint and L. P. Biró, *Materials Today: Proceedings*, 2014, **1**, 216–220.
116 Y. Kunugi, K. Nigorikawa, Y. Harima and K. Yamashita, *J. Chem. Soc., Chem. Commun.*, 1994, 873–874.
117 A. F. Holloway, A. Nabok, M. Thompson, A. K. Ray and T. Wilkop, *Sens. Actuators, B*, 2004, **99**, 355–360.
118 C. Surman, M. Pietrzykowski, N. Nagraj, W. Morris, A. Sundaresan, Z. Tang and R. A. Potyrailo, *IEEE Future Instrum. Intl. Workshop*, 2011, 28–31.
119 N. Shehada, G. Brönstrup, K. Funka, S. Christiansen, M. Leja and H. Haick, *Nano Lett.*, 2015, **15**, 1288–1295.
120 D. J. Wales, J. Grand, V. P. Ting, R. D. Burke, K. J. Edler, C. R. Bowen, S. Mintova and A. D. Burrows, *Chem. Soc. Rev.*, 2015, **44**, 4290–4321.
121 F. R. Baptista, S. A. Belhout, S. Giordani and S. J. Quinn, *Chem. Soc. Rev.*, 2015, **44**, 4433–4453.
122 X. Zhou, S. Lee, Z. Xu and J. Yoon, *Chem. Rev.*, 2015, **115**, 7944–8000.
123 H. S. Jung, P. Verwilst, W. Y. Kim and J. S. Kim, *Chem. Soc. Rev.*, 2016, **45**, 1242–1256.
124 A. Kaushik, R. Kumar, S. K. Arya, M. Nair, B. D. Malhotra and S. Bhansali, *Chem. Rev.*, 2015, **115**, 4571–4606.
125 C. Zhang, P. Chen and W. Hu, *Chem. Soc. Rev.*, 2015, **44**, 2087–2107.
126 K. L. Diehl and E. V. Anslyn, *Chem. Soc. Rev.*, 2013, **42**, 8596–8611.
127 L. Torsi, M. Magliulo, K. Manoli and G. Palazzo, *Chem. Soc. Rev.*, 2013, **42**, 8612–8628.
128 A. Ulman, *Chem. Rev.*, 1996, **96**, 1533–1554.
129 J. C. Love, L. A. Estroff, J. K. Kriebel, R. G. Nuzzo and G. M. Whitesides, *Chem. Rev.*, 2005, **105**, 1103–1169.
130 H. Wohltjen and A. W. Snow, *Anal. Chem.*, 1998, **70**, 2856–2859.
131 Q.-Y. Cai and E. T. Zellers, *Anal. Chem.*, 2002, **74**, 3533–3539.
132 W. H. Steinecker, M. P. Rowe and E. T. Zellers, *Anal. Chem.*, 2007, **79**, 4977–4986.
133 E. Dovgolevsky, G. Konvalina, U. Tisch and H. Haick, *J. Phys. Chem. C*, 2010, **114**, 14042–14049.
134 M. Y. Bashouti, A. S. De La Zerda, D. Geva and H. Haick, *J. Phys. Chem. C*, 2014, **118**, 1903–1909.
135 F. J. Ibañez and F. P. Zamborini, *Small*, 2012, **8**, 174–202.
136 S. Shan, W. Zhao, J. Luo, J. Yin, J. C. Switzer, P. Joseph, S. Lu, M. Poliks and C. J. Zhong, *J. Mater. Chem. C*, 2014, **2**, 1893–1903.
137 N. Olichwer, A. Meyer, M. Yesilmen and T. Vossmeyer, *J. Mater. Chem. C*, 2016, **4**, 8214–8225.
138 W. Zhao, L. F. Al-Nasser, S. Shan, J. Li, Z. Skeete, N. Kang, J. Luo, S. Lu, C. J. Zhong, C. J. Grausgruber and R. Harris, *Sens. Actuators, B*, 2016, **232**, 292–299.
139 Y. Yang, L. Cornwell, F. Ibanez and F. P. Zamborini, *ChemElectroChem*, 2016, **3**, 1230–1236.
140 M. K. Nakhleh, H. Amal, R. Jeries, Y. Y. Broza, M. Aboud, A. Gharra, H. Ivgi, S. Khatib, S. Badarneh and L. Har-Shai, *ACS Nano*, 2017, **11**, 112–125.
141 T. E. Mlsna, S. Cemalovic, M. Warburton, S. T. Hobson, D. Mlsna and S. V. Patel, *Sens. Actuators, B*, 2006, **116**, 192–201.
142 P. Pang, J. Guo, S. Wu and Q. Cai, *Sens. Actuators, B*, 2006, **114**, 799–803.
143 J. Guo, P. Pang and Q. Cai, *Sens. Actuators, B*, 2007, **120**, 521–528.
144 F. P. Zamborini, M. C. Leopold, J. F. Hicks, P. J. Kulesza, M. A. Malik and R. W. Murray, *J. Am. Chem. Soc.*, 2002, **124**, 8958–8964.
145 J. W. Grate, D. A. Nelson and R. Skaggs, *Anal. Chem.*, 2003, **75**, 1868–1879.
146 K. Scholten, L. K. Wright and E. T. Zellers, *IEEE Sens. J.*, 2013, **13**, 2146–2154.
147 K.-J. Chen and C.-J. Lu, *Talanta*, 2010, **81**, 1670–1675.

148 M. C. Dalfovo, R. C. Salvarezza and F. J. Ibañez, *Anal. Chem.*, 2012, **84**, 4886–4892.
149 R. Ionescu, U. Cindemir, T. G. Welearegay, R. Calavia, Z. Haddi, Z. Topalian, C. G. Granqvist and E. Llobet, *Sens. Actuators, B*, 2017, **239**, 455–461.
150 M. E. Franke, T. J. Koplin and U. Simon, *Small*, 2006, **2**, 36–50.
151 C. Drake, S. Deshpande, D. Bera and S. Seal, *Int. Mater. Rev.*, 2007, **52**, 289–316.
152 A. Zabet-Khosousi and A.-A. Dhirani, *Chem. Rev.*, 2008, **108**, 4072–4124.
153 E. Dovgolevsky, U. Tisch and H. Haick, *Small*, 2009, **5**, 1158–1161.
154 M. P. Rowe, K. E. Plass, K. Kim, Ç. Kurdak, E. T. Zellers and A. J. Matzger, *Chem. Mater.*, 2004, **16**, 3513–3517.
155 T. K. Sau and C. J. Murphy, *J. Am. Chem. Soc.*, 2004, **126**, 8648–8649.
156 Y. Joseph, B. Guse, A. Yasuda and T. Vossmeyer, *Sens. Actuators, B*, 2004, **98**, 188–195.
157 M. R. M. Hosseini, H. Jamalabadi and M. Najafi, *Measurement*, 2013, **46**, 3328–3332.
158 F. J. Ibañez and F. P. Zamborini, *Langmuir*, 2006, **22**, 9789–9796.
159 F. J. Ibañez and F. P. Zamborini, *J. Am. Chem. Soc.*, 2008, **130**, 622–633.
160 M. Moreno, F. J. Ibañez, J. B. Jasinski and F. P. Zamborini, *J. Am. Chem. Soc.*, 2011, **133**, 4389–4397.
161 M. F. Calderón, E. Zelaya, G. A. Benitez, P. L. Schilardi, A. H. Creus, A. G. Orive, R. C. Salvarezza and F. J. Ibañez, *Langmuir*, 2013, **29**, 4670–4678.
162 L. Wang, X. Shi, N. N. Kariuki, M. Schadt, G. R. Wang, Q. Rendeng, J. Choi, J. Luo, S. S. Lu and C.-J. Zhong, *J. Am. Chem. Soc.*, 2007, **129**, 2161–2170.
163 F. J. Ibañez and F. P. Zamborini, *ACS Nano*, 2008, **2**, 1543–1552.
164 Y. Joseph, A. Peie, X. Chen, J. Michl, T. Vossmeyer and A. Yasuda, *J. Phys. Chem. C*, 2007, **111**, 12855–12859.
165 G. Yang, L. Hu, T. D. Keiper, P. Xiong and D. T. Hallinan, *Langmuir*, 2016, **32**, 4022–4033.
166 K. Fu, S. Li, X. Jiang, Y. Wang and B. G. Willis, *Langmuir*, 2013, **29**, 14335–14343.
167 C. Kunstmann-Olsen, D. Belić, D. F. Bradley, M. P. Grzelczak and M. Brust, *Chem. Mater.*, 2016, **28**, 2970–2980.
168 E. García-Berríos, T. Gao, M. D. Woodka, S. Maldonado, B. S. Brunschwig, M. W. Ellsworth and N. S. Lewis, *J. Phys. Chem. C*, 2010, **114**, 21914–21920.
169 E. García-Berríos, T. Gao, J. C. Theriot, M. D. Woodka, B. S. Brunschwig and N. S. Lewis, *J. Phys. Chem. C*, 2011, **115**, 6208–6217.
170 L. J. Hubble, J. S. Cooper, A. Sosa-Pintos, H. Kiiveri, E. Chow, M. S. Webster, L. Wieczorek and B. Raguse, *ACS Comb. Sci.*, 2015, **17**, 120–129.
171 N. Krasteva, B. Guse, I. Besnard, A. Yasuda and T. Vossmeyer, *Sens. Actuators, B*, 2003, **92**, 137–143.
172 N. Krasteva, Y. Fogel, R. E. Bauer, K. Müllen, Y. Joseph, N. Matsuzawa, A. Yasuda and T. Vossmeyer, *Adv. Funct. Mater.*, 2007, **17**, 881–888.
173 M. D. Hanwell, S. Y. Heriot, T. H. Richardson, N. Cowlam and L. M. Ross, *Colloids Surf., A*, 2006, **284–285**, 379–383.
174 J. P. Choi, M. M. Coble, M. R. Branham, J. M. DeSimone and R. W. Murray, *J. Phys. Chem. C*, 2007, **111**, 3778–3785.
175 M. S. Webster, J. S. Cooper, E. Chow, L. J. Hubble, A. Sosa-Pintos, L. Wieczorek and B. Raguse, *Sens. Actuators, B*, 2015, **220**, 895–902.
176 N. Kahn, O. Lavie, M. Paz, Y. Segev and H. Haick, *Nano Lett.*, 2015, **15**, 7023–7028.
177 G. Neri, *Chemosensors*, 2015, **3**, 1–20.
178 C. Pacholski, *Sensors*, 2013, **13**, 4694–4713.
179 H.-L. Zhang, S. D. Evans, J. R. Henderson, R. E. Miles and T.-H. Shen, *Nanotechnology*, 2002, **13**, 439–444.
180 W. Zhao, T. Rovere, D. Weerawarne, G. Osterhoudt, N. Kang, P. Joseph, J. Luo, B. Shim, M. Poliks and C. J. Zhong, *ACS Nano*, 2015, **9**, 6168–6177.
181 G. Yang and D. T. Hallinan, *Nanotechnology*, 2016, **27**, 225604.
182 R. H. Terrill, T. A. Postlethwaite, C.-H. Chen, C.-D. Poon, A. Terzis, A. Chen, J. E. Hutchison, M. R. Clark, G. Wignall, J. D. Londono, R. Superfine, M. Falvo, C. S. Johnson Jr., E. T. Samulski and R. W. Murray, *J. Am. Chem. Soc.*, 1995, **117**, 12537–12548.
183 A. M. Kummer, A. Hierlemann and H. Baltes, *Anal. Chem.*, 2004, **76**, 2470–2477.
184 J. W. Grate, A. Snow, D. S. Ballantine, Jr., H. Wohltjen, M. H. Abraham, R. A. McGill and P. Sasson, *Anal. Chem.*, 1988, **60**, 869–875.
185 J. W. Grate, S. J. Patrash and M. H. Abraham, *Anal. Chem.*, 1995, **67**, 2162–2169.
186 J. M. Wessels, H. G. Nothofer, W. E. Ford, F. Von Wrochem, F. Scholz, T. Vossmeyer, A. Schroedter, H. Weller and A. Yasuda, *J. Am. Chem. Soc.*, 2004, **126**, 3349–3356.
187 H. Hövel, S. Fritz, A. Hilger, U. Kreibig and M. Vollmer, *Phys. Rev. B: Condens. Matter Mater. Phys.*, 1993, **48**, 18178–18188.
188 A. C. Templeton, J. J. Pietron, R. W. Murray and P. Mulvaney, *J. Phys. Chem. B*, 2000, **104**, 564–570.
189 X. Yu, N. Malvankar, R. Landis, S. Eymur, O. R. Miranda and V. M. Rotello, *Small*, 2015, **11**, 3814–3821.
190 R. A. Potyrailo and J. A. Dieringer, *ISOCS/IEEE International Symposium on Olfaction and Electronic Nose*, 2017, 4–6.
191 R. A. Potyrailo, *Intl. Conf. Sens. Electron. Instrum. Adv.*, Barcelona, 22–23 September, 2016.
192 F. I. Bohrer, E. Covington, Ç. Kurdak and E. T. Zellers, *Proc. Transducers '09*, 2009, 148–151.
193 A. W. Snow, F. K. Perkins, M. G. Ancona, J. T. Robinson, E. S. Snow and E. E. Foos, *IEEE Sens. J.*, 2015, **15**, 1301–1320.
194 F. I. Bohrer, E. Covington, C. Kurdak and E. T. Zellers, *Anal. Chem.*, 2011, **83**, 3687–3695.
195 L. Wang, J. Luo, J. Yin, H. Zhang, J. Wu, X. Shi, E. Crew, Z. Xu, Q. Rendeng, S. Lu, M. Poliks, B. Sammakia and C.-J. Zhong, *J. Mater. Chem.*, 2010, **20**, 907–915.
196 M. G. Ancona, A. W. Snow, E. E. Foos, W. Kruppa and R. Bass, *IEEE Sens. J.*, 2006, **6**, 1403–1413.

197 W. H. Steinecker, S. K. Kim, F. I. Bohrer, L. Farina, Ç. Kurdak and E. T. Zellers, *IEEE Sens. J.*, 2011, **11**, 469–480.
198 M. D. Porter, T. B. Bright, D. L. Allara and C. E. D. Chidsey, *J. Am. Chem. Soc.*, 1987, **109**, 3559–3568.
199 A. Demoz and J. Harrison, *Langmuir*, 1993, **9**, 1046–1050.
200 M. A. Rampi, O. J. A. Schueller and G. M. Whitesides, *Appl. Phys. Lett.*, 1998, **72**, 1781–1783.
201 R. A. Potyrailo, *TSensors Summit, Executive Vision Casting Forum*, Orlando, FL, December 08–10, http://tsensorssummit.org/Resources/XF%208%20-%20Potyrailo.pdf, 2015.
202 R. A. Potyrailo, J. M. Ashe, S. S. Hasan, N. K. Rao and K. Sundaresan, *Systems and methods for monitoring sensors*, *US Pat.*, 9389260, 2016.
203 R. A. Potyrailo, *Wearable Technology Show*, London, 2016.
204 J. R. Carey, K. S. Suslick, K. I. Hulkower, J. A. Imlay, K. R. C. Imlay, C. K. Ingison, J. B. Ponder, A. Sen and A. E. Wittrig, *J. Am. Chem. Soc.*, 2011, **133**, 7571–7576.
205 R. A. Potyrailo, N. Nagraj, Z. Tang, F. J. Mondello, C. Surman and W. Morris, *J. Agric. Food Chem.*, 2012, **60**, 8535–8543.
206 R. A. Potyrailo, C. M. Surman, S. Y. Go and Y. Lee, *Resonant sensor and an associated sensing method*, *US Pat.*, 9538657, 2017.
207 B. R. Goldsmith, J. J. Mitala, J. Josue, A. Castro, M. B. Lerner, T. H. Bayburt, S. M. Khamis, R. A. Jones, J. G. Brand, S. G. Sligar, C. W. Luetje, A. Gelperin, P. A. Rhodes, B. M. Discher and A. T. C. Johnson, *ACS Nano*, 2011, **5**, 5408–5416.
208 J. Im, S. K. Sengupta, M. F. Baruch, C. D. Granz, S. Ammu, S. K. Manohar and J. E. Whitten, *Sens. Actuators, B*, 2011, **156**, 715–722.
209 A. W. Snow, M. G. Ancona and D. Park, *Langmuir*, 2012, **28**, 15438–15443.
210 Q. Chen, A. Liu, J. Zhao and Q. Ouyang, *J. Pharm. Biomed. Anal.*, 2013, **84**, 77–83.
211 D. Huo, Y. Wu, M. Yang, H. Fa, X. Luo and C. Hou, *Food Chem.*, 2014, **145**, 639–645.
212 D. Dutta, S. Ghosh, M. Narjinary, N. Bhattacharyya and R. Bandyopadhyay, *Sens. Lett.*, 2016, **14**, 396–401.
213 I. A. Levitsky, *Sensors*, 2015, **15**, 19968–19991.
214 H. Butt, A. K. Yetisen, D. Mistry, S. A. Khan, M. U. Hassan and S. H. Yun, *Adv. Opt. Mater.*, 2016, **4**, 497–504.
215 K. R. Phillips, G. T. England, S. Sunny, E. Shirman, T. Shirman, N. Vogel and J. Aizenberg, *Chem. Soc. Rev.*, 2016, **45**, 281–322.
216 S. R. Mouchet, M. Lobet, B. Kolaric, A. M. Kaczmarek, R. Van Deun, P. Vukusic, O. Deparis and E. Van Hooijdonk, *Proc. R. Soc. B*, 2016, **283**, 20162334.
217 A. G. Dumanli and T. Savin, *Chem. Soc. Rev.*, 2016, **45**, 6698–6724.
218 T. Lu, S. Zhu, Z. Chen, W. Wang, W. Zhang and D. Zhang, *Nanoscale*, 2016, **8**, 10316–10322.
219 T. Lu, W. Peng, S. Zhu and D. Zhang, *Nanotechnology*, 2016, **27**, 122001.
220 Q. Li, Q. Zeng, L. Shi, X. Zhang and K.-Q. Zhang, *J. Mater. Chem. C*, 2016, **4**, 1752–1763.
221 Y. Y. Diao, X. Y. Liu, G. W. Toh, L. Shi and J. Zi, *Adv. Funct. Mater.*, 2013, **23**, 5373–5380.
222 Z. Xie, K. Cao, Y. Zhao, L. Bai, H. Gu, H. Xu and Z. Z. Gu, *Adv. Mater.*, 2014, **26**, 2413–2418.
223 Y. Zhang, J. Qiu, R. Hu, P. Li, L. Gao, L. Heng, B. Z. Tang and L. Jiang, *Phys. Chem. Chem. Phys.*, 2015, **17**, 9651–9658.
224 P. Ganter, K. Szendrei and B. V. Lotsch, *Adv. Mater.*, 2016, **28**, 7436–7442.
225 Y.-L. Ko, H.-P. Tsai, K.-Y. Lin, Y.-C. Chen and H. Yang, *J. Colloid Interface Sci.*, 2017, **487**, 360–369.
226 J. Gao, T. Gao and M. J. Sailor, *Appl. Phys. Lett.*, 2000, **77**, 901–903.
227 K. P. Raymond, I. B. Burgess, M. H. Kinney, M. Lončar and J. Aizenberg, *Lab Chip*, 2012, **12**, 3666–3669.
228 H. Zhang, L. Lin, D. Liu, Q. Chen and J. Wu, *Anal. Chim. Acta*, 2017, **953**, 71–78.
229 S. R. Mouchet, T. Tabarrant, S. Lucas, B.-L. Su, P. Vukusic and O. Deparis, *Opt. Express*, 2016, **24**, 12267–12280.
230 C. M. Eliason and M. D. Shawkey, *Opt. Express*, 2010, **18**, 21284–21292.
231 Y. Gao, Q. Xia, G. Liao and T. Shi, *J. Bionic Eng.*, 2011, **8**, 323–334.
232 M. D. Shawkey, L. D'Alba, J. Wozny, C. Eliason, J. A. H. Koop and L. Jia, *Zoology*, 2011, **114**, 59–68.
233 X. Yang, Z. Peng, H. Zuo, T. Shi and G. Liao, *Sens. Actuators, A*, 2011, **167**, 367–373.
234 S. Mouchet, O. Deparis and J. P. Vigneron, *Proc. SPIE*, 2012, **8424**, 842425.
235 K. Kertész, G. Piszter, E. Jakab, Z. Bálint, Z. Vértesy and L. P. Biró, *Appl. Surf. Sci.*, 2013, **281**, 49–53.
236 Z. Han, S. Niu, M. Yang, Z. Mu, B. Li, J. Zhang, J. Ye and L. Ren, *RSC Adv.*, 2014, **4**, 45214–45219.
237 W. Wang, W. Zhang, X. Fang, Y. Huang, Q. Liu, J. Gu and D. Zhang, *Sci. Rep.*, 2014, **4**, 5591.
238 T. Jiang, Z. Peng, W. Wu, T. Shi and G. Liao, *Sens. Actuators, A*, 2014, **213**, 63–69.
239 S. Niu, B. Li, Z. Mu, M. Yang, J. Zhang, Z. Han and L. Ren, *J. Bionic Eng.*, 2015, **12**, 170–189.
240 A. K. Wanekaya, M. Uematsu, M. Breimer and O. A. Sadik, *Sens. Actuators, B*, 2005, **110**, 41–48.
241 S. Zhang and Y. Chen, *Sci. Rep.*, 2015, **5**, 16637.
242 R. H. Siddique, S. Diewald, J. Leuthold and H. Hölscher, *Opt. Express*, 2013, **21**, 14351–14361.
243 M. Aryal, D.-H. Ko, J. R. Tumbleston, A. Gadisa, E. T. Samulski and R. Lopez, *J. Vac. Sci. Technol., B*, 2012, **30**, 061802.
244 O. Poncelet, G. Tallier, S. R. Mouchet, A. Crahay, J. Rasson, R. Kotipalli, O. Deparis and L. A. Francis, *Bioinspiration Biomimetics*, 2016, **11**, 036011.
245 R. H. Siddique, R. Hünig, A. Faisal, U. Lemmer and H. Hölscher, *Opt. Mater. Express*, 2015, **5**, 996–1005.
246 G. England, M. Kolle, P. Kim, M. Khan, P. Muñoz, E. Mazur and J. Aizenberg, *Proc. Natl. Acad. Sci. U. S. A.*, 2014, **111**, 15630–15634.
247 R. K. Bonam and J. G. Hartley, *J. Vac. Sci. Technol., B*, 2016, **34**, 06k606.

248 C. A. Tippets, Y. Fu, A. M. Jackson, E. U. Donev and R. Lopez, *J. Opt.*, 2016, **18**, 065105.
249 M. Garliauskas, E. Stankevičius and G. Račiukaitis, *Opt. Mater. Express*, 2017, **7**, 179–184.
250 H. Inan, M. Poyraz, F. Inci, M. A. Lifson, M. Baday, B. T. Cunningham and U. Demirci, *Chem. Soc. Rev.*, 2017, **46**, 366–388.
251 C. Steinberg, M. Rumler, M. Runkel, M. Papenheim, S. Wang, A. Mayer, M. Becker, M. Rommel and H.-C. Scheer, *Microelectron. Eng.*, 2017, **176**, 22–27.
252 F. Zhang, Q. Shen, X. Shi, S. Li, W. Wang, Z. Luo, G. He, P. Zhang, P. Tao, C. Song, W. Zhang, D. Zhang, T. Deng and W. Shang, *Adv. Mater.*, 2015, **27**, 1077–1082.
253 X. Guo, H. Zhou, T. Fan and D. Zhang, *Sens. Actuators, B*, 2015, **220**, 33–39.
254 I. Venditti, *Materials*, 2017, **10**, 97.
255 R. A. Potyrailo, in *New Developments in Coatings Technology ACS Symp. Series 962*, ed. P. Zarras, T. Wood, B. Richey and B. C. Benicewicz, American Chemical Society, Washington, DC, 2007, vol. 962, pp. 240–260.
256 R. Vargas-Bernal and G. Herrera-Pérez, in *Nanotechnology for optics and sensors*, ed. M. Aliofkhazraei, One Central Press, 2014, ch. 1.
257 J. Zhang, X. Liu, G. Neri and N. Pinna, *Adv. Mater.*, 2016, **28**, 795–831.
258 L. Srisombat, A. C. Jamison and T. R. Lee, *Colloids Surf., A*, 2011, **390**, 1–19.
259 Y. Joseph, B. Guse and G. Nelles, *Chem. Mater.*, 2009, **21**, 1670–1676.
260 C. Jin, P. Kurzawski, A. Hierlemann and E. T. Zellers, *Anal. Chem.*, 2008, **80**, 227–236.
261 N. Garg, A. Mohanty, N. Lazarus, L. Schultz, T. R. Rozzi, S. Santhanam, L. Weiss, J. L. Snyder, G. K. Fedder and R. Jin, *Nanotechnology*, 2010, **21**, 40550.
262 R. A. Potyrailo and V. M. Mirsky, *Chem. Rev.*, 2008, **108**, 770–813.
263 S. Curtarolo, G. L. Hart, M. B. Nardelli, N. Mingo, S. Sanvito and O. Levy, *Nat. Mater.*, 2013, **12**, 191–201.
264 K. Lejaeghere, G. Bihlmayer and T. Björkman, *Science*, 2016, **351**, aad3000.
265 M. G. Medvedev, I. S. Bushmarinov, J. Sun, J. P. Perdew and K. A. Lyssenko, *Science*, 2017, **355**, 49–52.
266 R. Gomez-Bombarelli, J. Aguilera-Iparraguirre, T. D. Hirzel, D. Duvenaud, D. Maclaurin, M. A. Blood-Forsythe, H. S. Chae, M. Einzinger, D. G. Ha, T. Wu, G. Markopoulos, S. Jeon, H. Kang, H. Miyazaki, M. Numata, S. Kim, W. Huang, S. I. Hong, M. Baldo, R. P. Adams and A. Aspuru-Guzik, *Nat. Mater.*, 2016, **15**, 1120–1127.
267 T. Ueno, T. D. Rhone, Z. Hou, T. Mizoguchi and K. Tsuda, *Mater. Disc.*, 2016, **4**, 18–21.
268 N. Nosengo, *Nature*, 2016, **533**, 22–25.
269 R. W. Friedrich and G. Laurent, *Science*, 2001, **291**, 889–894.
270 M. E. Staymates, W. A. MacCrehan, J. L. Staymates, R. R. Kunz, T. Mendum, T. H. Ong, G. Geurtsen, G. J. Gillen and B. A. Craven, *Sci. Rep.*, 2016, **6**, 36876.
271 J. Ying, X. Y. Yang, G. Tian, C. Janiak and B. L. Su, *Nanoscale*, 2014, **6**, 13370–13382.
272 J. A. Fan, C. Wu, K. Bao, J. Bao, R. Bardhan, N. J. Halas, V. N. Manoharan, P. Nordlander, G. Shvets and F. Capasso, *Science*, 2010, **328**, 1135–1138.
273 B. Luk'yanchuk, N. I. Zheludev, S. A. Maier, N. J. Halas, P. Nordlander, H. Giessen and C. T. Chong, *Nat. Mater.*, 2010, **9**, 707–715.
274 S. Zhang, K. Bao, N. J. Halas, H. Xu and P. Nordlander, *Nano Lett.*, 2011, **11**, 1657–1663.
275 G. Zheng, J. Cong, L. Xu and J. Wang, *Appl. Phys. Express*, 2017, **10**, 042202.
276 H. Li, Z. Chen, N. Borodinov, Y. Shao, I. Luzinov, G. Yu and P. Wang, *IEEE Sens. J.*, 2017, **17**, 3323–3331.
277 M. H. Zarifi and M. Daneshmand, *IEEE Microw. Wirel. Compon. Lett.*, 2017, **27**, 311–313.
278 T. Starkey, Doctoral thesis, School of Physics, University of Exeter, 2014.
279 D. Buso, M. Guglielmi, A. Martucci, G. Mattei, P. Mazzoldi, C. Sada and M. L. Post, *Cryst. Growth Des.*, 2008, **8**, 744–749.
280 E. M. Larsson, C. Langhammer, I. Zorić and B. Kasemo, *Science*, 2009, **326**, 1091–1094.
281 E. Della Gaspera, M. Guglielmi, S. Agnoli, G. Granozzi, M. L. Post, V. Bello, G. Mattei and A. Martucci, *Chem. Mater.*, 2010, **22**, 3407–3417.
282 N. A. Joy, P. H. Rogers, M. I. Nandasiri, S. Thevuthasan and M. A. Carpenter, *Anal. Chem.*, 2012, **84**, 10437–10444.
283 P. R. Ohodnicki Jr, C. Wang, S. Natesakhawat, J. P. Baltrus and T. D. Brown, *J. Appl. Phys.*, 2012, **111**, 064320.
284 E. Della Gaspera, M. Guglielmi, G. Perotto, S. Agnoli, G. Granozzi, M. L. Post and A. Martucci, *Sens. Actuators, B*, 2012, **161**, 675–683.
285 P. R. Ohodnicki, J. P. Baltrus and T. D. Brown, *Sens. Actuators, B*, 2015, **214**, 159–168.
286 International Sensor Technology, Irvine, CA, http://www.intlsensor.com/pdf/catalyticbead.pdf.
287 M. Aleixandre and M. Gerboles, *Chem. Eng. Trans.*, 2012, **30**, 169–174.
288 J. R. Stetter and M. Papageorge, *MEMS Technology Symposium, MEPTEC*, San Jose, CA, 2015, http://meptec.org/Resources/11%20-%20Stetter.pdf.
289 Sensistor ISH2000 Technical Reference Manual, www.infi con.com, 2012.
290 V. N. Bedekar and K. H. Tantawi, *Advanced Mechatronics and MEMS Devices II*, Springer, 2017, pp. 195–216.
291 FOODSniffer, http://www.myfoodsniffer.com/product.html, 2016.
292 S. H. Brongersma, *European Technology Platform on Smart Systems Integration (EPoSS) Annual Forum, Session 2*, 2011, http://www.smart-systems-integration.org/public/news-events/events/eposs-annual-forum-2011/programme.
293 C. Borrego, A. M. Costa, J. Ginja, M. Amorim, M. Coutinho, K. Karatzas, T. Sioumis, N. Katsifarakis, K. Konstantinidis, S. De Vito, E. Esposito, P. Smith, N. André, P. Gérard, L. A. Francis, N. Castell, P. Schneider, M. Viana, M. C. Minguillón, W. Reimringer, R. P. Otjes, O. von Sicard, R. Pohle, B. Elen,

D. Suriano, V. Pfister, M. Prato, S. Dipinto and M. Penza, *Atmos. Environ.*, 2016, **147**, 246–263.
294 P. Kumar, A. N. Skouloudis, M. Bell, M. Viana, M. C. Carotta, G. Biskos and L. Morawska, *Sci. Total Environ.*, 2016, **560–561**, 150–159.
295 L. Spinelle, M. Gerboles, M. G. Villani, M. Aleixandre and F. Bonavitacola, *Sens. Actuators, B*, 2015, **215**, 249–257.
296 L. Spinelle, M. Gerboles, M. G. Villani, M. Aleixandre and F. Bonavitacola, *Sens. Actuators, B*, 2017, **238**, 706–715.
297 T. Marshall, *Planet Earth, Natural Environment Research Council*, 2016, http://www.nerc.ac.uk/planetearth/stories/1837/.
298 Inside Activity Tracking, 2013, http://www.insideactivitytracking.com/tracking-accurately-how-is-it-done-why-is-it-difficult/.
299 C. Van Hoof, *EE Times*, 2014, http://www.eetimes.com/author.asp?section_id=36&doc_id=1321976.
300 R. Metz, *MIT Techn. Rev.*, 2015, https://www.technologyreview.com/s/538416/the-struggle-for-accurate-measurements-on-your-wrist/.
301 S. Richmond, *Wareable*, 2015, http://www.wareable.com/fitness-trackers/heart-rate-monitor-accurate-comparison-wrist.
302 M. A. Case, H. A. Burwick, K. G. Volpp and M. S. Patel, *JAMA*, 2015, **313**, 625–626.
303 K. R. Evenson, M. M. Goto and R. D. Furberg, *Int. J. Behav. Nutr. Phys. Act.*, 2015, **12**, 159.
304 E. Gibney, *Nature*, 2015, **528**, 26–28.
305 N. Savage, *Nature*, 2015, **527**, S12–S13.
306 Y. Zhu, *NC State Engineering FALL/WINTER*, 2015, https://news.engr.ncsu.edu/2015/2010/more-accurate-readings-without-the-goop/.
307 J. Ford, *The Engineer*, 2015, http://www.theengineer.co.uk/silver-nanowire-wearable-sensors-match-hospital-wet-electrode-accuracy/.
308 S. Del Din, A. Godfrey, C. Mazzà, S. Lord and L. Rochester, *Mov. Disord.*, 2016, **31**, 1293–1313.
309 W. Knight, *MIT Techn. Rev.*, 2016, https://www.technologyreview.com/s/602248/how-to-make-a-smartphone-detect-anemia/.
310 N. Yamazoe, *Sens. Actuators, B*, 2005, **108**, 2–14.
311 H. Wohltjen, *Plenary talk at the 11th International Meeting on Chemical Sensors*, University of Brescia, Italy, July 16–19, 2006, Elsevier Science, 2006.
312 F. Mayer, *Proc. Eng.*, 2010, **5**, 1–4.
313 E. J. Amis, *Nat. Mater.*, 2004, **3**, 83–85.
314 R. A. Potyrailo, W. G. Morris, A. M. Leach, L. Hassib, K. Krishnan, C. Surman, R. Wroczynski, S. Boyette, C. Xiao, P. Shrikhande, A. Agree and T. Cecconie, *Appl. Opt.*, 2007, **46**, 7007–7017.
315 *The Prism Awards for Photonics Innovation Winners*, 2011, www.photonicsprismaward.com/winners.aspx.
316 *Technology Readiness Assessment (TRA) Deskbook*, May 2005, https://acc.dau.mil/CommunityBrowser.aspx?id=18545, Department of Defence, Prepared by the Deputy Under Secretary of Defense for Science and Technology (DUSD(S&T)), 2005.
317 *OSD Manufacturing Technology Program*, 2011, www.dodmrl.com/MRL_Deskbook_V2.pdf.
318 Y. Lu, X. Fang and J. Zhan, *ACM International Conference Proceedings, BigDataScience '14*, 2014, 36.
319 F. Alborzi, R. Chirkova, J. Doyle and Y. Fathi, *Lect. Notes Comput. Sci.*, 2015, **9263**, 3–14.
320 E. Kujawski, *IEEE Trans. Syst., Man, Cybern., A*, 2013, **43**, 979–987.
321 E. McConkie, T. A. Mazzuchi, S. Sarkani and D. Marchette, *Syst. Eng.*, 2013, **16**, 391–400.
322 H. Wancura, R. Mubbala, R. Steinberger-Wilckens and A. Novak, *4th European PEFC and H2 Forum*, 2013, A1303.
323 *Technology To Market Plan*, https://arpa-e.energy.gov/, ARPA-E, 2014.
324 G. M. Whitesides, *Lab Chip*, 2013, **13**, 11–13.

